

Response to the editor and reviewer comments on

“Changes in glacier dynamics at the northern Antarctic Peninsula since 1985”

By Thorsten Seehaus et al.

First, we want to thank the editor and reviewer for constructive comments on our manuscript. All comments have been taken into account and a list of answers and undertaken actions is given below. Answers are indented and in bold face type and changes in manuscript are indented in *italic*.

Comments by editor Etienne Berthier Received: 19 December 2017

Your revised manuscript and your responses to the second round of comments have now been evaluated by one of the two initial referees. Although he found some clear improvements and clarification, your manuscript still need to be improved before it can be accepted for final publication in TC.

You will find the reviewer assessment below or attached. I also have myself several comments. My main comment is in line with the scepticism expressed by the referee about the use of the median along incomplete transverse velocity profiles as a metric to evaluate glacier velocity fluctuations.

We understand the editor’s concerns. The profiles have an average data coverage of 97% (now mentioned in the revised manuscript; see also answer to comment further down). Therefore, we think that it is justified to average along the profiles.

I appreciated the huge effort you made to extract the velocity variations at the thickest point along the transverse profile. However this alternative way of qualifying glacier velocity change is currently buried in the supplement although it is important to back up your results. I think that this alternative analysis would deserve to be better included in the manuscript than just by stating “Two approaches to measure and analyze the temporal changes in ice flow of the studied glacier are evaluated and the differences are discussed in the supplement Section S1. The favored measuring approach is explained in the following and its results are used for the subsequent analysis.” This does not need to be long I think: A few line of description in the method section and providing the results for the mean velocity change of the three sectors would do the job.

We agree with the editor and revised the methods and results section accordingly. More details and results of the second approach are now in the manuscript.

To facilitate the review process (possibly by one of the chief editors due to my 2.5-month absence), please attach to your revised manuscript a cover letter detailing the changes you made in response to all comments.

Best regards,

Etienne Berthier

Abstract: Currently, the sentence “By applying a hierarchical cluster analysis we show that this is associated with the geometric parameters of the individual glacier basins.” is a bit enigmatic to the reader. At least authors could list in parenthesis the geometric parameters examined.

According to the editor's comment, we listed the geometric parameters.

By applying a hierarchical cluster analysis, we show that this is associated with the geometric parameters of the individual glacier basins (Hypsometric Indexes, maximum surface elevation of the basin, flux gate to catchment size ratio).

2.16 "at the northern part of the peninsula" why not using "northern AP" here

We changed the wording accordingly.

2.27 Structure of the sentence starting with "Whereas" does not seem to be OK.

We appreciate this advice and restructured this sentence.

Whereas, glacier-wide surface lowering was observed by various author groups (e.g. Berthier et al., 2012; Rott et al., 2014; Scambos et al., 2014) at former ice shelf tributaries along the north-eastern AP.

3.7 "-" between "sub" and "regions" (I think)

Thank you for this advice, we looked it up in a dictionary, and removed the space.

4.1 delete "an area of"

We removed "an area of".

4.25 delete "in the area studied region"

We deleted "in the area studied".

5.31 "taking into account the effects on the local incidence angle by the topography" was not clear to me (I am not a SAR specialist as many others TC readers).

We rephrased this sentence to be clearer to the reader.

Finally, the displacement fields are transferred from slant range into ground range geometry, taking into account the contortion caused by the topography (topographic effects on the local SAR incidence angle).

6.5 Huber et al. (2017). Tell where they performed their accuracy assessment of the AP-DEM? Northern AP? Whole peninsula?

Huber et al. (2017) estimated the uncertainty, also based on their experiences with other DEMs. Thus, we conclude their accuracy value was used for the whole AP-DEM. We changed the wording accordingly.

Since the accuracy varies regionally, Huber et al. 2017 estimated the uncertainty to be ± 50 m for the AP-DEM, based on their experiences with other DEMs.

7.4 Indicate that this a transverse profile (right?)

Thank you for this advice. We changed the wording to be clearer

An across glacier profile is defined (red lines in Fig. 1) close to the terminus of each basin, considering the maximum retreat state of ice front position in the observation period.

7.7 I find the statement “Datasets with partial profile coverage or large data gaps, as well as those with still remaining tracking errors, are rejected.” rather vague. What is exactly “partial” (less than 80%, 50% coverage?) and “large data gaps”? Can authors make it clearer and reproducible?

We understand the editor’s concerns. The selection of the datasets was done manually (visual inspection) and no certain threshold was applied. However, we analyzed the profile coverage by velocity data and added this information in the manuscript.

The resulting average coverage by velocity measurements along the profiles is 97% and 90% of all extracted profiles have got a data coverage of more than 93%.

Moreover, we restructured the respective paragraph to be clearer.

7.10 The use of the median is a bit problematic (see also the referee statement). Authors should think twice about it in their future studies. Imagine that 40% of the profile had a drastic velocity change and not the rest of the profile. The median would not show any change in velocity where as the ice flow has clearly changed. This is why their alternative method should be included more in the manuscript.

The editor is right, regarding the limitation of median values. However, we also tested to use mean values, but the obtained results were noisier. Small scale outliers (single pixels or just a few pixels, which are remaining tracking errors after filtering) can bias the mean values measured along the profiles, whereas they are filtered out using median values.

“To minimize the impact of potential outliers (still remaining small scale tracking errors), median velocities along the profiles are calculated” (Section 3.2)

We did not want to reject the profiles which have some small-scale outliers. We wanted to keep the number of velocity measurements per glacier high, in order to obtain reasonable velocity change time series. Therefore, we decided to use median instead of mean values.

7.14 close parenthesis.

We closed the parenthesis.

9.22 Seems that “2” should be deleted before “256”

Please see also Table S1. In total 2256 profile measurements were used in this study. We changed the wording in order to not confuse this value with the number of obtained velocity fields.

...inspected and in total 2256 profile measurements passed the quality check...

11.5 I have a hard time understanding the statement “Moreover, slightly increased recession is also found in the time period (1995-2005, Fig. 4) at sector “East”.” in view of the two previous sentences. And then the next sentence deal with ice shelf disintegration but authors discuss here a sector where not ice shelf existed. Overall, the causal link between the successive sentences in this paragraph is unclear. Or did I miss something?

We understand the editor’s concerns and rephrased this paragraph to be clearer.

Davies et al. (2012) also reported higher retreat rates for most of the glaciers in this sector in the period 1988-2001 than in the period 2001-2009. However, another significant recession is also found at sector “East” after 1995 (Fig. 4). Davies et al. (2012) and Hulbe et al. (2004) supposed that the disintegration of a nearby ice shelf affects the local climate. The air temperatures would rise due to the presence of more ice free water in summers. Thus, the higher retreat rates at sector “East” after 1995 could be indirectly caused by the disintegration of Prince Gustav and Larsen A Ice Shelf.

12.8 why deleting Skvarca et al. (1998) and keeping it two lines later?

Here it was misplaced, since this sentence is about the observed cooling in the 21th century (cannot be observed in 1998) and the next sentence is about the warming since 1970s, which was reported by Skvarca et al. (1998) and Oliva et al. (2017).

12.25. Some textbook reference for surging glacier may be more appropriate (or a generic paper such as Sevestre and Benn, 2015). I do not really see the point at picking Alaska and Karakoram as examples here.

We appreciate the editor's comment. We just picked two regions which are famous for surge-type glaciers. According to the editor's comment we adjusted the wording and reference to two generic paper.

Surge-type glaciers (tidewater as well as land terminating), found in various regions worldwide, show similar behavior (Meier and Post, 1969; Sevestre and Benn, 2015).

13.14. Rott et al. (2017) is just published in TCD and has not passed the peer-review process. Should not be cited.

We removed the citation.

13.22 "higher flow speeds" higher than what?

We refer to pre-ice-shelf-collapse conditions. We added this information.

....albeit significant higher flow speeds (compared to pre-ice-shelf-collapse conditions) can be observed at the central sections of the terminus

14.5 delete "," in "Rott et al., (2014)"

Deleted

16.15 "along the west coast higher overall glacier flow" Do the author mean higher flow increase? In the rest of the paper they never compared their absolute flow magnitude to Pritchard & Vaughan (2007) but only compared the % of velocity increase.

The editor is right, we mean higher flow increase. We rephrased this sentence to be clearer.

The results are in general in line with findings of the previous studies; however, along the west coast a more accelerated glacier flow is determined and

16.26 "conclude" is very strong in this context. I think "suggest" or "speculate" would better reflect the level of understanding that we have here on these "East" glaciers.

We replaced "conclude" by "suggest" according to the editor's suggestion.

17.14 "M.B." instead of "MB"

Corrected

Ref to Lai. Volume/page numbers?

We revised the reference and added volume and page numbers.

Lai, Z., & Huang, M. 1989. Numerical Classification of Glaciers in China by Means of Glaciological Indices at the Equilibrium Line. In Snow Cover and Glacier Variations. Proceedings of a Symposium held in Baltimore, Maryland May 10-19, 1989, IAHS Publication 183, 103-111

Supplement.

Avoid so much parenthesis in the legend.

According to the editor's suggestion, we revised the overview legend.

S1. "along across glacier profiles" is not clear; " using obtained by the second approach" or " This mismatch does not influencing" is not correct. Check the supplement VERY carefully to make sure it is understandable. Proof reading may be useful for this supplementary text.

We are sorry for the errors. We checked the supplement and revised it. Additionally, we send it to a proofreading agency (therefore, most of the "tacked-changes" done by the authors, were removed by the agency and are not visible in the "tracked-changes" version of the revised supplement. We are sorry for this).

**Comment by Referee #2: Jan Wuite
Received: 18 December 2017**

General Comments

The comments here concern the second revised version of the manuscript by Seehaus et al. on changes in glacier dynamics in the northern Antarctic Peninsula since 1985. The authors have made substantial revisions to the original and revised manuscript in response to the reviewer's comments. These revisions include clarifications, corrections, additional references, as well as an added section and new figures in the supplemental material. The additional scrutiny appears to have led to significant changes in some of the reported velocity changes (individual glaciers & regions) and also to the discovery of errors in some of the figures/tables.

I appreciate the efforts by the authors to clarify their adopted approach, but would like to point out here that I am still rather unconvinced about the exact implementation of the across flow median velocity values in the presented analysis and my earlier worries on several issues still stand. The profiles presented in the manuscript's supplement illustrate to some degree the difficulties and problems that arise. If, as the authors mention in their reply document (1st reply), the erroneous/incomplete profiles were not used for the analysis there is little reason to include them, but in the way it is written currently it looks like all depicted profiles passed the quality check (Pg. 9 Ln. 12-15). Therefore, I mention here specifically: unrealistic fluctuations appear to occur along some of the profiles (e.g. Fig S155) and some profiles are incomplete (and were apparently not rejected as mentioned in the text – Pg. 6 Ln. 29/Pg. 7 Ln. 1).

Not all profiles with data gaps and remaining tracking errors were rejected, only those with partial coverage, large data gaps or large-scale tracking errors. However, the average profile coverage was kept at a high level of 97%, to facilitate a reasonable averaging along the profiles. In order to suppress the effect of the small-scale tracking errors we calculated median values instead of mean values (see also answer to editor comment above). We are sorry, that it was not clearly described. We revised the methods section (also taking in to account the comments of the editor) and hope that it is now clearer.

The results are visually inspected in order to remove unreliable measurements, based on the magnitude and direction of ice flow along the profiles. Datasets with partial profile coverage, large data gaps and large-scale tracking errors are rejected. The resulting average coverage by velocity measurements along the profiles is 97% and 90% of all extracted profiles have got a data coverage of more than 93%. To minimize the impact of potential outliers (still remaining small scale tracking errors), median velocities along the profiles are calculated

A crucial issue, however, is the treatment of velocity in the shear margins, some profiles seem to be cut off rather abruptly, some are smoother and go down to zero velocity, some appear to cover more glaciers and include intermediate (stationary?) areas, some have very high values at the margins (or do not seem to include the margin – e.g. S150). The sensor capabilities and to a certain degree the algorithm settings largely determine how well these margins can be captured. One should therefore be cautious when interpreting extracted values as they could reflect sensor limitations instead of real velocity changes.

We understand the reviewer's concerns. Some of the glacier basins consist of more than one major ice stream, which join towards the terminus. For some cases the intermediate areas have low flow speeds (e.g. Fig. S152 or S155). However, the delineation of the individual sections is not always clearly possible, and its width can vary temporally (as mentioned in Section 2, page 4, line 3-5). Therefore, we decided to merge coalescing glaciers for our analysis and use only one across terminus profile. Moreover, measuring velocities of a glacier system at a fix point can also lead to discrepancies, since the peak position and the shape of the across glacier velocity profile can vary (as discussed in Section S1 supplement). Regarding the velocity data in the margin of the glaciers: The

reviewer is right, that sensor capabilities and the tracking algorithm determine the capturing of the flow velocities in the lateral glacier sections. In order to minimize the limitations caused by the tracking algorithm, we used different tracking window sizes (small windows for the slow moving lateral section and larger windows to capture the displacements in the fast-flowing central sections (Section 3.2 page 6, line 9-16). The results were iteratively stacked to obtain the best spatial coverage. However, at some small and narrow glaciers the capturing of the velocity gradient in the margins is still mainly limited by the sensor resolution. Therefore, we present also the velocity profiles of small glaciers in the manuscript (e.g. TPE61 Glacier Fig. S 150, DGC14 Fig. S153, TPE8 Glacier Fig. S156) to illustrate the limitations. Moreover, we added a statement on this issue in the manuscript (Section 4.2 Results)

For small and narrow glaciers, the capturing of the flow velocity gradients in the margins is still mainly limited by the sensor resolution, even applying different tracking window sizes.

That said, in concordance with my main wish in the previous review rounds, at least the methods are now better documented and the inclusion of ice velocity cross profiles in concordance with calculated velocity median values (in the supplement) provide some means of traceability. I likewise welcome the inclusion of additional ice velocity maps for this reason as it shows the source material of some of the numbers and its potential or limitation. Also, the reported ice velocity changes for Drygalski (which I took as a primary example in my previous review) has been revised considerably.

A few more specific comments for consideration:

- The IV profiles are extracted from close to the terminus, but it is not mentioned in the text from which year nor is it very clear from fig 1.

We are sorry, but we do not know to which paragraph/section this comment refers. In Section 3.2 in the main manuscript we state: “A profile is defined (red lines in Fig. 1) close to the terminus of each glacier basin, considering the maximum retreat state of ice front position in the observation period.”

In the Supplemental Material Section S1 we link to this section: For the first approach, the flow velocities are extracted along across glacier profiles (see. Fig. 1 in the manuscript) close to the terminus and the median values along the profiles are calculated (see also Section 3.2 in the manuscript).

However, we rephrased this sentence in the Supplemental Material to be clearer:

For the first approach, the flow velocities are extracted along across glacier profiles, defined for each basin close to the terminus and considering the maximum frontal retreat state (see. Fig. 1 in the manuscript), and the median values along the profiles are calculated (see also Section 3.2 in the manuscript).

- In the conclusion it is now mentioned “Upcoming sensor [SIC] probably facilitate the region wide measurement of recent surface elevation, since current estimates have got only partial coverage or have got some issues due to the complex topography of the AP. “. Just a thought, what type of sensor is going to overcome the partial coverage and issues due to complex topography, or is this wishful thinking (in which case 'hopefully' is more apt than 'probably')?

We understand the reviewer’s concerns, and “hope” that sensors like e.g. ICESat-2 would overcome the partial coverage and the issues due to complex topography. However, this needs to be validated once it is in operation. Therefore, we replaced “probably” by “hopefully”.

• As mentioned above, please clarify whether profiles depicted in supp. material passed the quality check and if they were used or not used in the analysis.

All profiles shown in Fig. S149-S156 are used in the further analysis. See answer to comment above.

Grammar

Pg. 2 Ln. 27: “) The” → missing point

Pg. 7 Ln. 17&18: on average

Pg. 12 Ln. 2: van der Veen

Pg. 13 Ln. 8: observed

Sup Mat.

Pg. 2 2 nd paragraph: 2256 measurementS

Pg. 2 3 rd paragraph: using obtained by the second approach → seems like a word is missing here

Pg. 2 3 rd paragraph: This mismatch does not influencE the subsequent

Pg. 2 5 th paragraph: 'is little' → is small

Thank you for these advices. We corrected the manuscript and supplemental material accordingly.

Changes in glacier dynamics in the northern Antarctic Peninsula since 1985

Thorsten Seehaus¹, Alison J. Cook², Aline B. Silva³, Matthias Braun¹

¹ Institute of Geography, Friedrich-Alexander-University Erlangen-Nuremberg, Wetterkreuz 15, 91058 Erlangen, Germany

² Department of Geography, Durham University, South Road, Durham DH1 3LE, United Kingdom

³ Laboratório de Monitoramento da Criosfera, Universidade Federal do Rio Grande, Av. Itália, km 8, 96203-900, Rio Grande - RS Brazil

Correspondence to: Thorsten Seehaus (thorsten.seehaus@fau.de)

Abstract. The climatic conditions along the northern Antarctic Peninsula have shown significant changes within the last 50 years. Here we present a comprehensive analysis of temporally and spatially detailed observations of the changes in ice dynamics along both the east and west coastlines of the northern Antarctic Peninsula. Temporal evolutions of glacier area (1985-2015) and ice surface velocity (1992-2014) are derived from a broad multi-mission remote sensing database for 74 glacier basins on the northern Antarctic Peninsula (<65° S along the west coast and north of the Seal Nunataks on the east coast). A recession of the glaciers by 238.81 km² is found for the period 1985-2015, of which the glaciers affected by ice shelf disintegration showed the largest retreat by 208.59 km². Glaciers on the east coast north of the former Prince Gustav Ice Shelf extent in 1986 receded by only 21.07 km² (1985-2015) and decelerated by about 58% on average (1992-2014). A dramatic acceleration after ice shelf disintegration with a subsequent deceleration is observed at most former ice shelf tributaries on the east coast, combined with a significant frontal retreat. In 2014, the flow speed of the former ice shelf tributaries was 26% higher than before 1996. Along the west coast the average flow speeds of the glaciers increased by 41%. However, the glaciers on the western Antarctic Peninsula revealed a strong spatial variability of the changes in ice dynamics. By applying a hierarchical cluster analysis we show that this is associated with the geometric parameters of the individual glacier basins (*Hypsometric Indexes, maximum surface elevation of the basin, flux gate to catchment size ratio*). The heterogeneous spatial pattern of ice dynamic evolutions at the northern Antarctic Peninsula shows that temporally and spatially detailed observations as well as further monitoring are necessary to fully understand glacier change in regions with such strong topographic and climatic variances.

1 Introduction

During the last century, the northern Antarctic Peninsula (AP) and its outlying islands have undergone significant warming (Turner et al., 2005), leading to substantial glaciological changes. Skvarca et al. (1998) reported a significant increase in surface air temperatures at the north-eastern AP in the period 1960-1997 and correlated it with the recession of the Larsen and Prince Gustav Ice shelves (Fig. 1) and the observed retreat of tidewater glaciers on James Ross Island in the period

1975-1995 (Skvarca et al., 1995). However, a recent cooling trend on the AP was revealed by Oliva et al. (2017) and Turner et al. (2016) since the late 1990s. Shepherd et al. (2012) compiled a comprehensive glacier mass balance database of the polar ice sheets. The authors estimated a mass loss on the whole AP (<73° S) of $-36 \pm 10 \text{ Gt a}^{-1}$ for the period 2005-2010, which corresponds to 35% of the total mass loss of Antarctica. A projection of sea level rise contribution by the AP ice sheet amounts to 7-16 mm sea-level equivalent by 2100 and 10-25 mm by 2200 (Barrand et al., 2013a). However, along the western AP and on the higher elevation areas an increase in snow accumulation in the late 20th century was derived from ice cores (e.g. at Palmer Land, 73.59° S, 70.36° W, Thomas et al., 2008; Detroit Plateau, 64.08° S, 59.68° W, Potocki et al., 2011; at Bruce Plateau, 66.03° S, 64.07° W, Goodwind, 2013) and climate models (e.g. Dee et al., 2011), whereas Vvan Wessem et al. (2016) obtained insignificant trends in precipitation.

Numerous ice shelves along the AP have retreated widely (e.g. Müller, Wilkins, Wordie) or disintegrated in recent decades (e.g. Larsen A in 1995, Larsen B in 2002) (Braun and Humbert, 2009; Cook and Vaughan, 2010; Doake and Vaughan, 1991; Rack et al., 1998; Rack and Rott, 2003; Wendt et al., 2010). As a consequence to the reduced buttressing, former tributary glaciers showed increased ice discharge and frontal retreat (e.g. De Angelis and Skvarca, 2003; Rack and Rott, 2004; Rignot et al., 2004; Seehaus et al., 2015; Wendt et al., 2010). For the northern AP (<66° S), a mass loss rate of $-24.9 \pm 7.8 \text{ Gt a}^{-1}$ was reported by Scambos et al. (2014) for the period 2003-2008, indicating that major ice mass depletion happened at the northern ~~part of the peninsula~~ AP, especially along the eastern side where numerous glaciers have been affected by ice shelf collapses. Seehaus et al. (2015, 2016) quantified the ice loss of former ice shelf tributaries. Mass loss rates of $-2.14 \pm 0.21 \text{ Gt a}^{-1}$ (1995-2014) and $-1.16 \pm 0.16 \text{ Gt a}^{-1}$ (1993-2014) were found at Dinsmoor-Bombardier-Edgeworth Glacier System and Sjögren-Inlet glaciers, respectively. Glaciers that were not terminating in an ice shelf also showed considerable changes. Cook et al. (2005, 2014) have analyzed the variations of tidewater glacier fronts since the 1940s. The authors reported that 90% of the observed glaciers retreated, which they partly attributed to atmospheric warming. A more recent study revealed a mid-ocean warming along the southwestern coast of the AP, forcing the glacier retreat in this region (Cook et al., 2016). Pritchard and Vaughan (2007) observed an acceleration of ice flow by ~12% along the west coast of the AP (1995-2005) and linked it to frontal retreat and dynamic thinning of the tidewater glaciers. Observations by Kunz et al. (2012) support this supposition. They analyzed surface elevation changes of 12 glaciers on the western AP based on stereoscopic digital elevation models (DEM) over the period 1947-2010. Frontal surface lowering was found at all glaciers. Whereas, glacier-wide surface lowering ~~of former ice shelf tributaries~~ was observed ~~along the north-eastern AP~~ by various author groups (e.g. Berthier et al., 2012; Rott et al., 2014; Scambos et al., 2014) ~~at former ice shelf tributaries along the north-eastern AP~~. The collected observations suggest that the ice masses on the AP are contributing to sea level rise and show that glaciers' response to climate change on the AP is not homogeneous and that more detailed knowledge of various aspects on the glacier changes are required. Previous studies often cover a specific period or area, or focus on one particular aspect of glacier change. By now, the availability of remote sensing data time series data and other datasets in this region facilitates

the comprehensive analysis of glacier change. Therefore, we study the changes in glacier extent in combination with detailed investigations on ice dynamics as well as other derived geometrical attributes of glaciers on the northern AP (<65° S along the west coast and north of the Seal Nunataks on the east coast, Fig. 1b colored polygons) between 1985 and 2015. We analyze various multi-mission remote sensing datasets in order to obtain methodologically consistent and temporally detailed time series of ice dynamic changes of 74 glacier basins. The observations are individually discussed for the sub-regions, considering the different atmospheric, glaciological and oceanic conditions and changes.

2 Study site

The AP is the northern-most region of Antarctica and stretches from 63-75°S (Huber et al., 2017). It covers only 3% of the entire continent in area, but receives 13% of the total mass input (Van Lipzig et al., 2002, 2004). The AP's mountain chain (typically 1500-2000 m high) acts as an orographic barrier for the circumpolar westerly air streams leading to very high precipitation values on the west coast and on the plateau region of up to 5000 mm we a⁻¹, as well as frequent foehn type wind occurrences on the east coast (Cape et al., 2015, Marshall et al., 2006, Van Wessem et al. 2016). The foehn events are characterized by strong winds and high air temperatures. Consequently, the climatic mass balance (b_{clim}) shows a strong gradient across the mountain chain (Turner, 2002; Van Wessem et al., 2016). Aside from those that are ice shelf tributaries, almost all glaciers on the AP are marine terminating, and the majority of the glacier catchments extend up to the high elevation plateau regions (north to south: Laclavère, Louis Philippe, Detroit, Herbert, Foster, Forbidden, Bruce, Avery, Hemimont, Dyer). Typically the AP plateau is separated from the outlet glaciers by escarpments and ice-falls. Glaciers on the west coast drain into the Bellingshausen Sea and on the east coast into the Weddell Sea. Since the 1980s, the ice shelves along the east coast have substantially recessed and disintegrated (Larsen Inlet in 1987-89, Prince Gustav and Larsen A in 1995 and Larsen B in 2002) (Cook and Vaughan, 2010; Rott et al., 1996; Skvarca et al., 1999), which Scambos et al. (2003) attributed to higher summer air temperatures and surface melt. A more recent study by Holland et al. (2015) discovered that significant thinning of the Larsen C Ice Shelf is caused by basal melting and that ungrounding from an ice rise and frontal recession could trigger its collapse. The northern AP has a maritime climate and is the only region of Antarctica that frequently experiences widespread surface melt (Barrand et al., 2013b; Rau and Braun, 2002).

Our study site stretches approximately 330 km from the northern tip of the AP mainland southwards to Drygalski Glacier on the east coast and Grubb Glacier on the west coast (Fig. 1). This facilitates the analyses of the temporal evolution (~20 years) of the response of tributary glaciers to ice shelf disintegration at the former Larsen A and Prince Gustav ice shelves on the east coast, the investigation of glaciers north of the former Prince Gustav Ice Shelf, where no information on change in ice flow is currently available, and the comparison with temporal variations in ice dynamics along the west coast at the same latitude. The study site covers an area of ~11,000 km² (~11% of the whole AP including islands, Cook et al., 2014; Huber et al., 2017) with elevations stretching from sea level up to 2220 m. The glacier basin delineations are based on the Antarctic

Digital Database ADD 6.0 (Cook et al., 2014). Glacier names are taken from the Global Land Ice Measurements from Space (GLIMS) project database. The local GLIMS glacier IDs (e.g. TPE62, LAB2) are used for unnamed glaciers and further missing glacier basin names are replaced with the ADD 6.0 glacier IDs. Neighboring basins with coalescing ice flow at the termini are merged (many are already merged in the ADD 6.0), as the delineation of the individual glacier sections is not always possible and the width can vary temporally (due to changes in mass flux of the individual glaciers). In these cases, the names of the glaciers are also merged (e.g. Sikorsky-Breguet-Gregory – SBG, see Table 1 for abbreviations of glacier names). Due to the sparse data coverage (fewer than three good quality velocity measurements), no time series analysis of the glaciers at the northern tip of the AP or at some capes and peninsulas (e.g. Sobral Peninsula, Cape Longing) is possible. Therefore, the northern-most analyzed catchments are Broad-Valley Glacier on the east coast and TPE8 Glacier on the west coast, resulting in 74 studied glacier basins. Furthermore, the study site is divided into three sectors, taking into account the different climatic settings and drainage orientation as well as former ice shelf extent: sector “West” - glaciers on the west coast, draining into the Bransfield and Gerlache Strait; sector “East” – glaciers on the east coast, draining into the Prince Gustav Channel; and sector “East-Ice-Shelf” – glaciers on the east coast, that were former tributaries to the Larsen A, Larsen Inlet and Prince Gustav Ice Shelf.

3 Data & Methods

A large number of various remote sensing datasets are analyzed in order to obtain temporally and spatially detailed information on changes in ice dynamics in the study area. Glacier area changes are derived from satellite and aerial imagery. Repeat-pass Synthetic Aperture Radar (SAR) satellite acquisitions are used to compute surface velocity fields in order to obtain information on changes in glacier flow speed. Auxiliary data from sources such as a digital elevation model and glacier inventory are included in the further analyses and discussion of the results.

3.1 Area changes

Changes in glacier area are derived by differencing glacier outlines from various epochs. All observed glaciers are tidewater glaciers and only area changes along the calving front were considered. Information on the positions of the glacier fronts ~~in the area studied~~ are taken from Cook et al. (2014), and are available for the whole AP in the ADD 6.0 (1945-2010). This coastal-change inventory is based on manually digitized ice front positions using imagery from various satellites (e.g. Landsat, ERS) and aerial photo campaigns. This dataset is updated (up to 2015) and gaps are filled by manual mapping of the ice front positions based on SAR and optical satellite images. Consistent with Cook et al. (2014), the ice-front positions are assigned to 5-year intervals in order to analyze temporal trends in glacier area changes in the period 1985-2015. Before 1985, only sparse information on ice front positions for the whole study site is available, and the coverage by SAR data for

analyzing glacier flow starts in 1992. Additionally, the analysis of the area changes for the Larsen A and Prince Gustav Ice Shelf tributaries is limited to the period 1995-2015, as the ice shelves disintegrated in 1995.

The uncertainties of the glacier change measurements strongly depend on the specifications of the imagery used (e.g. spatial resolution, geodetic accuracies) as well as the methods used. To each record in the coastal-change inventory from the ADD 6.0, a reliability rating is assigned according to Ferrigno et al. (2006). The rating ranges from 1 to 5 (reliability within 60 m to 1 km) and takes into account errors due to manual digitization and interpretation (see Ferrigno et al., 2006 for a detailed description). This approach is also applied on the updated ice-front positions. Nearly all mapped ice fronts in the area studied have a good reliability rating of 1 (76%) and 2 (21%). Only a few glacier fronts (3%) have a rating of 3. No ice fronts with reliability ratings of 4 and 5 are mapped in the study area.

3.2 Surface velocities

Surface velocity maps are derived from repeat-pass Synthetic Aperture Radar (SAR) acquisitions. SAR image time series of the satellite missions ERS-1/2, Envisat, RadarSAT-1, ALOS, TerraSAR-X (TSX) and TanDEM-X (TDX) are analyzed, covering the period 1992-2014. Specifications of the SAR sensors are listed in Table 2. The large number of SAR images was provided by the German Aerospace Center (DLR), the European Space Agency (ESA) and the Alaska Satellite Facility (ASF). To obtain displacement fields for the glaciers, the widely used and well approved intensity offset tracking method is applied on co-registered single look complex SAR image pairs (Strozzi et al., 2002). In order to improve the co-registration of the image pairs, we mask out fast moving and unstable regions such as outlet glaciers and the sea during the co-registration processes. Furthermore, single SAR image tiles acquired during the same satellite flyover are concatenated in the along-track direction. This helps to further improve the co-registration in coastal regions (by including more stable areas in the co-registration process) but also simplifies the analysis of the final results as no mosaicking of the results is needed. Image pairs with low quality co-registration are filtered out. A moving window technique (step-size see Table 2) is used by the intensity offset tracking method to compute the cross-correlation function of each image patch and to derive its azimuth and slant range displacement. The resolution of the obtained displacement fields depends on the combination of the step-size and the resolution of the images in slant-range geometry. A resolution of the velocity fields of ~50 m for the high resolution sensors TSX, TDX and ~100 m for all other sensors was targeted. Less reliable offset measurements are filtered out by means of the signal-to-noise ratio of the normalized cross-correlation function. Moreover, we apply an additional filter algorithm based on a comparison of the magnitude and alignment of the displacement vector relative to its surrounding offset measurements. This technique removes more than 90% of incorrect measurements (Burgess et al., 2012). Finally, the displacement fields are transferred from slant range into ground range geometry, taking into account ~~the contortion-the effects on the local incidence angle by the~~ [caused by the topography \(topographic effects on the local SAR incidence angle\)](#). The results are then geocoded, orthorectified, resampled and converted into velocity fields (with 100 m pixel spacing for all

sensors) by means of the time span between the SAR acquisitions. The mean date of the consecutive SAR acquisitions is assigned to each velocity field. The ASTER Global Digital Elevation Model of the Antarctic Peninsula (AP-DEM, Cook et al., 2012) is used as elevation reference. It is currently the best available digital elevation model of the Antarctic Peninsula. It has a mean elevation bias of -4 m (± 25 m RMSE) from ICESat data and horizontal accuracy better than 2 pixels. ~~However~~
5 ~~Since the accuracy varies regionally~~, Huber et al. 2017 estimated the uncertainty to be ± 50 m ~~for the AP-DEM, based on their experiences with other DEMs since it varies regionally~~. -Velocity data is analyzed close to the calving front (see further down) where the slope of the glaciers at the AP is typically quite low. Thus, the impact of the DEM accuracy on the velocity fields is insignificant (see Seehaus et al., 2015 supplemental material).

Depending on the displacement rate and resolution of the SAR sensor, the tracking window size needs to be adapted (de
10 Lange et al. 2007). For the fast flowing central glacier sections, larger window sizes are needed since large displacements cannot be tracked by using small correlation patches. Small tracking window sizes are suitable for the slow moving lateral sections of the outlet glaciers. Wide parts of large tracking patches cover the stable area next to the glacier, which biases the tracking results towards lower velocities. Consequently, we compute surface velocity fields of the same image pairs for different correlation patch sizes in order to get the best spatial coverage. Table 2 shows the different tracking window sizes
15 for each sensor. The results of each image pair are stacked by starting with the results of smallest tracking window size and filling the gaps with the results of the next biggest tracking window size.

The accuracy of the velocity measurements strongly depends on the coregistration quality and the intensity offset tracking algorithm settings. The mismatch of the coregistration σ_v^C is quantified by measuring the displacement on stable reference areas close to the coast line, such as rock outcrops and nunataks. Based on the Bedmap2 (Fretwell et al., 2013) and ADD 6.0
20 rock outcrop masks, reference areas are defined and the median displacements magnitude of each velocity field is measured at these areas. The uncertainty of the tracking process σ_v^T is estimated according to McNabb et al. (2012) and Seehaus et al. (2015) depending on accuracy of the tracking algorithm C , image resolution dx , oversampling factor z , time interval dt .

$$\sigma_v^T = \frac{Cdx}{zdt} \quad (1)$$

The accuracy of the tracking algorithm is estimated to be 0.2 pixels and an oversampling factor $z=2$ is applied to tracking
25 patches in order to improve the accuracy of the tracking process. Both independent error estimates are quadratically summed to compute the uncertainties of the individual velocity fields σ_v .

$$\sigma_v = \sqrt{(\sigma_v^T)^2 + (\sigma_v^C)^2} \quad (2)$$

Two approaches to measure and analyze the temporal changes in ice flow of the studied glacier are evaluated (~~see also and the differences are discussed in the supplement~~ Section S1 ~~in the supplement~~).

First approach: An across glacier profile is defined (red lines in Fig. 1) close to the terminus of each glacier-basin, considering the maximum retreat state of the ice front position in the observation period. The changes in the ice flow of each the individual glaciers are analyzed by measuring the surface velocities along the profiles. In order to reduce the number of data gaps along the profile due to pixel size data voids in the velocity fields, the velocity data is extracted within a buffer zone of 200 m around the profiles. The results are visually inspected in order to remove unreliable measurements, based on the magnitude and direction of ice flow along the profiles. Datasets with partial profile coverage, ~~or~~ large data gaps or large scale tracking errors are rejected. ~~The changes in the ice flow of each glacier are analyzed by measuring the surface velocities along the profiles. In order to reduce the number of data gaps along the profile due to pixel size data voids in the velocity fields, the velocity data is extracted within a buffer zone of 200 m around the profiles.~~ The resulting average coverage by velocity measurements along the profiles is 97% and 90% of all extracted profiles have ~~got~~ a data coverage of more than 93%. To minimize the impact of potential outliers (still remaining tracking errors), median velocities along the profiles are calculated and their temporal developments are plotted for each basin (Fig. S1-S74 in the supplement).

Second approach: The velocity values are picked at the location of the maximum ice thickness at the across glacier profiles (taken from the firstst approach). Ice thickness is obtained from the ice thickness reconstruction of the AP by Huss and Farinotti (2014). By means of visual inspection of the velocity profiles obtained by the firstst approach, outliers in the measurements using the secondnd approach are manually filtered out and the resulting evolutions of the flow speed of each glacier are plotted (Fig. S75-S148 in the supplement).

The glaciers are manually classified in six categories according to the temporal evolution of the ice flow speeds (see Table 3), since automatic classification attempts did not achieve satisfying results-sueeed. Only glaciers with three or more observations and an observation period of more than 10 years are considered in the categorization, resulting in 74 categorized glacier basins (colored polygons in Fig. 1b). ~~There is a minimum of seven velocity measurements per categorized basin and the shortest observation period is 14.83 years (see Table S1; average number of velocity measurements per glacier is 30.5 and average observation period is 19.25 years).~~ The GAMMA Remote Sensing software is used for processing of the SAR data.

3.3 Catchment geometries and settings

Glacier velocities and area change measurements provide information on the ice dynamics of the individual glaciers. To facilitate a better and comprehensive interpretation of these observations, additional attributes regarding the different geometries and settings of the glaciers are derived. In addition to glacier attributes derived by Huber et al. (2017), we calculated the Hypsometric Index and the ratio of the flux gate cross section divided by the glacier catchment area.

Mass input strongly affects the dynamics of a glacier. The climatic mass balance at the northern AP shows a strong spatial variability, with very high accumulation rates along the west coast (3769 mm we a⁻¹ ~~on~~ average in sector “West”, 1992-2014, RACMO2.3), significantly lower values on the east coast (1119 mm we a⁻¹ ~~in~~ average in sector “East”, 1992-2014, RACMO2.3) and an increase towards higher altitudes along both coast lines (Turner, 2002; ~~V~~van Wessem et al. 2016).

5 Consequently, the mass input depends on the basin orientation (east coast or west coast), elevation range and the hypsometry. For each glacier basin a Hypsometric Index (*HI*), defined by Jiskoot et al. (2009), is calculated by means of surface elevations from the AP-DEM. Based on this index the glaciers are grouped into the five categories according to Jiskoot et al. (2009), ranging from very top-heavy to very bottom heavy (Table 4). Moreover, the maximum elevations of the individual glacier catchments are derived from the AP-DEM, which represents the altitude range of the catchment, since all
10 observed glaciers are marine terminating.

In order to characterize the catchment shape, the ratios (*FA*) of the flux gate cross sections divided by the glacier catchment areas are calculated. The flux gates are defined along the profiles used for the glacier flow analysis (Section 3.2). Lower values of *FA* indicate a channelized outflow (narrowing towards the glacier front), whereas higher *FA* ratios imply a broadening of the glacier towards the calving front. Ice thickness at the flux gates is taken from the AP Bedmap dataset from
15 Huss and Farinotti (2014).

3.4 Cluster analysis

The glaciers in the sector “West” (Fig. 1, red shaded area) show a heterogeneous spatial pattern of ice dynamics as compared to the other sectors changes (Section 4.1, 4.2). In order to analyze the influence of the glacier geometries on the glaciological changes and to find similarities, a cluster analysis is carried out in sector “West”. This is a proven method to classify glaciers
20 based on a set of variables (Lai and Huang, 1989; Sagredo and Lowell, 2012). Variables of the glacier dynamics used are the derived area changes (in percent) and velocity changes (ratings of the categories, Table 3). Glaciers categorized as “stable” showed a temporal variability in flow speeds of less than 0.25 m d⁻¹. Therefore, we used the same rating for the velocity change categories “stable” and “fluctuating” to perform the cluster analysis. The glacier geometry parameters used are the Hypsometric Indexes *HI*, maximum surface elevation h_{max} of the basin and the flux gate to catchment size ratio *FA*. The
25 variables are standardized in the traditional way of calculating their standard scores (also known as z-scores or normal scores). It is done by subtracting the variables mean value and dividing by its standard deviation (Miligan and Cooper, 1988). Afterwards a dissimilarity matrix is calculated using the Euclidean distances between the observations (Deza and Deza, 2009). A hierarchical cluster analysis (Kaufman and Rousseeuw, 1990) is applied on the dissimilarities using Ward's minimum variance method (Ward, 1963). At the start, the most similar glaciers (samples) are grouped. The resulting clusters
30 are iteratively joined based on their similarities until only one cluster is left, resulting in a dendrogram (see Section 4.4). The

distances between the clusters are updated in each iteration step by applying the Lance-Williams algorithms (Lance and Williams, 1967).

4 Results

4.1 Area changes

5 Area changes relative to the measurements in the epoch 1985-1989 (1995-2000 for the former Larsen A and Prince Gustav
Ice Shelf tributaries, see Section 5.2) of the observed glaciers are plotted in Fig. S1-S74 (supplement). The glaciers are
classified in three groups based on the latest area change measurements, which are illustrated in Fig. 2: retreat (Fig. 2a, b, c,
f) – loss of glacier area by frontal retreat; stable (Fig. 2e) – no significant area changes (within the error bars); advance (Fig.
2d) – gain of glacier area by frontal advance. In Fig. 3 the spatial distribution of the area change classification is illustrated.
10 All glaciers along the east coast, including the former ice shelf tributaries, retreated, whereas along the west coast, numerous
glaciers show stable ice front positions and some glaciers even advanced. In total, 238.81 km² of glacier area was lost in the
survey area in the period 1985-2015, which corresponds to a relative loss of 2.2%. All sectors show glacier area loss (Table
5), of which the area loss by 5.7% (208.59 km²) at sector “East-Ice-Shelves” clearly dominates. The glaciers in sector
“West” and “East” recessed by 0.2% (9.14 km²) and 1.4% (21.07 km²), respectively. The temporal trends of total glacier area
15 and area loss of all observed glaciers and of each sector are presented in Fig. 4. Catchment areas and changes between 1985
and 2015 of the individual basins are listed in Table S1 (supplement) and relative changes are illustrated in Fig. 5.

4.2 Surface velocities

A total of 282 stacked and filtered velocity fields are derived from the SAR acquisitions covering the period from 25th
December, 1992 until 16th December, 2014. Figure S157-S160 (supplement) show exemplary velocity fields of the studied
20 area obtained for ERS, Envisat, ALOS and TSX/TDX data. The average total uncertainty of the velocity fields amounts to
 $0.08 \pm 0.07 \text{ m d}^{-1}$ and the values for each SAR sensor are provided in Table 2. In Table S3 (supplement) the error estimates
of each velocity field are listed. The mean sample count to estimate the coregistration quality is 11717 and the average
mismatch amounts to 0.07 m d^{-1} . The error caused by the tracking algorithm strongly varies depending on the source of the
SAR data (sensor). A mean value of 0.05 m d^{-1} is found. ERS image pairs with time intervals of one day have very large
25 estimated tracking uncertainties, biased by the very short temporal baselines. Therefore, only the errors caused by the
mismatch of the coregistration are considered in the total error computations of the seven ERS tracking results with one day
temporal baselines.

All measured velocity profiles of the 74 observed glaciers are visually inspected and in total 2256 [profile measurements](#)
([first1st](#) approach) and 2736 [point measurements](#) ([second2nd](#) approach) [datasets](#) passed the quality check ([on average -31 per](#)

Formatiert: Hochgestellt

Formatiert: Hochgestellt

glacier). The shortest observation period is 14.83 years at DBC31 Glacier, the average number of velocity measurements per glacier is 30.5 and 37.0 and the average observation period is 19.25 years ($\sigma = 2.06$ years) and 19.21 years ($\sigma = 1.96$ years) for the first^{4th} and second^{2nd} measuring approach, respectively). Figure 2 shows by example the temporal evolution of the ice flow (using the first^{4th} approach) for each velocity change category (see Table 3) and Fig. S149-S156 (supplement) show surface velocity profiles across the terminus for the same glaciers as well as for the small glacier catchments DGC14 and TPE61. For small and narrow glaciers, the capturing of the flow velocity gradients in the margins is still limited mainly by the sensor resolution, even applying different tracking window sizes (see Section 3.2).

Formatiert: Hochgestellt

Formatiert: Hervorheben

The temporal evolution of the surface velocities at the termini of each glacier are depicted plotted in the supplement (-Fig. S1-S74 for the first^{4th} approach, Fig. S75-148 for the second^{2nd} approach) (supplement) and the related categories are listed in Table S1 and S2 (supplement).

Formatiert: Hochgestellt

Formatiert: Hochgestellt

For both velocity measuring approaches and each glacier, the flow velocities in the first v_S and last year v_E of the observation period as well as the absolute and relative change Δv is presented in Table S1 and S2 (supplement). The mean values of v_S , v_E and Δv of all analyzed glaciers and for each sector are listed in Table 5. On average the ice flow in the whole studied area increased by 0.061 m/d (13%), and 0.071 m/d (7%) for the first^{4th} and second^{2nd} approach respectively, but the average changes of the individual sectors are more pronounced. Along the west coast an average acceleration by 41% (0.177 m/d) and 44% (0.369 m/d) occurred and the former ice shelf tributaries on the east coast accelerated by 26% (0.118 m/d) and 41% (0.312 m/d) for both approaches respectively. In the sector "East" the glaciers decelerated resulting in a mean velocity change of -58% (-0.423 m/d) and -69% (-1.272 m/d) for the first^{4th} and second^{2nd} approach respectively. The presented average flow speed change values are based on the observed changes of all glaciers in the respective sector (Table S1), ignoring the different size of the individual glaciers. The shortest observation period is 14.83 years at DBC31 Glacier, the longest observation period is 21.99 years at TPE31 and Sjögren glaciers and on average velocity changes are analyzed over a period of 19.25 years ($\sigma = 2.06$ years).

Formatiert: Hochgestellt

Formatiert: Hochgestellt

Formatiert: Hochgestellt

Formatiert: Hochgestellt

Detailed results and differences of both approaches to measure the glacier velocities are presented and discussed in the supplement Section S1. Based on this discussion, we decided to favor the first^{4th} approach and its results are used for the subsequent analysis.

The spatial distribution of the categories is illustrated in Fig. 3. At nearly all glaciers in sector "East-Ice-Shelf" a peak in ice velocities is observed. In the sector "East", most glaciers showed a decrease in flow velocities in the observation period. The glaciers on the west coast show a more irregular distribution than along the east coast, but a local clustering of accelerating glaciers can be observed at Wilhelmina Bay. In order to analyze the quality of obtained velocity change signal, the ratio of the maximum measured velocity difference (maximum velocity minus minimum velocity) divided by the average error of the velocity measurements is calculated for each glacier. An average signal to noise ratio of 14.6 is found. At three glaciers

(DGC14, DGC22 and Orel) a signal to noise ratio of less than 2 is observed. These glaciers are characterized as “stable”, which justifies the low signal to noise ratio.

For each glacier the flow velocities in the first v_{1s} and last year v_{1e} of the observation period as well as the absolute and relative change Δv is presented in Table S1 (supplement). The mean values of v_{1s} , v_{1e} and Δv of all analyzed glaciers and for each sector are listed in Table 5. On average the ice flow in the whole studied area increased by 0.061 m/d (13%), but the average changes of the individual sectors are more pronounced. Along the west coast an average acceleration by 41% (0.177 m/d) occurred and the former ice shelf tributaries on the east coast accelerated by 26% (0.118 m/d). In the sector “East” the glaciers decelerated resulting in a mean velocity change of -58% (-0.423 m/d). The presented average flow speed change values are based on the observed changes of all glaciers in the respective sector (Table S1), ignoring the different size of the individual glaciers. The shortest observation period is 14.83 years at DBC31 Glacier, the longest observation period is 21.09 years at TPE31 and Sjögren glaciers and on average velocity changes are analyzed over a period of 19.25 years ($\sigma = 2.06$ years).

4.3 Catchment geometries and settings

The spatial distribution of Hypsometric Indexes and categories of the glacier basins is presented in Fig. 3 and the values are listed in Table S1 (supplement). The HI values range between -4.6 and 9.1 (mean: 0.88, σ : 2.10). No clear spatial distribution pattern can be identified, reflecting the heterogeneous topography of the AP. The maximum elevation of the catchments and the FA factors are also listed in Table S1 (supplement).

4.4 Cluster analysis

The resulting dendrogram of the hierarchical cluster analysis is plotted in Fig. 6. Four groups are distinguished. The boxplots of each input variable are generated based on this grouping and are shown in Fig. 7. The characteristics of the groups are discussed in Section 5.3.

5 Discussion

Most of the observed glaciers (62%) retreated and only 8% advanced in the study period. These findings are comparable to the results of Cook et al. (2005, 2014, 2016). Only glaciers along the west coast showed stable or advancing calving fronts and all glaciers on the east coast receded since 1985. This heterogeneous area change pattern was also observed by Davies et al. (2012) on western Trinity Peninsula. Most significant retreat occurred in the sector “East-Ice-Shelf”. In the period 1985-1995, the Larsen Inlet tributaries (APPE-glaciers) lost 45.0 km² of ice. After the disintegration of Prince Gustav and Larsen A Ice Shelf, the tributaries rapidly retreated in the period 1995-2005. The recession slowed down in the latest observation interval (2005-2010). This trend is comparable to detailed observations by Seehaus et al. (2015, 2016) at individual glaciers

(DBE glaciers and Sjøgren-Inlet glaciers). At sector “East” the highest area-loss is found in the earliest observation interval (1985-1990). Davies et al. (2012) also reported higher retreat rates for most of the glaciers in this sector in the period 1988-2001 than in the period 2001-2009. ~~Moreover~~However, another slightly-increased significant recession is also found ~~in the time-period (1995-2005, Fig. 4)~~ at sector “East” after 1995 (Fig. 4). Davies et al. (2012) and Hulbe et al. (2004) supposed that the disintegration of a nearby ice shelf affects the local climate. The air temperatures would rise due to the presence of more ice free water in summers. Thus, This might explain the slightly the higher retreat rates at sector “East” after 1995 could be indirectly caused by the disintegration of Prince Gustav and Larsen A Ice Shelf in Sector “East-Ice-Shelf”. At Base Marambio, ~100 km east of this sector, approximately 2°C higher mean annual air temperatures were recorded in the period 1996-2005 as compared to the period 1986-1995 (Oliva et al., 2017). Unfortunately, no temperature data recorded within sector “East” is available covering this period that could be used to validate this hypothesis.

The average changes of flow velocities at each sector also vary strongly (Table 5) in the observation period 1992-2014. On the west coast an increase of 41% is found, whereas in sector “East” the glaciers slowed down by approximately 58% and at the ice shelf tributaries the ice flow increased on average by 26%. Pritchard and Vaughan (2007) reported an increase in mean flow rate of 7.8% in frame 4923 (the central and much of the northern part of sector “West”) and 15.2% in frame 4941 (the southern part of sector “West”) for the period 1992-2005 (frame numbers correspond to European Space Agency convention for identifying ERS coverage). This spatial trend corresponds to our observations, since most of the glaciers which accelerated are located at the southern end of sector “West”. However, for the same observation period we derived a mean increase in flow velocity by 18.9 % in sector “West”, which is an approximately 1.6 times higher acceleration. Pritchard and Vaughan (2007) estimated the mean velocity change by measuring the flow speed at profiles along the flow direction of the glacier, whereas we measured the velocity across glacier profiles at the terminus. If a tidewater glacier speeds up due to the destabilization of its front, the highest acceleration is found at the terminus (see Seehaus et al., 2015, Fig. 3). Consequently, the different profile locations explain the deviations between both studies.

In the following section the observed changes in the individual sectors are discussed in more detail.

5.1 East

The glaciers north of the former Prince Gustav Ice Shelf show a general deceleration. Eyrie, Russell East, TPE130, TPE31, TPE32, TPE34, and “2731” glaciers experienced a rapid decrease and, except “2731” Glacier, a subsequent stabilization or even gentle acceleration of flow velocities (Fig. S2, S6, S7 and S9-S12). A significant retreat followed by a stabilization or slight re-advance of the calving front position is also observed at these glaciers. According to Benn and Evans (1998), a small retreat of a glacier with an overdeepening behind its grounding line (i.e. where the bed slopes away from the ice front) can result in a rapid recession into the deepening fjord. The increased calving and retreat of the ice front cause stronger up-glacier driving stress, higher flow speed as well as glacier thinning and steepening (Meier and Post, 1987; Veen, 2002). The

glacier front stabilizes when the grounding line reaches shallower bathymetry and ice flow also starts to slowdown. A delay between the front stabilization and slowdown can be caused by thinning and steepening of the glacier. Additionally, the accelerated ice flow can surpass the retreat rates and cause short-term glacier advances in the period of high flow speeds (e.g. Eyrie, Russel East, TPE130 and TPE32 glaciers, Fig. S6, S7, S9 and S11) (Meier and Post, 1987). This process can be initiated by climatic forcing (Benn and Evans, 1998). Significant higher surface air temperature at the north-eastern AP and a cooling trend in the 21st century was reported by Oliva et al. (2017) and Turner et al. (2016) (see Section 1). Hence, we assume that the initial recessions of the glaciers in sector “East” were forced by the warming observed by Oliva et al. (2017) and Skvarca et al. (1998) since the 1970s. Therefore, this initial frontal destabilization and retreat led to high flow speeds at the beginning of our ice dynamics time series (earliest velocity measurements from 1992) and the subsequently observed frontal stabilization (after 1985) caused the deceleration of the ice flow. The fjord geometry significantly affects the dynamics of the terminus of a tidewater glacier (Benn and Evans, 1998; ~~v~~Van der Veen, 2002). The tongues of Aitkenhead and “2707” glaciers are split into two branches by nunataks, resulting in rather complex fjord geometries. A retreat from pinning points (e.g. fjord narrowing) causes further rapid recession and higher flow speeds until the ice front reaches a new stable position as observed at “2707” and Aitkenhead Glacier (Fig. S1 and S3). At TPE10 Glacier (Fig. S8 and S82) a “peaked” flow velocity evolution is observed as at Aitkenhead Glacier (Fig. S3 and S77). No nunatak is present at the terminus, but small rock outcrops, indicating a shallow bedrock bump, are identified north of the center of the ice front by visual inspection of optical satellite imagery. Most probably, this shallow bedrock acts as a pinning point and prevents further retreat. The front of Broad Valley Glacier (Fig. S4) is located in a widening fjord. This geometry makes the glacier less vulnerable to frontal changes (Benn and Evans, 1998). Therefore, no significant changes in flow velocities are observed as a consequence of the frontal recession and re-advance.

Diplock and Victory glaciers (Fig. S5 and S13) show a decrease of flow speed during retreat (1995-2010) followed by an acceleration combined with frontal advance (2010-2015). Surge-type glaciers (tidewater as well as land terminating), found for example in Alaska (tidewater) (Motyka and Truffer, 2007; Walker and Zenone, 1988) or Karakoram (land-terminating) (Rankl et al., 2014) in various regions worldwide, show similar behavior (Meier and Post, 1969; Sevestre and Benn, 2015). They are characterized by episodically rapid down-wasting, resulting in a frontal acceleration and strong advance. Regarding tidewater glaciers the advance can be strongly compensated by increased calving rates in deepwater in front of the glacier. It is therefore possible that these glaciers may have experienced a surge cycle in our observation period; however, a longer time series analysis is necessary to prove this hypothesis.

5.2 East-Ice-Shelf

In the sector “East-Ice-Shelf” the tributary glaciers in the Larsen A embayment (“2558”, Arron Icefall, DBE, Drygalski, LAB2, LAB32, TPE61 and TPE62; Fig. S14, S17, S19-S22, S25 and S26) and Sjögren-Inlet (Boydell, Sjögren and TPE114;

Fig. S18, S23 and S24) lost the downstream Larsen A and Prince Gustav Ice Shelf in 1995. Nearly all glaciers showed a rapid and significant acceleration after ice shelf break up and a subsequent slow down. A gentle peak in flow speeds is obtained at LAB32 and TPE114 glaciers. They are classified as “stable”, since the variations are below the threshold of 0.25 m d^{-1} , according to the categorization in Table 3. Dramatic speed up with subsequent deceleration of former ice shelf tributaries was reported by various authors; e.g. in this sector by Seehaus et al., (2015, 2016) at DBE and Sjögren-Inlet glaciers and further south at Larsen B embayment by Rott et al. (2011) and Wuite et al. (2015). The velocities reported by Rott et al. (2014) at Sjögren, Pyke, Edgeworth and Drygalski glaciers are generally higher than our findings. The authors measured the velocities at locations near the center of the glacier fronts, where the ice flow velocities are typically highest, whereas we measured the median velocities at cross profiles close to the glacier fronts (Seehaus et al. 2015). The different approaches result in different absolute values (see also Section S1 in the supplement), but comparable temporal developments in glacier flow speeds are observed by both author groups. For example Rott et al. (2015, ~~2017~~) presented surface velocity measured along a central flow line of Drygalski Glacier. Figure S149 shows our surface velocity measurements across the terminus of Drygalski Glacier and Fig S94 velocity measurements at the maximum ice thickness across the terminus profile. Both studies show comparable values (e.g. in 1995: this study $\sim 2.7 \text{ m/d}$, Rott et al. (2015) $\sim 2.8 \text{ m/d}$; in 2009: this study $\sim 5.5 \text{ m/d}$, Rott et al. (2015) $\sim 6.0 \text{ m/d}$) at the terminus.

Highest peak values of 6.3 m d^{-1} are found at TPE61 Glacier in November 1995 and January 1996. Most glaciers (Arron Icefall, Drygalski, LAB2, TPE61, TPE62) strongly decelerated after the initial acceleration and show almost constant flow speeds in recent years, indicating that the glaciers adjusted to the new boundary conditions, albeit significant higher flow speeds ([compared to pre-ice-shelf-collapse conditions](#)) can be observed at the central sections of the terminus (see Section S1 and Fig. S149 in the supplement). At “2558”, Boydell, DBE and Sjögren glaciers the deceleration is ongoing and Boydell and DBE glaciers still show increased flow speeds at the glacier fronts. We suppose that these tributary glaciers show a prolonged response to ice shelf disintegration, caused by local settings (e.g. bedrock topography or fjord geometry), and are still adjusting to the new boundary conditions, as suggested by Seehaus et al. (2015, 2016).

In the 1980s, Prince Gustav Ice Shelf gradually retreated (see Fig. 1) and “2668” Glacier (Fig. S15) has not been buttressed by the ice shelf since the early 1990s. A deceleration is found in the period 2005-2010. Hence, this glacier may also have experienced a speed up in the early 1990s due to the recession of Prince Gustav Ice Shelf in the 1980s. However, the earliest velocity measurement at “2668” Glacier is only available from February 1996.

The ice shelf in Larsen Inlet disintegrated in 1987-1988 and earliest velocity measurements are obtained in 1993. As for “2668” Glacier no sufficient cloud free coverage by Landsat imagery is available which facilitates the computation of surface velocities for the 1980s. The ice flow speeds at APPE glaciers (Fig. S16) are nearly stable with short term variations in the order of $0.2\text{-}0.5 \text{ m d}^{-1}$ between 1993 and 2014. Rott et al.; (2014) also found nearly constant flow velocities at Pyke

Glacier (part of the APPE basin, Table 1). The authors suggest that the ice flow of APPE glaciers was not strongly disturbed by the ice shelf removal due to the steep glacier surfaces and shallow seabed topography at the glacier fronts (Pudsey et al., 2001).

5.3 West

5 The glacier geometries differ strongly along the west coast. In the southern part of sector “West” the shoreline is more ragged and islands are near the coast. An impact of the islands on the climatic conditions at the AP mainland’s coastline (e.g. orographic barrier) is not obvious (visual inspection of RACMO2.3 5.5 km grid cell model results (Van Wessem et al., 2016)). However, the climatic conditions on the AP show strong spatial and temporal variability (see Section 1.2 and 3.3). These factors cause the heterogeneous spatial pattern of area and flow speed changes in sector “West” as compared to the
10 eastern sectors.

Kunz et al. (2012) observed thinning at the glacier termini along the western AP, by analyzing airborne and spaceborne stereo imagery in the period 1947-2010. Two of the twelve studied glaciers are located within our study area; Leonardo Glacier (1968-2010) and Rozier Glacier (1968-2010). An acceleration and terminus retreat can be caused by frontal thinning as shown by Benn et al. (2007). However, Benn et al. (2007) also point out that changes in ice thickness do not necessarily
15 affect the ice flow and that calving front positions and ice dynamics are strongly dependent on the fjord and glacier geometries, derived from modeling results which have higher uncertainties especially for smaller basins.

The large number of glaciers in this sector is analyzed by means of a hierarchical cluster analysis (Section 3.4) and assorted into four groups based on the resulting dendrogram (Fig. 6). Boxplots of the individual input variables of each group are shown in Fig. 7. The correlation between the observed ice dynamics and the glacier geometries of each group are discussed
20 in the following sections (see also Fig. 7).

Group 1 (14 glaciers):

Most glaciers experienced acceleration in the period 1992-2014. The majority of the glacier basins are “very top-heavy” or “top-heavy” (median $HI = -1.8$), stretching from sea level up to 1892 m on average. The b_{etim} increases toward higher altitudes (Van Wessem et al., 2016) and highest values are found in the zone between 1000 and 1700 m a.s.l. Consequently
25 these glaciers receive high mass input in their large high altitude accumulation areas. The accumulation is known to have significantly increased on the AP by 20% since 1850 (Thomas et al., 2008). Pritchard and Vaughan (2007) reported that only a small fraction of the acceleration can be attributed to glacier thickening due to increased mass input. Up-glacier thickening combined with frontal thinning (reported by Kunz et al., 2012) leads to a steepening of the glacier and an increase in driving stress, resulting in faster ice flow (Meier and Post, 1987) as observed in this study. Moreover, a thinning of the terminus
30 reduces the effective basal stress of a tidewater glacier and facilitates faster ice flow (Pritchard and Vaughan, 2007). The flux

gate cross sections to catchment size ratios are relatively small, indicating narrowing catchments towards the ice front. The channelized increased ice flow almost compensates for the increased calving rates (due to frontal thinning), resulting in an average recession of the glaciers by only 0.2% in the period 1985-2015. The high flow speeds may outweigh the calving and lead to ice-front advances as measured at Krebs and TPE46 Glacier. The glacier termini of this group are typically located in narrow fjords (Fig. 5) and are clustered in Charcot, Charlotte and Andvord Bay.

Group 2 (19 glaciers)

Glaciers of group 2 are spread all over sector “West”, with a local clustering in Wilhelmina Bay. Group 2 shows similar h_{max} and FA characteristics to group 1. Area changes are also quite small (-0.1%). Most of the glaciers experienced acceleration or show a “peaked” evolution of the flow velocities. In contrast to group 1 the catchments are in general “bottom-heavy” and some are even “very bottom-heavy”. We assume that the constraints are similar to group 1 (increasing b_{clim} , frontal thinning and steepening). However, the additional mass accumulation in the upper areas is smaller due to the “bottom-heavy” glacier geometries. Consequently, the imbalance due to the frontal thinning and up-glacier mass gain is less pronounced as in group 1 and numerous glaciers (“peak” type) started to decelerate after the speed-up, indicating that these glaciers are adjusting to the new boundary conditions.

Group 3 (13 glaciers)

These basins typically show a “bottom-heavy” hypsometry and smaller elevation ranges (in average up to 1103 m a.s.l.). Thus, b_{clim} is relatively low. The smaller mean ice thickness at the termini (161 m, compared to 211 m of all glaciers) of group 3 implies less interaction with the ocean, leading to a small average frontal retreat of ~0.1%. The low frontal ablation does not significantly affect the ice flow, probably due to the flat glacier topography and the low mass input. Consequently, the flow speed is in general stable or even slightly decreases in the observation period. Glaciers of group 3 usually face the open ocean, and do not terminate in narrow fjords (especially in the northern part, Trinity Peninsula).

Group 4 (3 glaciers)

All basins in this group have a “very bottom-heavy” hypsometry and an elevation range comparable to group 3 glaciers. The FA factors are in general higher than in group 3, implying that outflow of the catchments is less channelized and the glacier fronts are long compared to the catchment sizes. Therefore, the largest relative area changes, in average -5.1%, are found at glaciers in group 4. However, the absolute frontal retreat is small and does not significantly affect the glacier flow. Note: Group 4 consists of only three samples, limiting the significance.

6 Conclusions

Our analysis expands on previous work (Pritchard and Vaughan, 2007) on ice dynamic changes along the west coast of AP between TPE8 and Bagshawe-Grubb Glacier, both in regard to temporal coverage and analysis methods. It also spatially extends previous work on changes in ice dynamics along the east coast between Eyrie Bay and the Seal Nunataks. The spatially and temporally detailed analysis of changes in ice flow speeds (1992-2014) and ice front positions (1985-2015) reveal varying temporal evolution in glacier dynamics along the northern AP. The results are in general in line with findings of the previous studies; however along the west coast a more accelerated higher overall glacier flow is determined and on the eastern side temporal evolution of ice dynamics of 21 glaciers is observed for the first time. A large variety of temporal variations in glacier dynamics were observed in our studied area and attributed to different forcing and boundary conditions.

On the east side all glacier fronts retreated in the study period (relative to 1985, relative to 1995 for former Larsen-A and Prince Gustav Ice Shelf tributaries, see also Section 5.2), with highest retreat rates observed at former tributaries of the Prince Gustav, Larsen Inlet and Larsen A ice shelves. Moreover, nearly all the glaciers affected by ice shelf disintegration showed similar temporal evolutions of ice velocities. The glaciers reacted with a strong acceleration to ice shelf break up followed by a deceleration, indicating that the glaciers adjusted or are still adjusting to the new boundary conditions. Glaciers on the east coast north of the former Prince Gustav Ice Shelf showed in general a significant deceleration and a reduction in frontal ablation. Based on the observed warming trend since the 1960s and the subsequent cooling since the mid-2000s in the northern AP, we suggesteoneclude that the initial recession and speed up of the glaciers took place before the start of our observation and that the glaciers are now close to a new equilibrium.

The average flow speed of the glaciers along the west coast of the Antarctic Peninsula significantly increased in the observation period but the total frontal change is negligible. No general evolution in ice dynamics of the glaciers at the west coast is obvious. However, correlations between the changes in ice dynamics and the glacier geometries of the individual catchments are obtained by applying a hierarchical cluster analysis. Thus, the geometry of the individual glacier basin strongly affects the reaction of the glacier to external forcing.

We conclude that for regions with such a strong spatial variation in topographic and climatic parameters as the AP, it is impossible to derive a regional trend in glacier change by simply analyzing individual glaciers in this region. Therefore further detailed observation of the glaciological changes along the AP is needed. Upcoming sensor probably-hopefully facilitate the region wide measurement of recent surface elevation, since current estimates have got only partial coverage or have got some issues due to the complex topography of the AP. Moreover, future activities should link remote sensing derived ice dynamics and glacier extent with ocean parameters and ocean models, as well as regional climate models and ice dynamic models, in order to provide a better quantification of mass changes and physical processes leading to the observed changes.

Author contributions. T.S. designed the study, processed the SAR data, performed the data analysis and led the writing of the manuscript, in which he received support from all authors. A.C. and A.S. compiled and provided glacier front position data sets. M.B. initiated the project and coordinated the research.

5 *Competing interests.* The authors declare no competing financial interests.

Acknowledgements. This work was supported by the Deutsche Forschungsgemeinschaft (DFG) in the framework of the priority programme "Antarctic Research with comparative investigations in Arctic ice areas" by a grant to M.B. (BR 2105/9-1). MB and TS would like to thank the HGF Alliance "Remote Sensing of Earth System Dynamics" (HA-310) and Marie-Curie-Network International Research Staff Exchange Scheme IMCONet (EU FP7-PEOPLE-2012-IRSES) for additional support. Access to satellite data was kindly provided by various space agencies, e.g. under ESA AO 4032, DLR TerraSAR-X Background Mission Antarctic Peninsula & Ice Shelves, TSX AO LAN0013, TanDEM-X Mission TDX AO XTI_GLAC0264, ASF, GLIMS as well as NASA and USGS.

10

References

- Barrand, N.E., Hindmarsh, R.C.A., Arthern, R.J., Williams, C.R., Mougnot, J., Scheuchl, B., Rignot, E., Ligtenberg, S.R.M., Van Den Broeke, M.R., Edwards, T.L., Cook, A.J., Simonsen, S.B., 2013a. Computing the volume response of the Antarctic Peninsula ice sheet to warming scenarios to 2200. *J. Glaciol.* 59, 397–409. doi:10.3189/2013JoG12J139
- Barrand, N.E., Vaughan, D.G., Steiner, N., Tedesco, M., Kuipers Munneke, P., van den Broeke, M.R., Hosking, J.S., 2013b. Trends in Antarctic Peninsula surface melting conditions from observations and regional climate modeling. *J. Geophys. Res. Earth Surf.* 118, 315–330. doi:10.1029/2012JF002559
- Benn, D.I., Evans, D.J.A., 1998. *Glaciers & Glaciation*. Arnold.
- Benn, D.I., Hulton, N.R.J., Mottram, R.H., 2007. “Calving laws”, “sliding laws” and the stability of tidewater glaciers. *Ann. Glaciol.* 46, 123–130. doi:10.3189/172756407782871161
- Braun, M., Humbert, A., 2009. Recent Retreat of Wilkins Ice Shelf Reveals New Insights in Ice Shelf Breakup Mechanisms. *IEEE Geosci. Remote Sens. Lett.* 6, 263–267. <https://doi.org/10.1109/LGRS.2008.2011925>
- Berthier, E., Scambos, T.A., Shuman, C.A., 2012. Mass loss of Larsen B tributary glaciers (Antarctic Peninsula) unabated since 2002. *Geophys. Res. Lett.* 39, L13501. doi:10.1029/2012GL051755
- Burgess, E.W., Forster, R.R., Larsen, C.F., Braun, M., 2012. Surge dynamics on Bering Glacier, Alaska, in 2008–2011. *The Cryosphere* 6, 1251–1262. doi:10.5194/tc-6-1251-2012
- Cape, M.R., Vernet, M., Skvarca, P., Marinsek, S., Scambos, T., Domack, E., 2015. Foehn winds link climate-driven warming to ice shelf evolution in Antarctica. *J. Geophys. Res. Atmospheres* 2015JD023465. Doi: 10.1002/2015JD023465
- Cook, A.J., Vaughan, D.G., 2010. Overview of areal changes of the ice shelves on the Antarctic Peninsula over the past 50 years. *The Cryosphere* 4, 77–98. <https://doi.org/10.5194/tc-4-77-2010>
- Cook, A.J., Vaughan, D. g., Luckman, A. j., Murray, T., 2014. A new Antarctic Peninsula glacier basin inventory and observed area changes since the 1940s. *Antarct. Sci.* 26, 614–624. doi:10.1017/S0954102014000200
- Cook, A.J., Fox, A.J., Vaughan, D.G., Ferrigno, J.G., 2005. Retreating Glacier Fronts on the Antarctic Peninsula over the Past Half-Century. *Science* 308, 541–544. doi:10.1126/science.1104235

- Cook, A.J., Holland, P.R., Meredith, M.P., Murray, T., Luckman, A., Vaughan, D.G., 2016. Ocean forcing of glacier retreat in the western Antarctic Peninsula. *Science* 353, 283–286. doi:10.1126/science.aae0017
- Cook, A.J., Murray, T., Luckman, A., Vaughan, D.G., Barrand, N.E., 2012. A new 100-m Digital Elevation Model of the Antarctic Peninsula derived from ASTER Global DEM: methods and accuracy assessment. *Earth Syst. Sci. Data* 4, 129–142. doi:10.5194/essd-4-129-2012
- Cook, A.J., Vaughan, D.G., 2010. Overview of areal changes of the ice shelves on the Antarctic Peninsula over the past 50 years. *The Cryosphere* 4, 77–98. doi:10.5194/tc-4-77-2010
- Davies, B.J., Carrivick, J.L., Glasser, N.F., Hambrey, M.J., Smellie, J.L., 2012. Variable glacier response to atmospheric warming, northern Antarctic Peninsula, 1988–2009. *The Cryosphere* 6, 1031–1048. doi:10.5194/tc-6-1031-2012
- De Angelis, H., Skvarca, P., 2003. Glacier Surge After Ice Shelf Collapse. *Science* 299, 1560–1562. doi:10.1126/science.1077987
- de Lange, R., Luckman, A., Murray, T., 2007. Improvement of Satellite Radar Feature Tracking for Ice Velocity Derivation by Spatial Frequency Filtering. *IEEE Trans. Geosci. Remote Sens.* 45, 2309–2318. doi:10.1109/TGRS.2007.896615
- Dee, D.P., Uppala, S.M., Simmons, A.J., Berrisford, P., Poli, P., Kobayashi, S., Andrae, U., Balmaseda, M.A., Balsamo, G., Bauer, P., Bechtold, P., Beljaars, A.C.M., van de Berg, L., Bidlot, J., Bormann, N., Delsol, C., Dragani, R., Fuentes, M., Geer, A.J., Haimberger, L., Healy, S.B., Hersbach, H., Hólm, E.V., Isaksen, I., Kållberg, P., Köhler, M., Matricardi, M., McNally, A.P., Monge-Sanz, B.M., Morcrette, J.-J., Park, B.-K., Peubey, C., de Rosnay, P., Tavolato, C., Thépaut, J.-N., Vitart, F., 2011. The ERA-Interim reanalysis: configuration and performance of the data assimilation system. *Q. J. R. Meteorol. Soc.* 137, 553–597. doi:10.1002/qj.828
- Deza, E., Deza, M.M., 2009. *Encyclopedia of Distances*. Springer Berlin Heidelberg, Berlin, Heidelberg.
- Doake, C.S.M., Vaughan, D.G., 1991. Rapid disintegration of the Wordie Ice Shelf in response to atmospheric warming. *Nature* 350, 328–330. <https://doi.org/10.1038/350328a0>
- Ferrigno, J.G., Cook, A.J., Foley, K.M., Williams, R.S., Swithinbank, C., Fox, A.J., Thomson, J.W., Sievers, J., 2006. Coastal-change and glaciological map of the Trinity Peninsula area and South Shetland Islands, Antarctica, 1843–2001.
- Fretwell, P., Pritchard, H.D., Vaughan, D.G., Bamber, J.L., Barrand, N.E., Bell, R., Bianchi, C., Bingham, R.G., Blankenship, D.D., Casassa, G., Catania, G., Callens, D., Conway, H., Cook, A.J., Corr, H.F.J., Damaske, D.,

- Damm, V., Ferraccioli, F., Forsberg, R., Fujita, S., Gim, Y., Gogineni, P., Griggs, J.A., Hindmarsh, R.C.A., Holmlund, P., Holt, J.W., Jacobel, R.W., Jenkins, A., Jokat, W., Jordan, T., King, E.C., Kohler, J., Krabill, W., Riger-Kusk, M., Langlely, K.A., Leitchenkov, G., Leuschen, C., Luyendyk, B.P., Matsuoka, K., Mouginot, J., Nitsche, F.O., Nogi, Y., Nost, O.A., Popov, S.V., Rignot, E., Rippin, D.M., Rivera, A., Roberts, J., Ross, N., Siegert, M.J., Smith, A.M., Steinhage, D., Studinger, M., Sun, B., Tinto, B.K., Welch, B.C., Wilson, D., Young, D.A., Xiangbin, C., Zirizzotti, A., 2013. Bedmap2: improved ice bed, surface and thickness datasets for Antarctica. *The Cryosphere* 7, 375–393. doi:10.5194/tc-7-375-2013
- Goodwin, B.P., 2013. Recent Environmental Changes on the Antarctic Peninsula as Recorded in an ice core from the Bruce Plateau. The Ohio State University.
- Holland, P.R., Brisbourne, A., Corr, H.F.J., McGrath, D., Purdon, K., Paden, J., Fricker, H.A., Paolo, F.S., Fleming, A.H., 2015. Oceanic and atmospheric forcing of Larsen C Ice-Shelf thinning. *The Cryosphere* 9, 1005–1024. doi:10.5194/tc-9-1005-2015
- Huber, J., Cook, A.J., Paul, F., Zemp, M., 2017. A complete glacier inventory of the Antarctic Peninsula based on Landsat 7 images from 2000 to 2002 and other preexisting data sets. *Earth Syst. Sci. Data* 9, 115–131. doi:10.5194/essd-9-115-2017
- Hulbe, C.L., MacAyeal, D.R., Denton, G.H., Kleman, J., Lowell, T.V., 2004. Catastrophic ice shelf breakup as the source of Heinrich event icebergs. *Paleoceanography* 19, PA1004. doi:10.1029/2003PA000890
- Huss, M., Farinotti, D., 2014. A high-resolution bedrock map for the Antarctic Peninsula. *The Cryosphere* 8, 1261–1273. doi:10.5194/tc-8-1261-2014
- Jiskoot, H., Curran, C.J., Tessler, D.L., Shenton, L.R., 2009. Changes in Clemenceau Icefield and Chaba Group glaciers, Canada, related to hypsometry, tributary detachment, length–slope and area–aspect relations. *Ann. Glaciol.* 50, 133–143. doi:10.3189/172756410790595796
- Kaufman, L., Rousseeuw, P.J., 1990. Finding groups in data: an introduction to cluster analysis, Wiley series in probability and mathematical statistics. Wiley, New York.
- Kunz, M., King, M.A., Mills, J.P., Miller, P.E., Fox, A.J., Vaughan, D.G., Marsh, S.H., 2012. Multi-decadal glacier surface lowering in the Antarctic Peninsula. *Geophys. Res. Lett.* 39, L19502. doi:10.1029/2012GL052823
- Lance, G.N., Williams, W.T., 1967. A general theory of classificatory sorting strategies: II. Clustering systems. *Comput. J.* 10, 271–277. doi:10.1093/comjnl/10.3.271

~~Lai, Z.M., Huang, M.H., 1989. A numerical classification of glaciers in China by means of glaciological indices at the equilibrium line. Snow Cover Glacier Var. Proc. Baltim. Symp.~~

~~Lai, Z., & Huang, M. 1989. Numerical Classification of Glaciers in China by Means of Glaciological Indices at the Equilibrium Line. In Snow Cover and Glacier Variations. Proceedings of a Symposium held in Baltimore, Maryland May 10-19, 1989, IAHS Publication 183, 103-111~~

Marshall, G.J., Orr, A., van Lipzig, N.P.M., King, J.C., 2006. The Impact of a Changing Southern Hemisphere Annular Mode on Antarctic Peninsula Summer Temperatures. *J. Clim.* 19, 5388–5404. doi:10.1175/JCLI3844.1

McNabb, R.W., Hock, R., O’Neel, S., Rasmussen, L.A., Ahn, Y., Braun, M., Conway, H., Herreid, S., Joughin, I., Pfeffer, W.T., Smith, B.E., Truffer, M., 2012. Using surface velocities to calculate ice thickness and bed topography: a case study at Columbia Glacier, Alaska, USA. *J. Glaciol.* 58, 1151–1164. doi:10.3189/2012JoG11J249

~~Meier, M.F., Post, A., 1969. What are glacier surges? *Can. J. Earth Sci.* 6, 807–817. <https://doi.org/10.1139/e69-081>~~

Formatiert: Englisch (Vereinigte Staaten)

~~Meier, M.F., Post, A., 1987. Fast tidewater glaciers. *J. Geophys. Res. Solid Earth* 92, 9051–9058. doi:10.1029/JB092iB09p09051~~

Formatiert: Deutsch (Deutschland)

Meredith, M.P., King, J.C., 2005. Rapid climate change in the ocean west of the Antarctic Peninsula during the second half of the 20th century. *Geophys. Res. Lett.* 32, L19604. doi:10.1029/2005GL024042

Milligan, G.W., Cooper, M.C., 1988. A study of standardization of variables in cluster analysis. *J. Classif.* 5, 181–204. doi:10.1007/BF01897163

~~Motyka, R.J., Truffer, M., 2007. Hubbard Glacier, Alaska: 2002 closure and outburst of Russell Fjord and postflood conditions at Gilbert Point. *J. Geophys. Res. Earth Surf.* 112, F02004. doi:10.1029/2006JF000475~~

Oliva, M., Navarro, F., Hrbáček, F., Hernández, A., Nývlt, D., Pereira, P., Ruiz-Fernández, J., Trigo, R., 2017. Recent regional climate cooling on the Antarctic Peninsula and associated impacts on the cryosphere. *Sci. Total Environ.* 580, 210–223. doi:10.1016/j.scitotenv.2016.12.030

Potocki, M., Mayewski, P.A., Kurbatov, A., Handley, M., Simoes, J.C., Jaña, R., 2011. Detailed Glaciochemical Records from a Northern Antarctic Peninsula Site - Detroit Plateau. *AGU Fall Meet. Abstr.* 43.

Pritchard, H.D., Vaughan, D.G., 2007. Widespread acceleration of tidewater glaciers on the Antarctic Peninsula. *J. Geophys. Res.* 112. doi:10.1029/2006JF000597

- Pudsey, C.J., Evans, J., Domack, E.W., Morris, P., Valle, R.A.D., 2001. Bathymetry and acoustic facies beneath the former Larsen-A and Prince Gustav ice shelves, north-west Weddell Sea. *Antarct. Sci.* 13, 312–322. doi:10.1017/S095410200100044X
- Rack, W., Rott, H., 2003. Further retreat of the northern Larsen Ice Shelf and collapse of Larsen B, in: 16th International Workshop of the Forum for Research on Ice Shelf Processes (FRISP), June 25.
- Rack, W., Rott, H., Nagler, T., Skvarca, P., 1998. Areal Changes and Motion of Northern Larsen Ice Shelf, Antarctic Peninsula, in: *Geoscience and Remote Sensing Symposium Proceedings, 1998. IGARSS'98. 1998 IEEE International. IEEE*, pp. 2243–2245.
- Rack, W., Rott, H., 2004. Pattern of retreat and disintegration of the Larsen B ice shelf, Antarctic Peninsula. *Ann. Glaciol.* 39, 505–510.
- ~~Rankl, M., Kienholz, C., Braun, M., 2014. Glacier changes in the Karakoram region mapped by multiresolution satellite imagery. *The Cryosphere* 8, 977–989. doi:10.5194/tc-8-977-2014~~
- Rau, F., Braun, M., 2002. The regional distribution of the dry-snow zone on the Antarctic Peninsula north of 70°S. *Ann. Glaciol.* 34, 95–100. doi:10.3189/172756402781817914
- Rignot, E., Casassa, G., Gogineni, P., Krabill, W., Rivera, A., Thomas, R., 2004. Accelerated ice discharge from the Antarctic Peninsula following the collapse of Larsen B ice shelf. *Geophys. Res. Lett.* 31. doi:10.1029/2004GL020697
- ~~Rott, H., Abdel Jaber, W., Wuite, J., Scheiblauer, S., Floricioiu, D., van Wessem, J.M., Nagler, T., Miranda, N., van den Broeke, M.R., 2017. Changing pattern of ice flow and mass balance for glaciers discharging into the Larsen A and B embayments, Antarctic Peninsula, 2011 to 2016. *Cryosphere Discuss* 2017, 1–34. <https://doi.org/10.5194/tc-2017-259>~~
- Rott, H., Floricioiu, D., Wuite, J., Scheiblauer, S., Nagler, T., Kern, M., 2014. Mass changes of outlet glaciers along the Nordenskjöld Coast, northern Antarctic Peninsula, based on TanDEM-X satellite measurements. *Geophys. Res. Lett.* 2014GL061613. doi:10.1002/2014GL061613
- Rott, H., Müller, F., Nagler, T., Floricioiu, D., 2011. The imbalance of glaciers after disintegration of Larsen-B ice shelf, Antarctic Peninsula. *The Cryosphere* 5, 125–134. doi:10.5194/tc-5-125-2011

- Rott, H., Skvarca, P., Nagler, T., 1996. Rapid Collapse of Northern Larsen Ice Shelf, Antarctica. *Science* 271, 788–792. <https://doi.org/10.1126/science.271.5250.788>
- Rott, H., Wuite, J., Floricioiu, D., Nagler, T., Scheiblauer, S., 2015. Synergy of TanDEM-X DEM differencing and input-output method for glacier monitoring, in: 2015 IEEE International Geoscience and Remote Sensing Symposium (IGARSS). Presented at the 2015 IEEE International Geoscience and Remote Sensing Symposium (IGARSS), pp. 5216–5219. doi:10.1109/IGARSS.2015.7327010
- Sagredo, E.A., Lowell, T.V., 2012. Climatology of Andean glaciers: A framework to understand glacier response to climate change. *Glob. Planet. Change* 101–109.
- Scambos, T., Hulbe, C., Fahnestock, M., 2003. Climate-Induced Ice Shelf Disintegration in the Antarctic Peninsula, in: Domack, E., Levente, A., Burnet, A., Bindschadler, R., Convey, P., Kirby, P., Thew (Eds.), *Antarctic Peninsula Climate Variability: Historical and Paleoenvironmental Perspectives*. American Geophysical Union, pp. 79–92.
- Scambos, T.A., Berthier, E., Haran, T., Shuman, C.A., Cook, A.J., Ligtenberg, S.R.M., Bohlander, J., 2014. Detailed ice loss pattern in the northern Antarctic Peninsula: widespread decline driven by ice front retreats. *The Cryosphere* 8, 2135–2145. doi:10.5194/tc-8-2135-2014
- Scambos, T.A., Bohlander, J., Shuman, C.A., Skvarca, P., 2004. Glacier acceleration and thinning after ice shelf collapse in the Larsen B embayment, Antarctica. *Geophys. Res. Lett.* 31. doi:10.1029/2004GL020670
- Seehaus, T., Marinsek, S., Helm, V., Skvarca, P., Braun, M., 2015. Changes in ice dynamics, elevation and mass discharge of Dinsmoor–Bombardier–Edgeworth glacier system, Antarctic Peninsula. *Earth Planet. Sci. Lett.* 427, 125–135. doi:10.1016/j.epsl.2015.06.047
- Seehaus, T.C., Marinsek, S., Skvarca, P., van Wessem, J.M., Reijmer, C.H., Seco, J.L., Braun, M.H., 2016. Dynamic Response of Sjøgren Inlet Glaciers, Antarctic Peninsula, to Ice Shelf Breakup Derived from Multi-Mission Remote Sensing Time Series. *Front. Earth Sci.* 4. doi:10.3389/feart.2016.00066
- [Sevestre, H., Benn, D.I., 2015. Climatic and geometric controls on the global distribution of surge-type glaciers: implications for a unifying model of surging. *J. Glaciol.* 61, 646–662. <https://doi.org/10.3189/2015JoG14J136>](https://doi.org/10.3189/2015JoG14J136)
- Skvarca, P., Rack, W., Rott, H., Donángelo, T.I., 1999. Climatic trend and the retreat and disintegration of ice shelves on the Antarctic Peninsula: an overview. *Polar Res.* 18, 151–157.

- Skvarca, P., Rack, W., Rott, H., Ibarzábal y Donángelo, T., 1998. Evidence of recent climatic warming on the eastern Antarctic Peninsula. *Ann. Glaciol.* 27, 628–632.
- Skvarca, P., Rott, H., Nagler, T., 1995. Satellite imagery, a base line for glacier variation study on James Ross Island, Antarctica. *Ann. Glaciol.* 21, 291–296.
- Strozzi, T., Luckman, A., Murray, T., Wegmuller, U., Werner, C.L., 2002. Glacier motion estimation using SAR offset-tracking procedures. *IEEE Trans. Geosci. Remote Sens.* 40, 2384–2391. doi:10.1109/TGRS.2002.805079
- Thomas, E.R., Marshall, G.J., McConnell, J.R., 2008. A doubling in snow accumulation in the western Antarctic Peninsula since 1850. *Geophys. Res. Lett.* 35. doi:10.1029/2007GL032529
- Turner, J., 2002. Spatial variability of Antarctic Peninsula net surface mass balance. *J. Geophys. Res.* 107. doi:10.1029/2001JD000755
- Turner, J., Colwell, S.R., Marshall, G.J., Lachlan-Cope, T.A., Carleton, A.M., Jones, P.D., Lagun, V., Reid, P.A., Iagovkina, S., 2005. Antarctic climate change during the last 50 years. *Int. J. Climatol.* 25, 279–294. doi:10.1002/joc.1130
- Turner, J., Lu, H., White, I., King, J.C., Phillips, T., Hosking, J.S., Bracegirdle, T.J., Marshall, G.J., Mulvaney, R., Deb, P., 2016. Absence of 21st century warming on Antarctic Peninsula consistent with natural variability. *Nature* 535, 411–415. doi:10.1038/nature18645
- van Lipzig, N.P.M., King, J.C., Lachlan-Cope, T.A., van den Broeke, M.R., 2004. Precipitation, sublimation, and snow drift in the Antarctic Peninsula region from a regional atmospheric model. *J. Geophys. Res. Atmospheres* 109, D24106. doi:10.1029/2004JD004701
- van Lipzig, N.P.M., Meijgaard, E. van, Oerlemans, J., 2002. The spatial and temporal variability of the surface mass balance in Antarctica: results from a regional atmospheric climate model. *Int. J. Climatol.* 22, 1197–1217. doi:10.1002/joc.798
- van Wessem, J.M., Ligtenberg, S.R.M., Reijmer, C.H., van de Berg, W.J., van den Broeke, M.R., Barrand, N.E., Thomas, E.R., Turner, J., Wuite, J., Scambos, T.A., van Meijgaard, E., 2016. The modelled surface mass balance of the Antarctic Peninsula at 5.5 km horizontal resolution. *The Cryosphere* 10, 271–285. doi:10.5194/tc-10-271-2016
- van der Veen, C.J., 2002. Calving glaciers. *Prog. Phys. Geogr.* 26, 96–122. doi:10.1191/0309133302pp327ra

~~Walker, K.M., Zenone, C., 1988. Multitemporal Landsat multispectral scanner and thematic mapper data of the Hubbard Glacier region, southeast Alaska. *Photogramm. Eng. Remote Sens.* 54, 373–376.~~

- Ward, J.H., 1963. Hierarchical Grouping to Optimize an Objective Function. *J. Am. Stat. Assoc.* 58, 236–244. doi:10.1080/01621459.1963.10500845
- Wendt, J., Rivera, A., Wendt, A., Bown, F., Zamora, R., Casassa, G., Bravo, C., 2010. Recent ice-surface-elevation changes of Fleming Glacier in response to the removal of the Wordie Ice Shelf, Antarctic Peninsula. *Ann. Glaciol.* 51, 97–102.
- Wuite, J., Rott, H., Hetzenecker, M., Floricioiu, D., De Rydt, J., Gudmundsson, G.H., Nagler, T., Kern, M., 2015. Evolution of surface velocities and ice discharge of Larsen B outlet glaciers from 1995 to 2013. *The Cryosphere* 9, 957–969. doi:10.5194/tc-9-957-2015

5

10

Figures

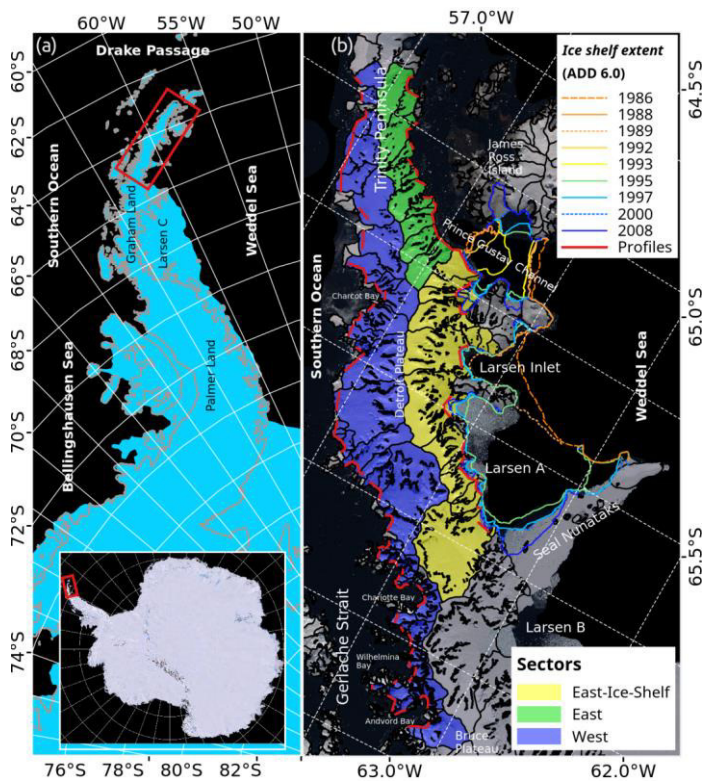


Figure 1. Panels (a) Location of study site on the Antarctic Peninsula and on the Antarctic continent (inset). Panel (b). Separation of study site in 3 sectors and retreat states of Prince Gustav and Larsen A ice shelves. Red lines: profiles at glacier front for velocity measurements. Map base, Landsat LIMA Mosaic USGS, NASA, BAS, NSF, coastlines (ice shelf extent) and catchment delineations from SCAR Antarctic Digital Database 6.0.

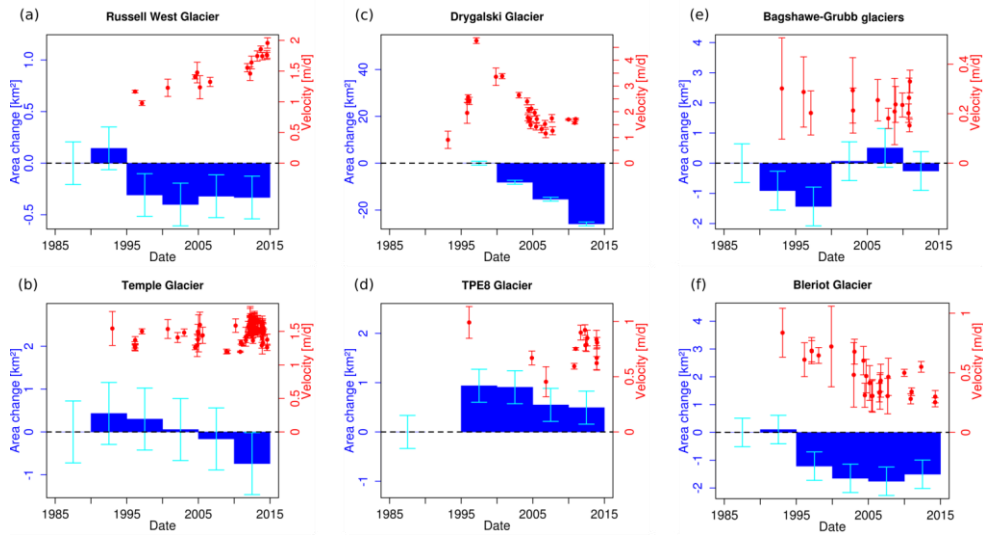


Figure 2. Temporal evolution of surface velocity (red, using 1st measuring approach) and area (blue) changes of selected glaciers in the study area for each velocity change category (see Table 3).

Formatiert: Hochgestellt

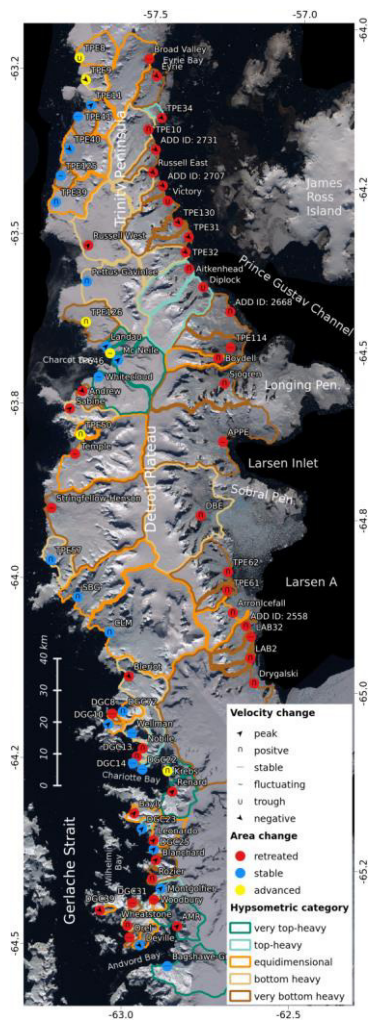


Figure 3. Categorizations of glaciers based on the temporal variations of area changes (dots) and flow velocities (symbols). Colors of catchment delineation indicate Hypsometric categories according to Jiskoot et al. (2009). Background: Landsat LIMA Mosaic USGS, NASA, BAS, NSF

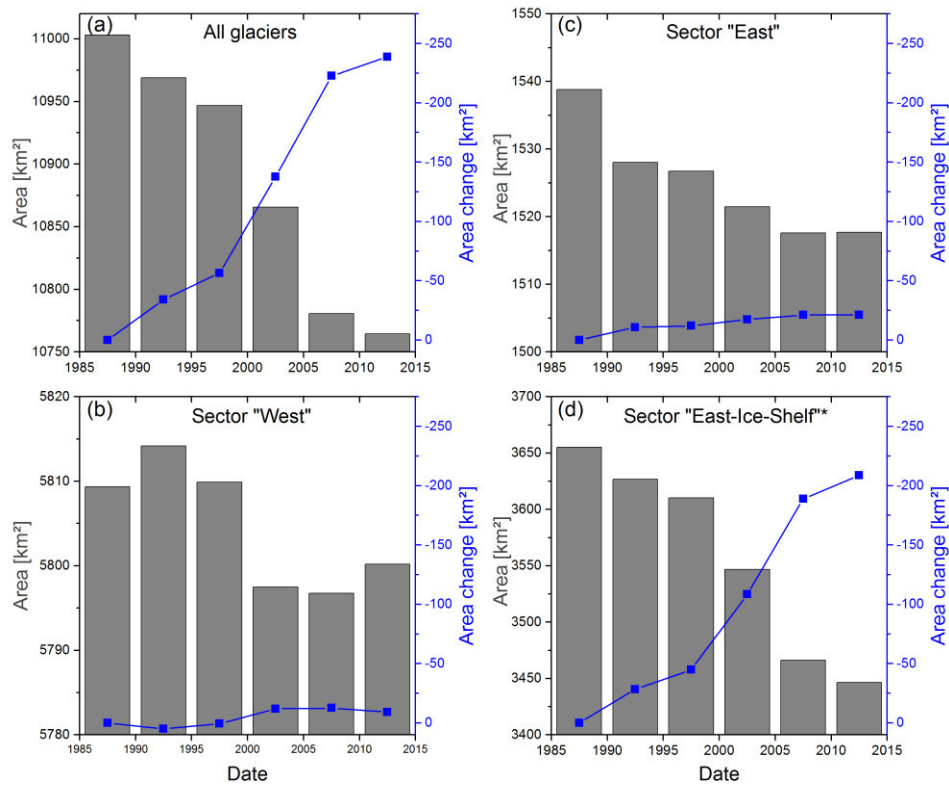


Figure 4. Total glacier area (gray bars) of the whole study site (Panel (a)) and of the individual sectors (Panels (b)-(d)) in the period 1985-2015. Changes in glacier area (blue points) are relative to the measurements in time interval 1985-1990. Note the different scaling of the left y-axes. *In sector "East-Ice-Shelf", area changes before 1995 are only measured at Larsen Inlet tributaries (APPE glaciers).

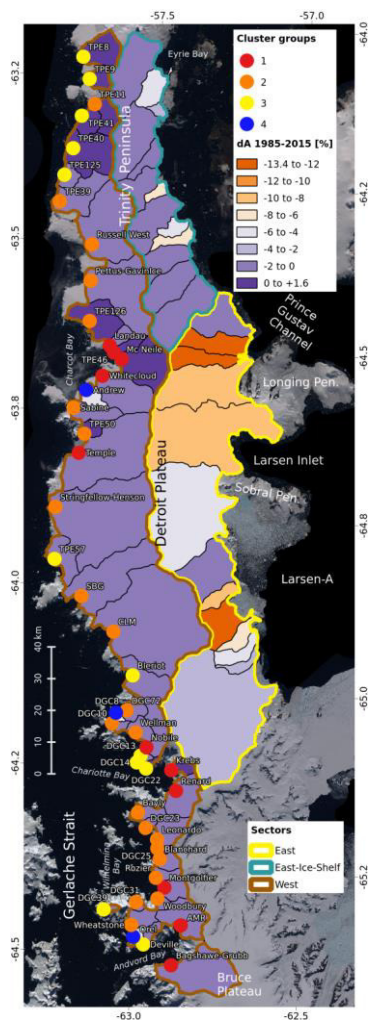


Figure 5. Spatial distribution of glacier types along the west coast. Glaciers are group based on a hierarchical cluster analysis (dots). In Section 5.3 the characteristics of the groups are discussed in detail. Individual glacier catchment colors: relative area change in the period 1985-2015. Colored polygon outlines: Boundaries of the three sectors. Background: Landsat LIMA Mosaic USGS, NASA, BAS, NSF

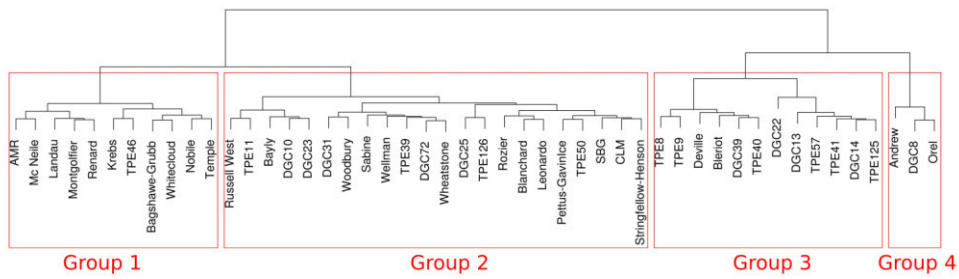


Figure 6. Dendrogram of hierarchical cluster analysis of glaciers in sector "West". The glaciers are assorted in four groups (red rectangles). See also Section 5.3.

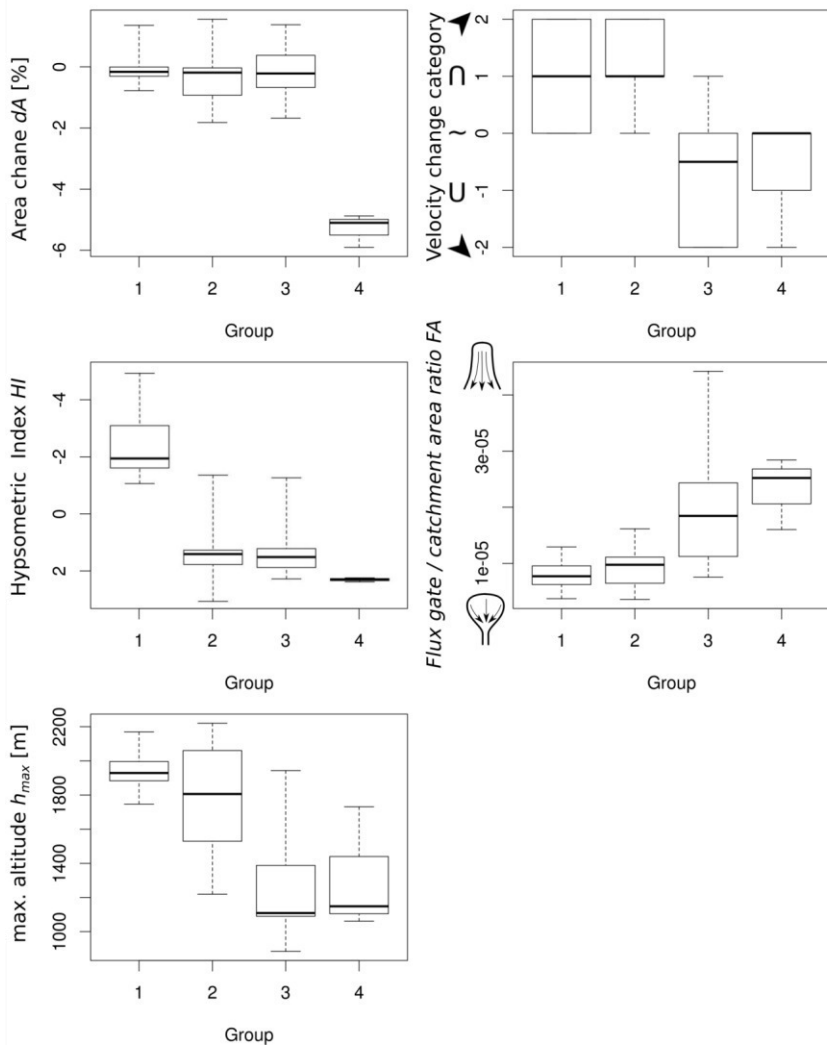


Figure 7. Boxplots of cluster analysis input variables (Sector “West”) for each group. Whiskers extend to the most extreme data points.

Tables

Table 1. Abbreviations of glacier names

Abbreviation	Glacier names
AMR	Arago-Moser-Rudolph
APPE	Albone-Pyke-Polaris-Eliason
CLM	Cayley-Lilienthal-Mouillard
DBE	Dinsmoor-Bombardier-Edgeworth
SBG	Sikorsky-Breguet-Gregory

Table 2. Overview of SAR sensors and specifications used in this study.

Platform	Sensor	Mode	SAR band	Repetition cycle	Time interval	Ground range resolution [m]*	Tracking patch sizes [p x p] ⁺	Tracking step size [p x p] ⁺	Mean uncertainty of tracking results [m/d]
ERS-1/2	SAR	IM	C band	35/1	08. December 1992	30	48x240	5x25	0.15±0.10
					02. April 2010		64x320		
RADARSAT 1	SAR	ST	C band	24	10. September 2000	30	48x192	5x20	0.11±0.03
					03. September 2006		64x256		
Envisat	ASAR	IM	C band	35	05. December 2003	30	32x160	5x25	0.12±0.05
					16. August 2009		64x320		
							128x640		
ALOS	PALSAR	FBS	L band	46	18. May 2006	10	64x192	10x30	0.05±0.06
					17. March 2011		96x192		
							128x384		
TerraSAR-X TanDEM-X	SAR	SM	X band	11	14. October 2008	3	128x128	25x25	0.06±0.04
					22. December 2014		256x256		
							512x512		

* nominal resolution; depending on the incidence angle.

* intensity tracking parameters are provided in pixels [p] in slant range geometry.

Table 3. Description of velocity change categories.

Category	Description	Rating ^a
positive	General increase of flow speed	2
peak	Increase of flow speed with subsequent deceleration	1
stable	Variability of measurements < 0.25 m d ⁻¹	0
fluctuating	Short term speed-ups and deceleration, no clear trend	0
trough	Decrease of flow speed with subsequent acceleration	-1
negative	General decrease of flow speed	-2

^aratings used for cluster analysis Section 3.4

Table 4. Hypsometric Index and glacier basin category descriptions.

Hypsometric Index (<i>HI</i>) [*]	Hypsometric categories	Number of Glaciers
$HI < -1.5$	Very top-heavy	8
$-1.5 < HI < -1.2$	Top-heavy	7
$-1.2 < HI < 1.2$	Equidimensional	18
$1.2 < HI < 1.5$	Bottom-heavy	13
$HI > 1.5$	Very bottom-heavy	28

^{*}according to Jiskoot et al., (2009)

Table 5. Summary of observed parameters for each sector and all glaciers.

	SectorEast	East-Ice-ShelfWest	All glaciers	
N	13	13	48	74
l_f [m]	85114	127909	268763	481786
$A_{1985-1990}$ [km ²]	1538.78	3655.13	5809.33	11003.23
$A_{2010-2015}$ [km ²]	1517.71	3446.54	5800.18	10764.42
dA [km ²]	-21.07	-208.59	-9.14	-238.81
dt [a]	18.22	19.05	19.58	19.25
First^{1st} velocity measuring approach				
v_S [m d ⁻¹]	0.729	0.480	0.428	0.490
v_E [m d ⁻¹]	0.306	0.562	0.605	0.545
dv [m d ⁻¹]	-0.423	0.081	0.177	0.055
n_v	277	550	1429	2256
Second^{2nd} velocity measuring approach				
v_S [m d ⁻¹]	<u>1.834</u>	<u>0.760</u>	<u>0.831</u>	<u>0.994</u>
v_E [m d ⁻¹]	<u>0.562</u>	<u>1.071</u>	<u>1.200</u>	<u>1.065</u>
dv [m d ⁻¹]	<u>-1.272</u>	<u>0.312</u>	<u>0.369</u>	<u>0.071</u>
n_v	<u>355</u>	<u>639</u>	<u>1742</u>	<u>2736</u>

N – number of studied glaciers

l_f – length of ice front

A – glacier area in the respective period (subscript)*

dA – change in glacier area between 1985 and 2015*

Formatierte Tabelle

Formatiert: Links

Formatiert: Hochgestellt

Formatiert: Links

Formatiert: Hochgestellt

Formatiert: Links

dt - mean time period of velocity measurements

vs - mean of earliest velocity measurements (1992-1996)

vE - mean of latest velocity measurements (2010-2014)

dv - mean velocity change

5 n_v - sum of velocity measurements in the observation period (dt)

*since 1995 for the former Larsen-A and Prince Gustav Ice Shelf tributaries (see Section 5.2)

Supplement to

Detailed analysis of changes in glacier dynamics in the northern Antarctic Peninsula since 1985

Thorsten Seehaus¹, Alison Cook², Aline B. Silva³, Matthias Braun¹

¹Institute of Geography, Friedrich-Alexander-University Erlangen-Nuremberg, Wetterkreuz 15, 91058 Erlangen, Germany

²Department of Geography, Durham University, Lower Mountjoy South Road, Durham DH1 3LE, United Kingdom

³Laboratório de Monitoramento da Criosfera, Universidade Federal do Rio Grande, Av. Itália, km 8, 96203-900, Rio Grande – RS, Brazil

Correspondence to: Thorsten Seehaus (thorsten.seehaus@fau.de)

Overview:

Section S1: Velocity change measurements

Figures:

Figure S1-S74: Temporal changes in glacier area and flow speed (~~median values of measurements along the terminus profiles~~) ~~and glacier area~~

Figure S75-S148: Temporal changes in glacier area and flow speed (~~measured at maximum ice thickness at the terminus profiles~~) ~~and glacier area~~

Figure S149-S156: Surface velocity across the terminus and respective median values of Drygalski, TPE61, Bagshawe-Grubb, Bleriot, DGC14, Russell West, Temple and TPE8 glaciers

Figure S157-S160: Velocity fields obtained from ERS, ENVISAT, ALOS PALSAR and TerraSAR/TanDEM-X data

Figure S161: Categorizations of glaciers based on the temporal variations of area changes and flow velocities (~~measured at maximum ice thickness at the terminus profiles~~)

Figure S162: Spatial distribution of glacier types along the west coast ~~(Cluster analysis based on velocity measurements at the maximum ice thickness at the terminus profiles)~~

Figure S163: Boxplots of cluster analysis (~~velocity measurements at the maximum ice thickness at the terminus profiles~~)

Figure S164: Dendrogram of hierarchical cluster analysis ~~(velocity measurements at the maximum ice thickness at the terminus profiles)~~

Tables:

Table S1: Observed parameters of the individual glaciers - median velocity measurements along terminus profiles

Table S2: Observed parameter of the individual glaciers - velocities measured at maximum ice thickness at terminus profiles

Table S3: Uncertainties of intensity tracking results

S1: Velocity change measurements

Two approaches to measure and analyze the temporal changes in flow velocities of the studied glaciers are evaluated. For the first approach, the flow velocities are extracted at across glacier profiles, defined for each basin close to the terminus, considering the maximum frontal retreat state (see Fig. 1 in the manuscript), and the median values along the profiles are then calculated (see also Section 3.2 in the manuscript). For the second approach, the flow velocities are measured at the location of maximum ice thickness at the respective across glacier terminus profile (same as for the first approach). The ice thickness information is taken from the Huss and Farinotti (2014) ice thickness reconstruction dataset of the Antarctic Peninsula. The temporal evolution of the ice velocities of all observed glaciers is plotted in Fig. S1-S74 (for the first approach) and Fig. S75-S148 (for the second approach).

For the first approach, velocity profiles with partial profile coverage (for glaciers located at the border of a velocity field) or large data gaps are sorted out. Data voids usually occur towards the lateral parts of the glacier (e.g. regions affected by SAR shadow, caused by the valley side walls), whereas the maximum ice thickness is usually found towards the center of the terminus. Therefore, some more velocity measurements are obtained using the second approach (2256 measurements for the first approach; 2736 measurements for the second approach; see Table S1 and S2).

The temporal changes in the flow speed of all studied glaciers are categorized according to Table 3 (manuscript) for both approaches (see Table S1 and S2). The same categories are used for 50 glaciers (68%) by both approaches. Taking the first approach as a reference, the largest mismatch (9 glaciers) between both approaches is found for the category “stable”. However, most of these “mismatched” glaciers are categorized as “fluctuating” glaciers, using measurements obtained by the second approach (note: this mismatch does not influence the subsequent cluster analysis since both velocity change categories have the same numerical rating, see manuscript Section 3.4 and Table 3). For both approaches, the same threshold of 0.25 m/d for the temporal variability of the measurements is applied for the category “stable” in order to carry out a comparable analysis. However, the comparison of Fig. S1-S74 and S75-S148 shows that the magnitude of the temporal variability of the flow speed is typically higher for the second approach, since the values obtained using the first approach are smoothed by averaging along the profiles.

Small differences in the mean velocity change rate (dv in %) in the observation period are found for Sector “East” (-58.0% for the first approach, -69% for the second approach) and “West” (+41.3% for the first approach, +44.5% for the second approach). At sector “EastIS”, an average increase in flow speed by +26.5% for the first approach and +41.0% for the second approach is obtained. This divergence can be explained by the different forcing at sector “EastIS”. The glaciers were buttressed by the Larsen-A and Prince Gustav ice shelves until they broke up in 1995. The subsequent acceleration of the glaciers led to changes in the across glacier velocity profiles (see Fig. S149). The highest acceleration is found towards the center of the glacier terminus (where usually the ice thickness is the greatest). Thus, the change in glacier type from ice shelf terminating to tide water glaciers differently affects both velocity measuring methods and leads to the observed deviations. However, a general acceleration is revealed by both approaches.

The impact of the velocity measuring approach on the cluster analysis (Section 3.4, manuscript) is small. The results of the cluster analysis (boxplots, dendrogram and the spatial distribution of the glacier groups) using the first velocity measuring approach are presented in the manuscript and the results using the second velocity measuring approach are shown in Fig. S162-S164. Most of the glaciers, 42 out of 48, are assorted to equal groups. Compared to the grouping based on the first velocity measuring approach, group 2 lost 6 glaciers using the second velocity measuring approach. Two glaciers are attributed to group 1 and four glaciers to group 3. Hence, these glaciers are only assorted to neighboring groups, which have the greatest similarity to the original group.

To sum it up, both velocity measuring approaches reveal comparable results at our study region. The results of both approaches are provided in this supplement to facilitate a better comparison with results from other studies. As discussed above, the shape of the across glacier velocity profiles can change over time and the peak position as well (see Fig. S149-S156). Moreover, the maximum ice thickness does not necessarily overlap with the peak in the velocity profiles, since estimates of the former also have significant uncertainties. These cases can impact on the observed temporal evolution of the flow speed using a fixed position to measure the velocities, as performed by applying the second velocity measuring approach (at maximum ice thickness at the terminus profile) or by other studies using manually defined measuring positions. Therefore, we decided to use the results of the first approach for the detailed analysis and discussion in the manuscript since it takes into account the changes in flow speed across the whole glacier terminus and, in our opinion, this method is more representative for the changes in ice dynamics and ice discharge of a glacier system.

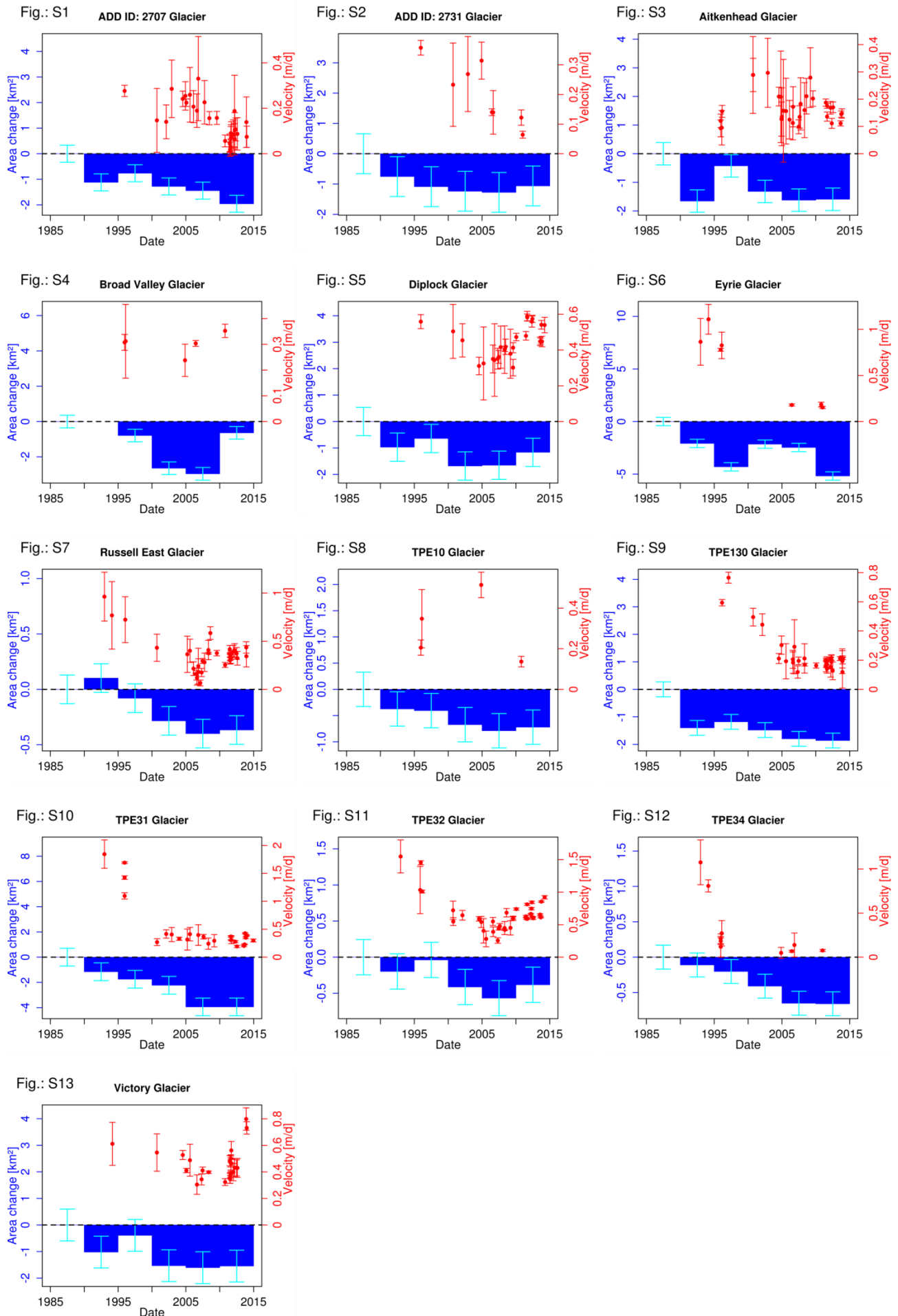


Figure S1-S13. Temporal changes of surface velocity (median values of measurements along terminus profiles) (red) and area (blue) changes of glaciers in sector "East".

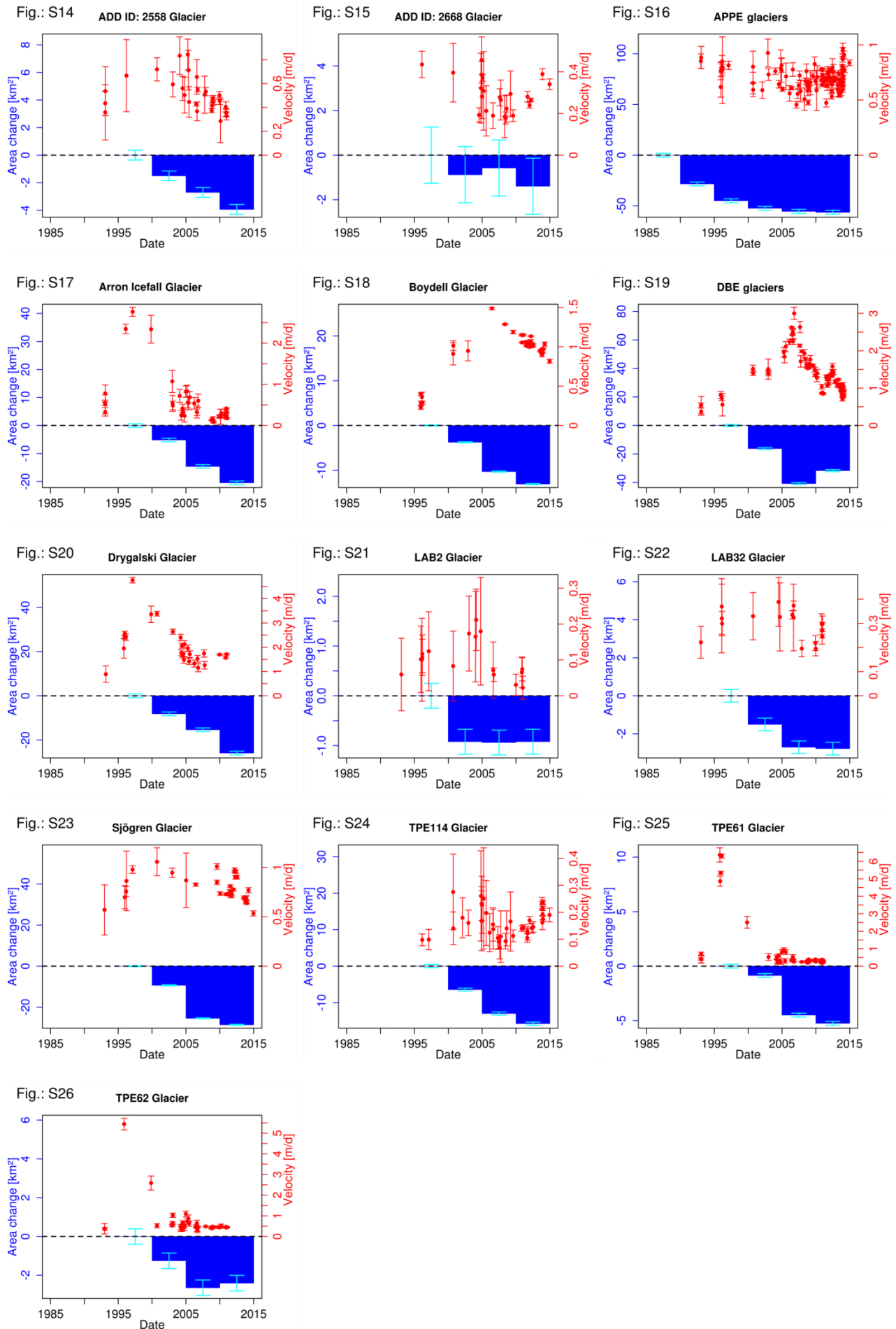


Figure S14-S26. Temporal changes of surface velocity (median values of measurements along terminus profiles) (red) and area (blue) changes of glaciers in sector "East-Ice-Shelf".

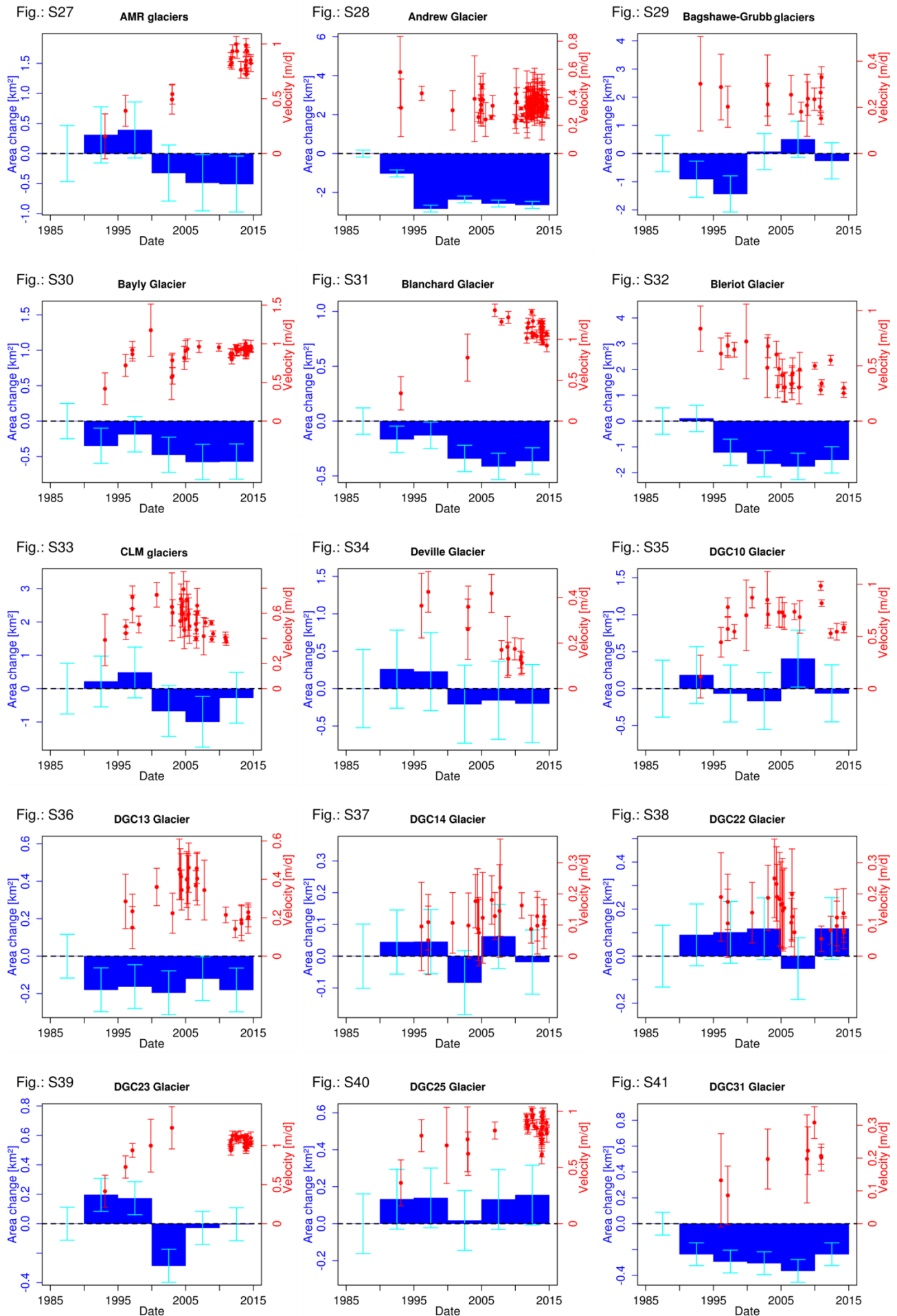


Figure S27-S41. Temporal changes of surface velocity (median values of measurements along terminus profiles) (red) and area (blue) changes of glaciers in sector "West".

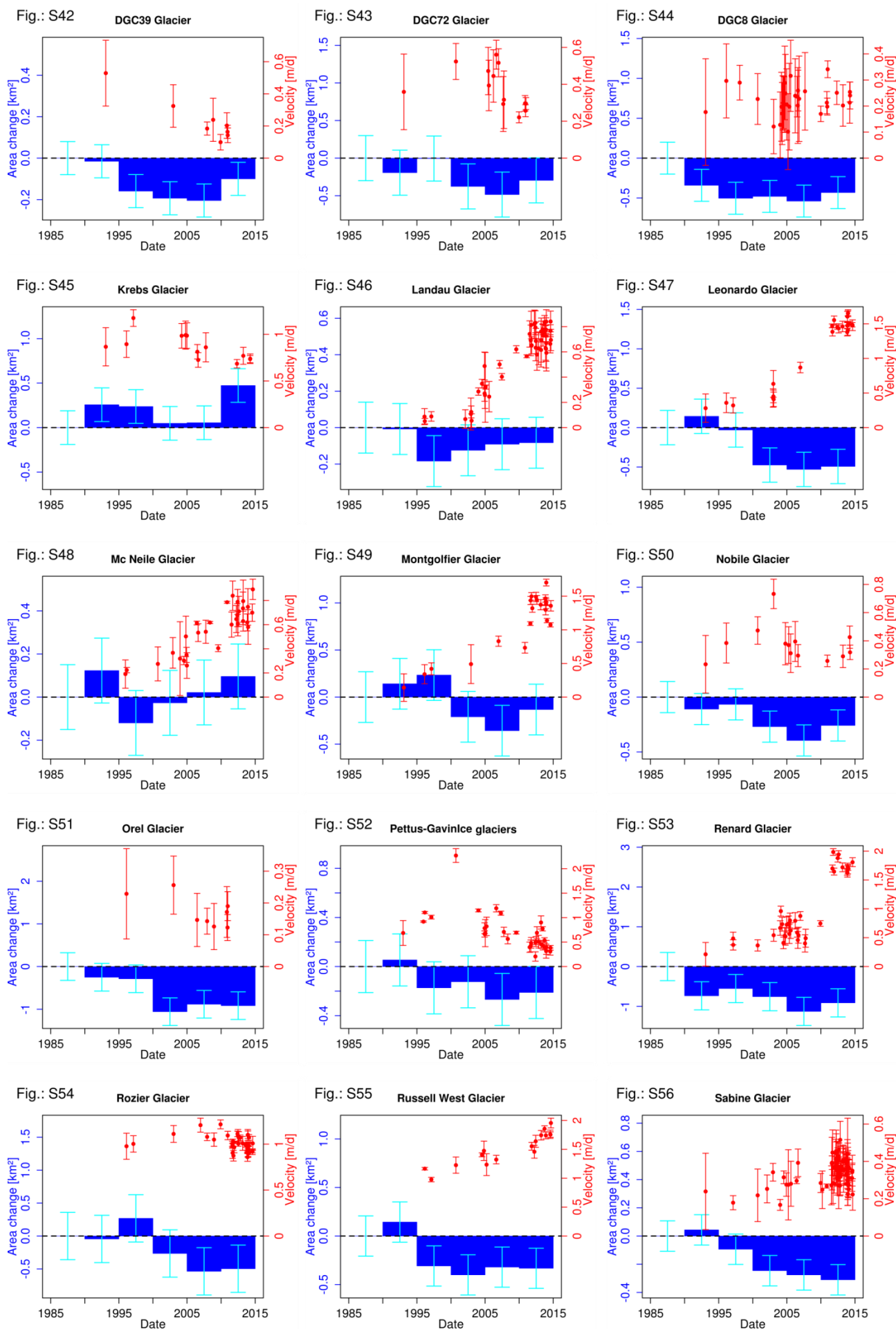


Figure S42-S56. Temporal changes of surface velocity (median values of measurements along terminus profiles) (red) and area (blue) changes of glaciers in sector "West".

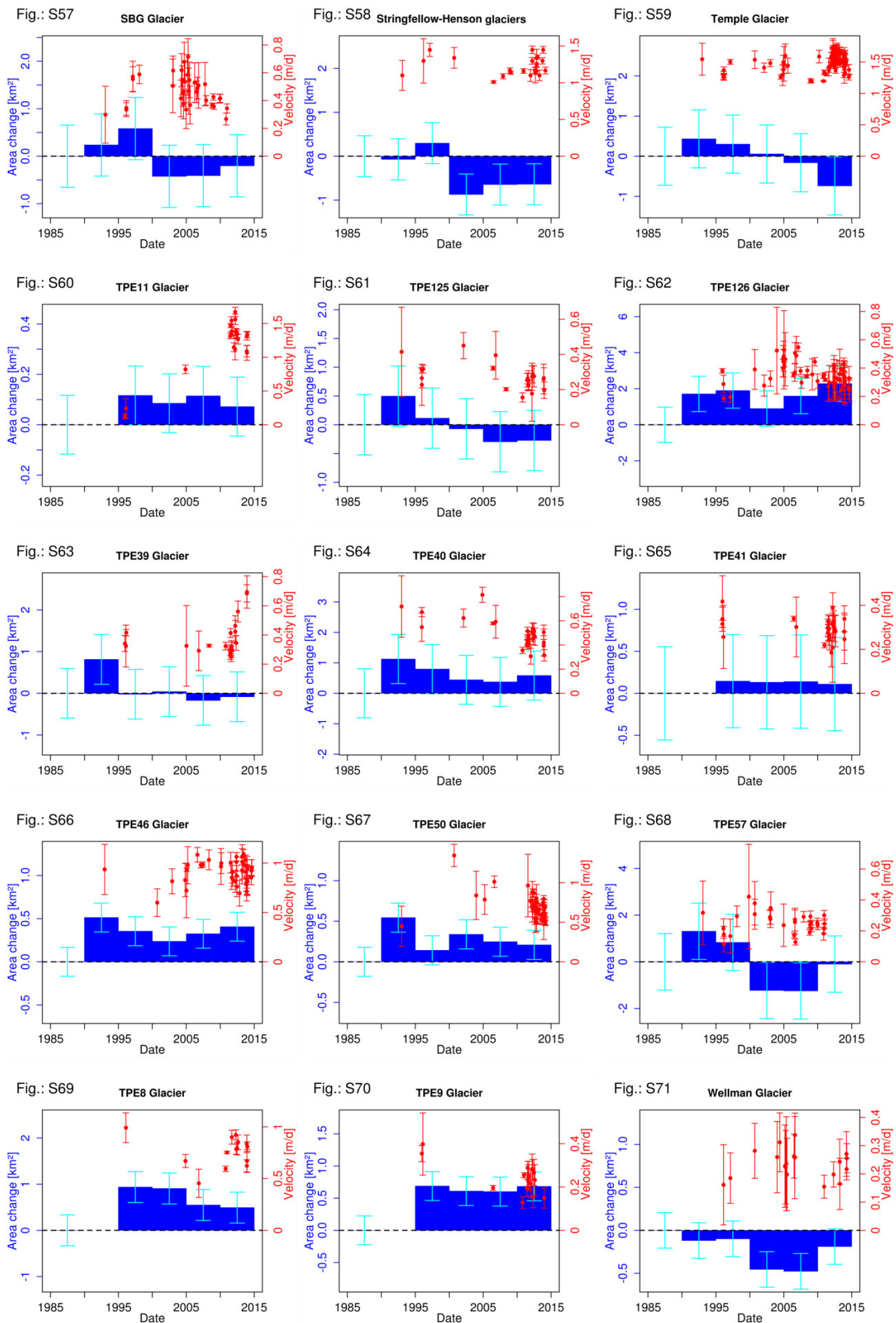


Figure S57-S71. Temporal changes of surface velocity (median values of measurements along terminus profiles) (red) and area (blue) changes of glaciers in sector "West".

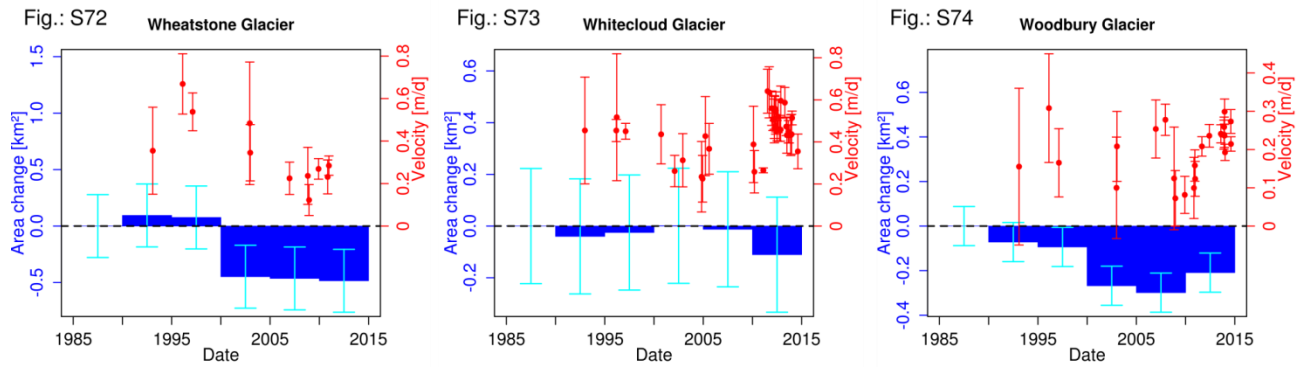


Figure S72-S74. Temporal changes of surface velocity (median values of measurements along terminus profiles) (red) and area (blue) changes of glaciers in sector "West".

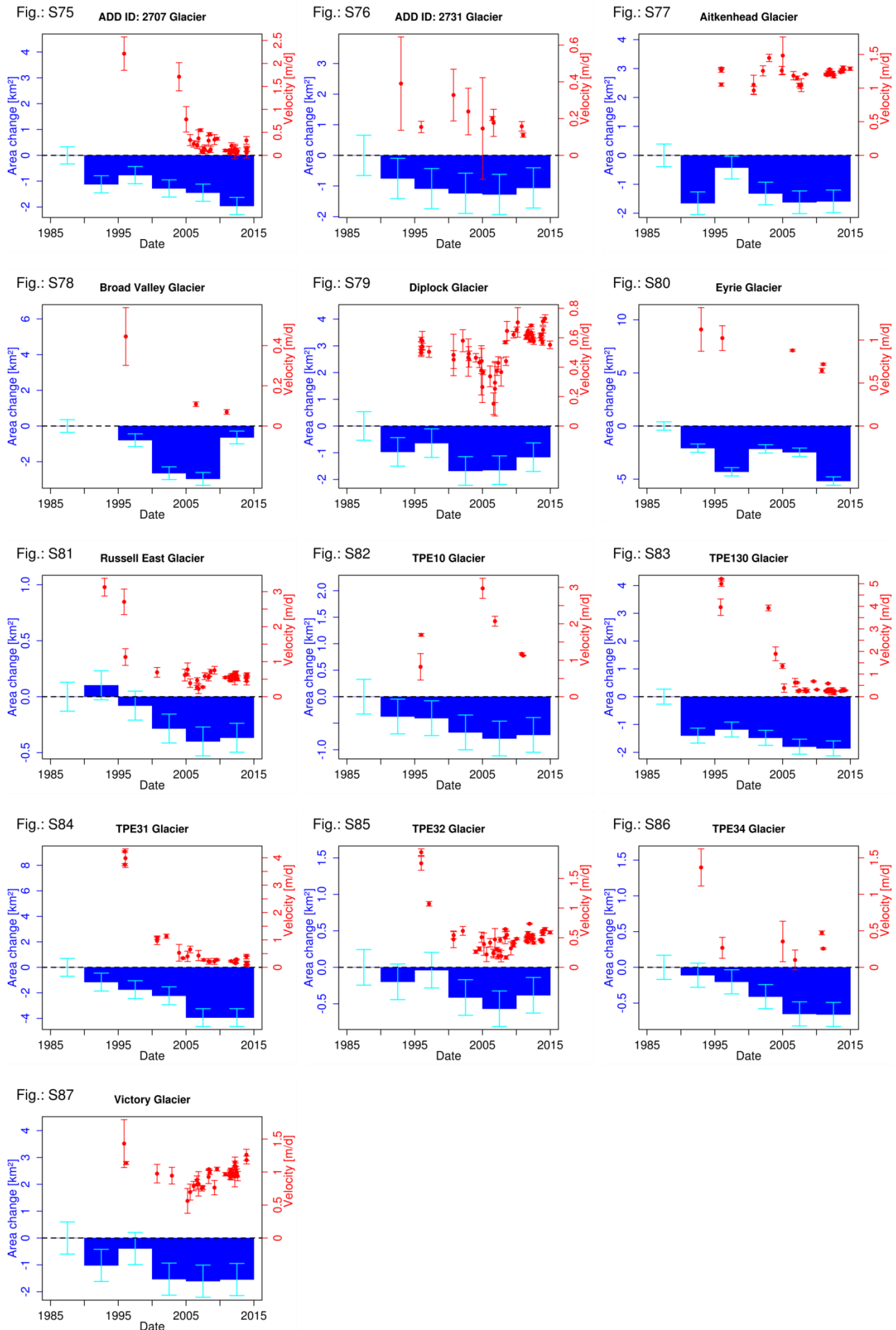


Figure S75-S87. Temporal trend of surface velocity measured at maximum ice thickness at terminus profiles (red) and area (blue) changes of glaciers in sector "East".

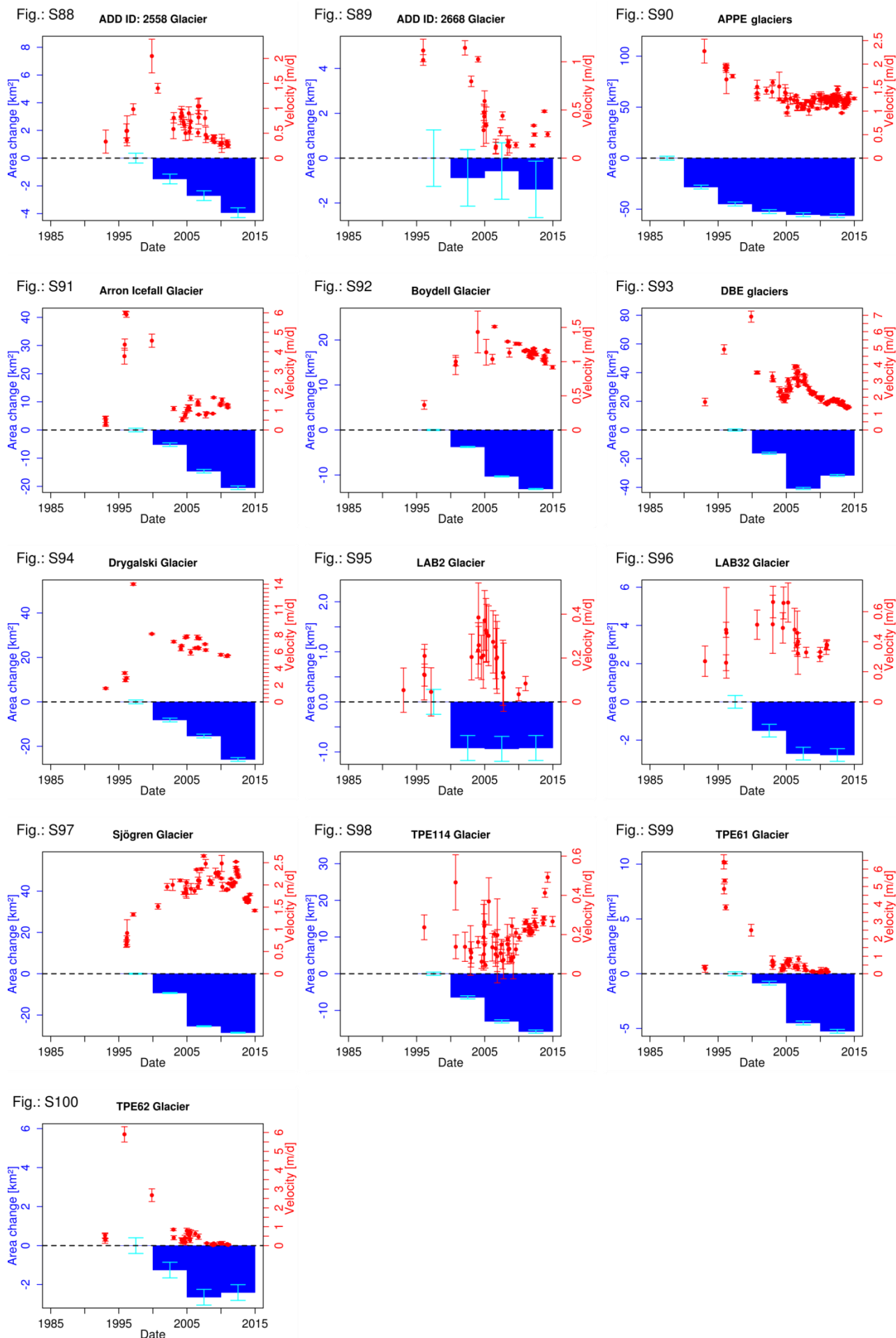


Figure S88-S100. Temporal trend of surface velocity measured at maximum ice thickness at terminus profiles (red) and area (blue) changes of glaciers in sector "EastIS".

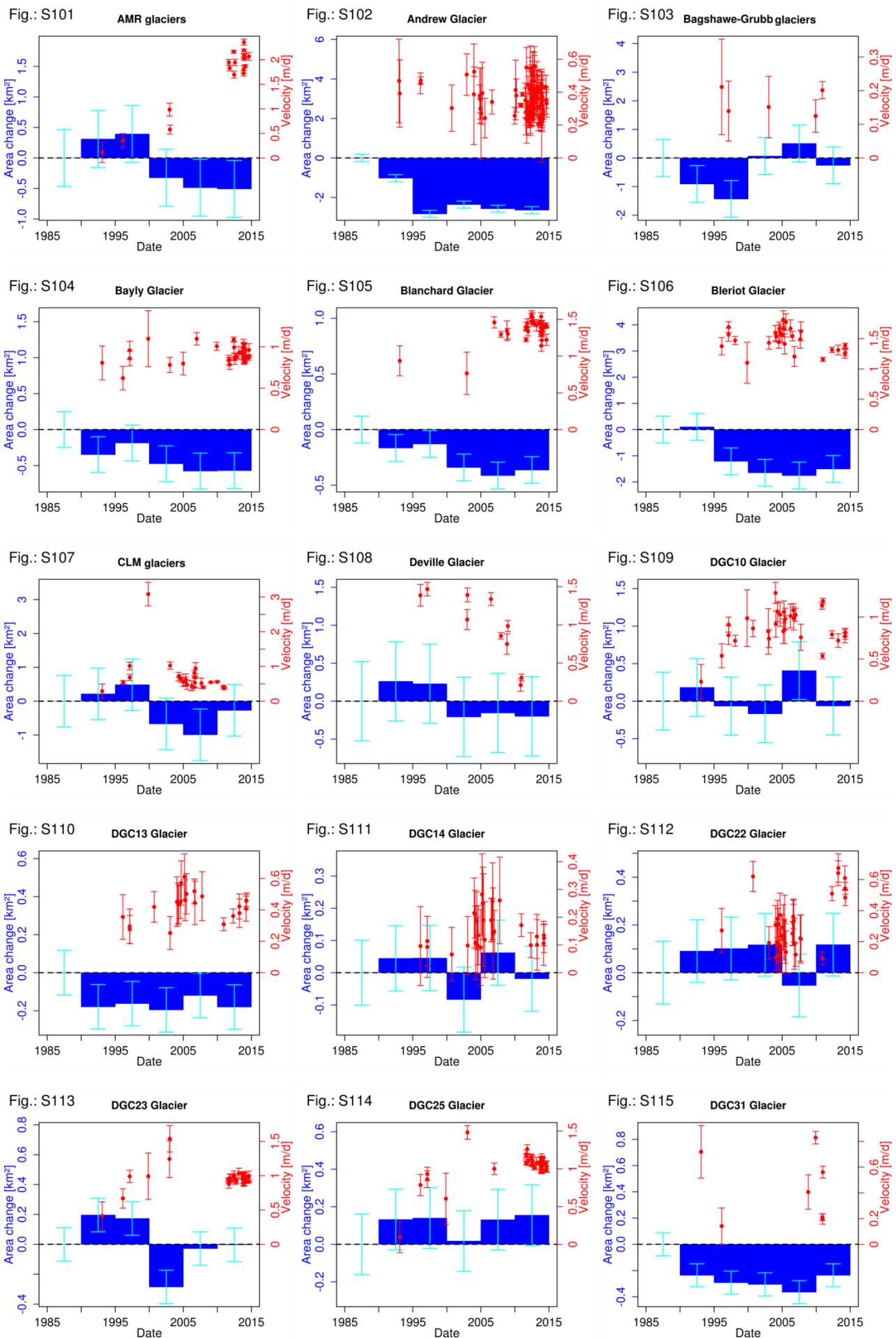
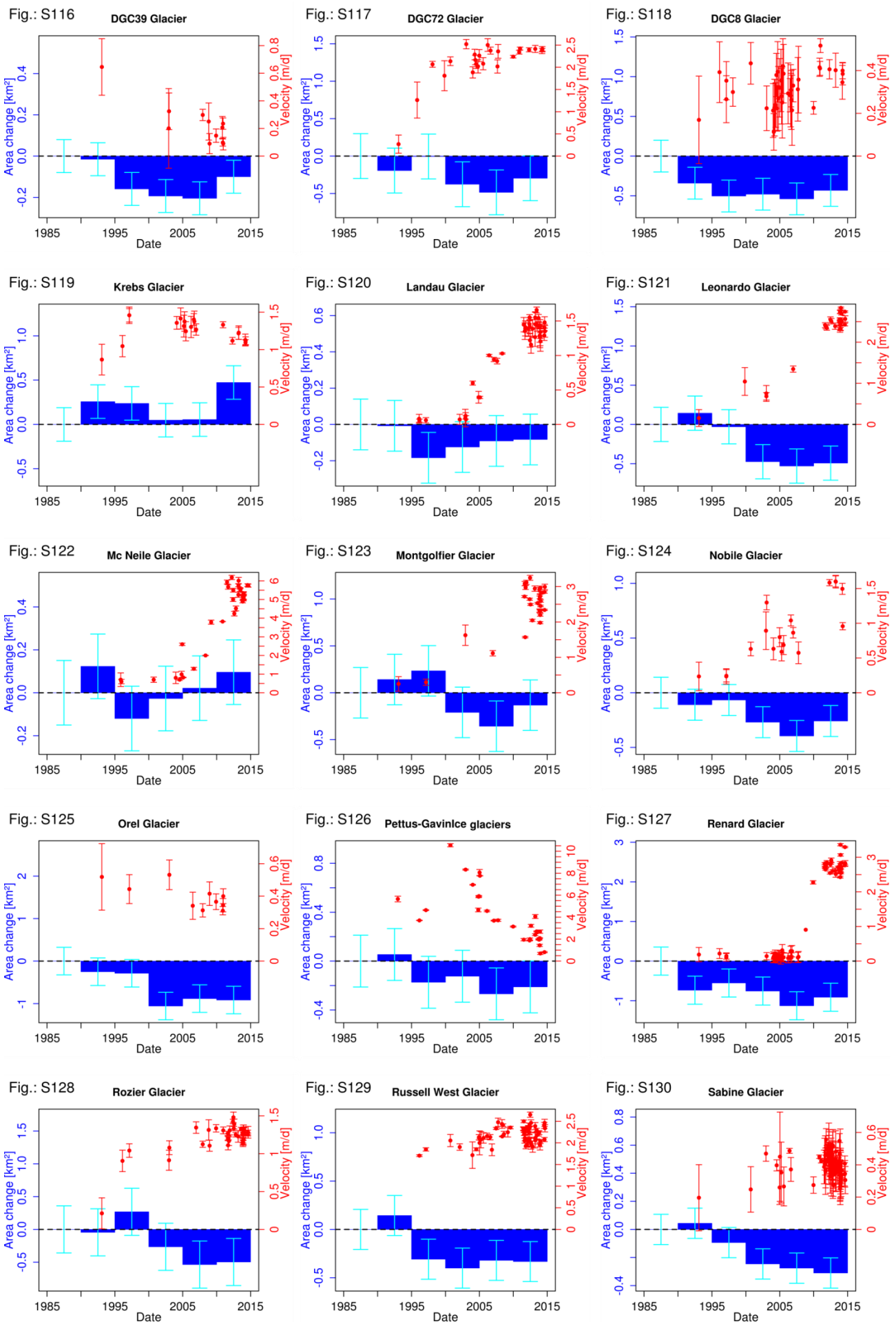


Figure S101-S115. Temporal trend of surface velocity measured at maximum ice thickness at terminus profiles (red) and area (blue) changes of glaciers in sector "West".



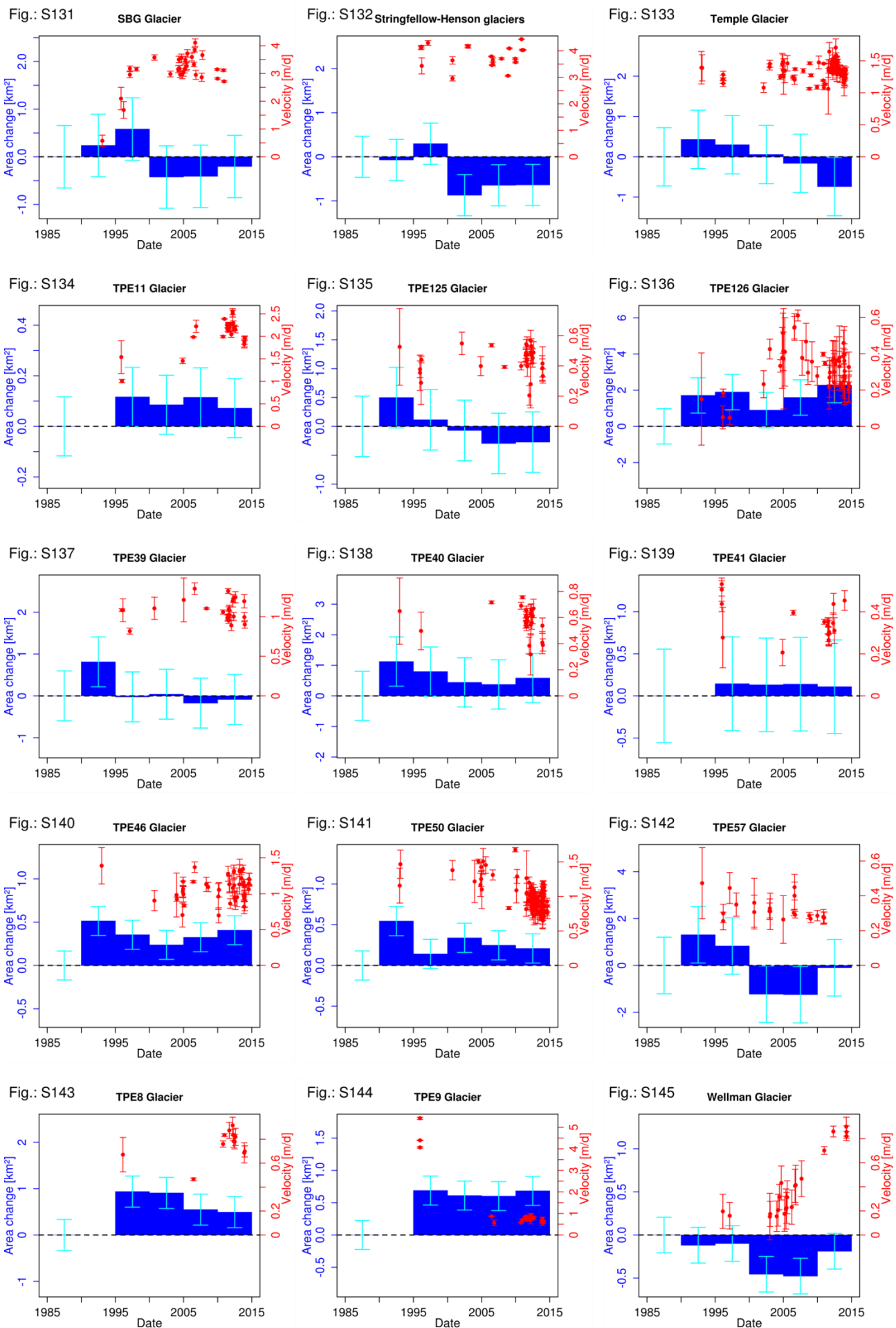


Figure S131-S145. Temporal trend of surface velocity measured at maximum ice thickness at terminus profiles (red) and area (blue) changes of glaciers in sector "West".

Fig.: S146 Wheatstone Glacier

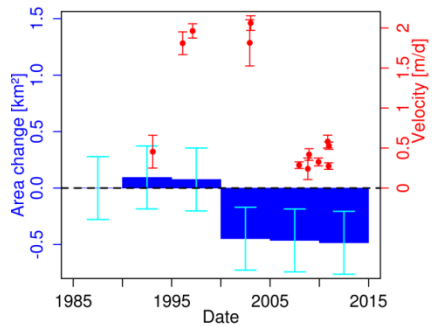


Fig.: S147 Whitecloud Glacier

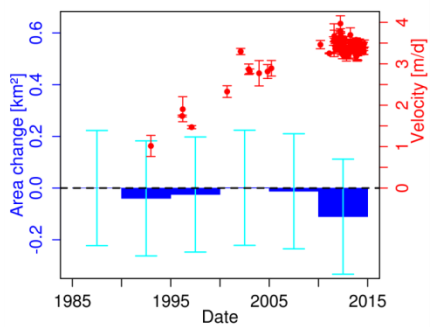


Fig.: S148 Woodbury Glacier

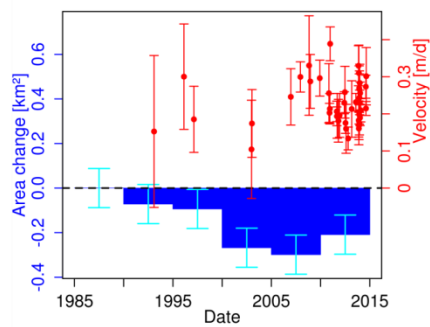


Figure S146-S148. Temporal trend of surface velocity measured at maximum ice thickness at terminus profiles (red) and area (blue) changes of glaciers in sector "West".

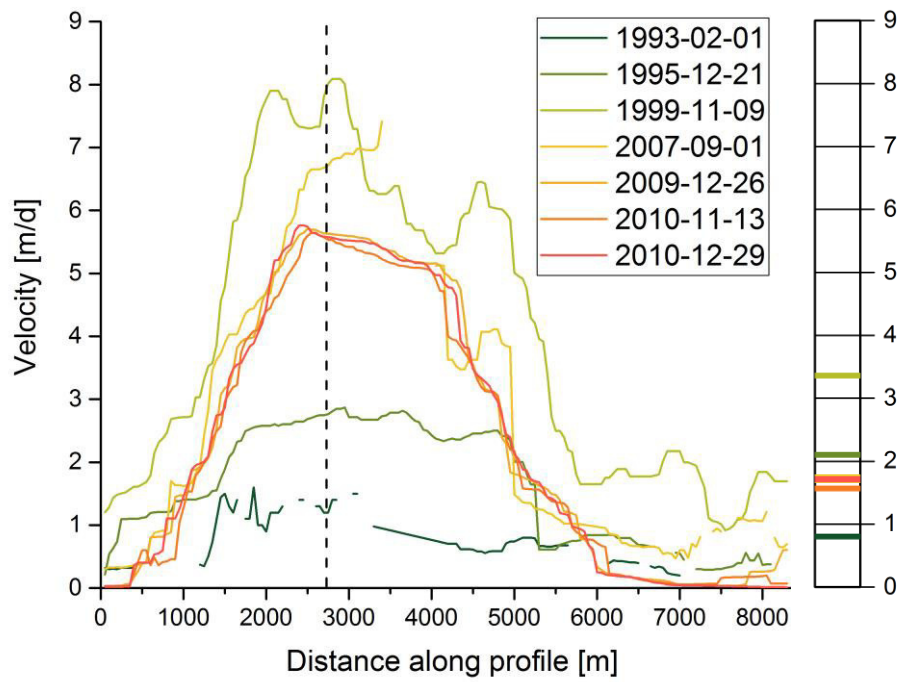


Figure S149. Surface velocity across the terminus of Drygalski Glacier (left) and median values of each profile (right). Dashed line: maximum ice thickness of across glacier profile

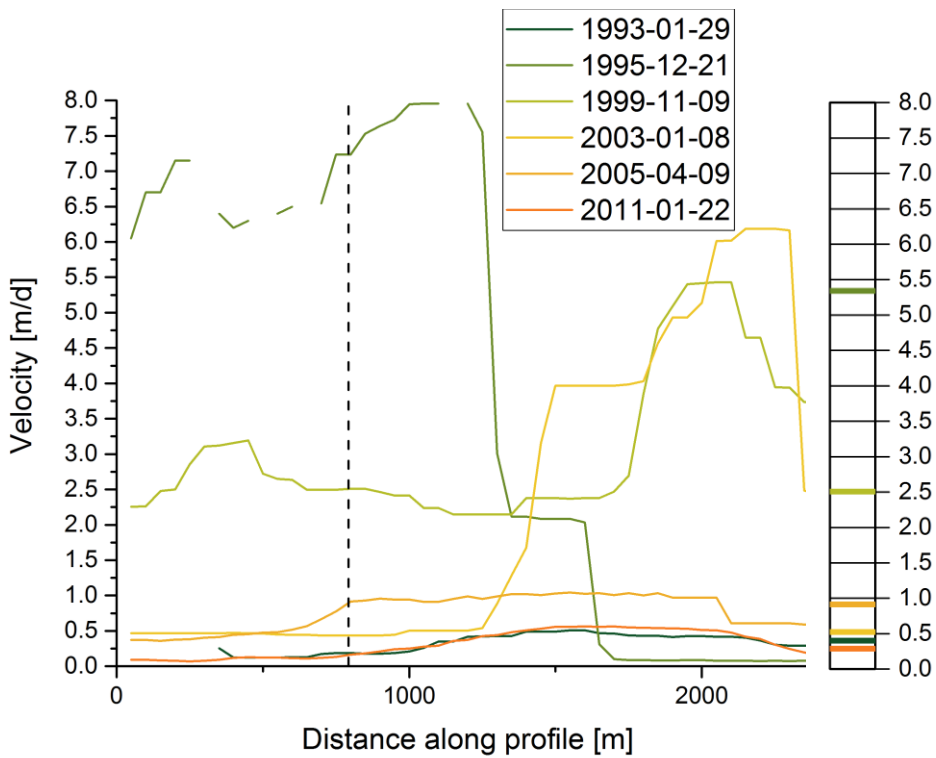


Figure S150. Surface velocity across the terminus of TPE61 Glacier (left) and median values of each profile (right). Dashed line: maximum ice thickness of across glacier profile

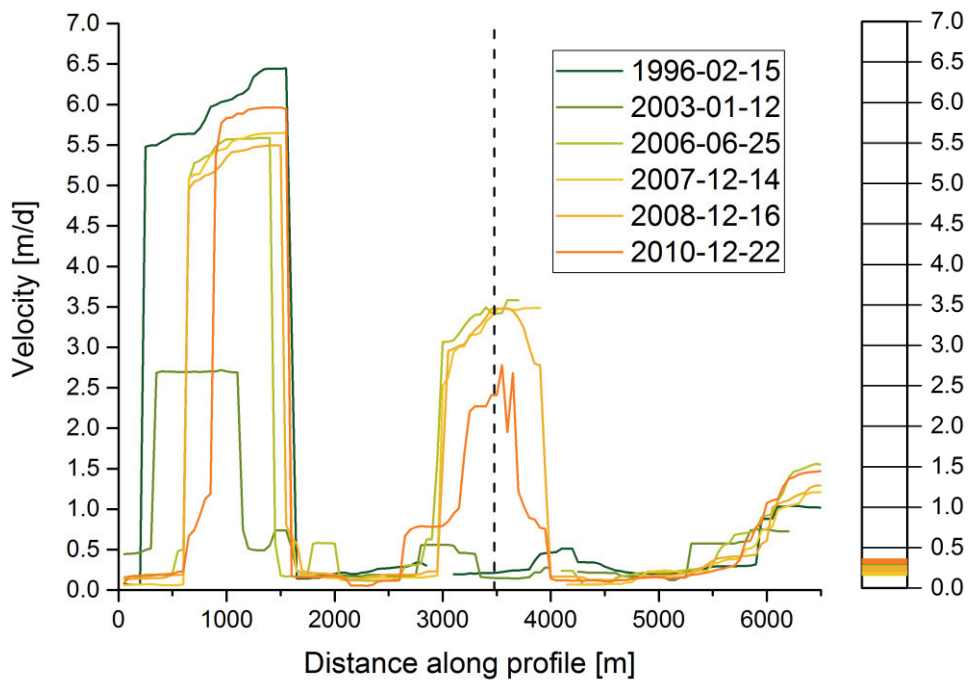


Figure S151. Surface velocity across the terminus of Bagshawe-Grubb glaciers (left) and median values of each profile (right). Dashed line: maximum ice thickness of across glacier profile

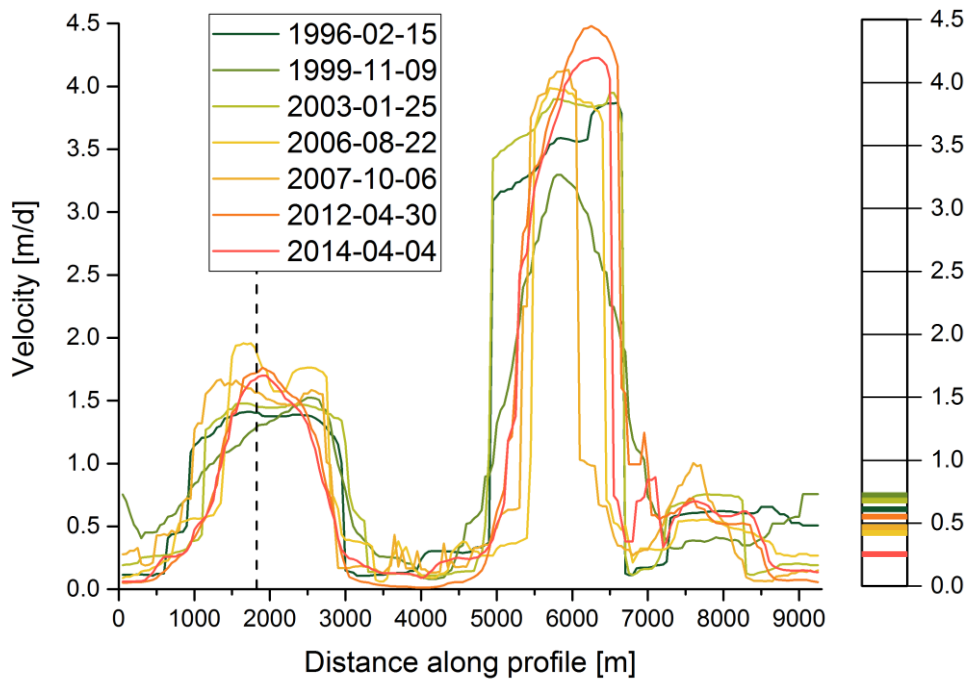


Figure S152. Surface velocity across the terminus of Bleriot Glacier (left) and median values of each profile (right). Dashed line: maximum ice thickness of across glacier profile

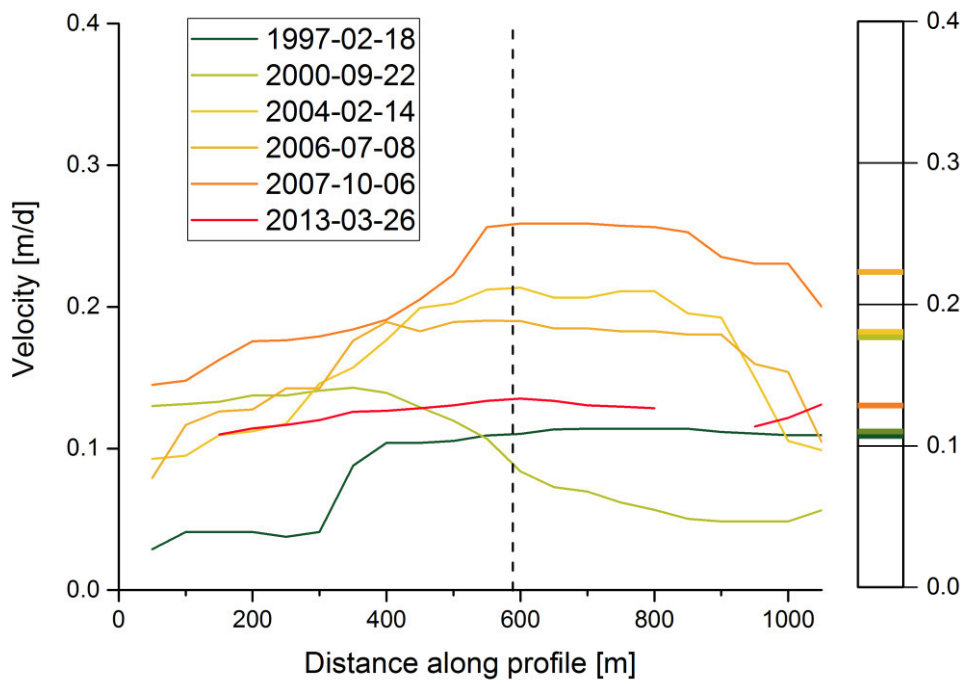


Figure S153. Surface velocity across the terminus of DGC14 Glacier (left) and median values of each profile (right). Dashed line: maximum ice thickness of across glacier profile

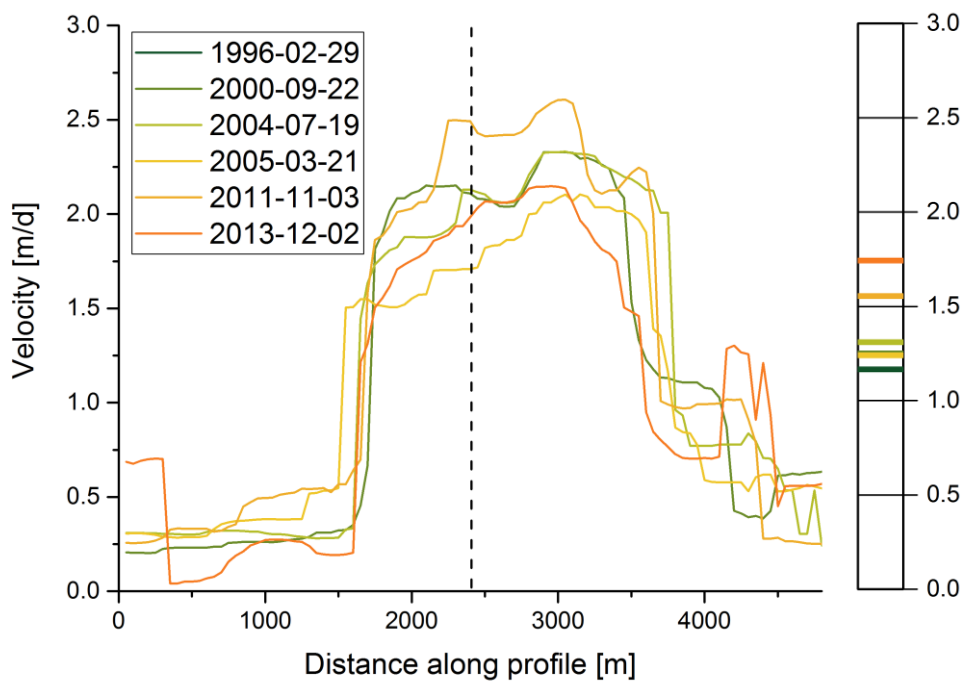


Figure S154. Surface velocity across the terminus of Russell West Glacier (left) and median values of each profile (right). Dashed line: maximum ice thickness of across glacier profile

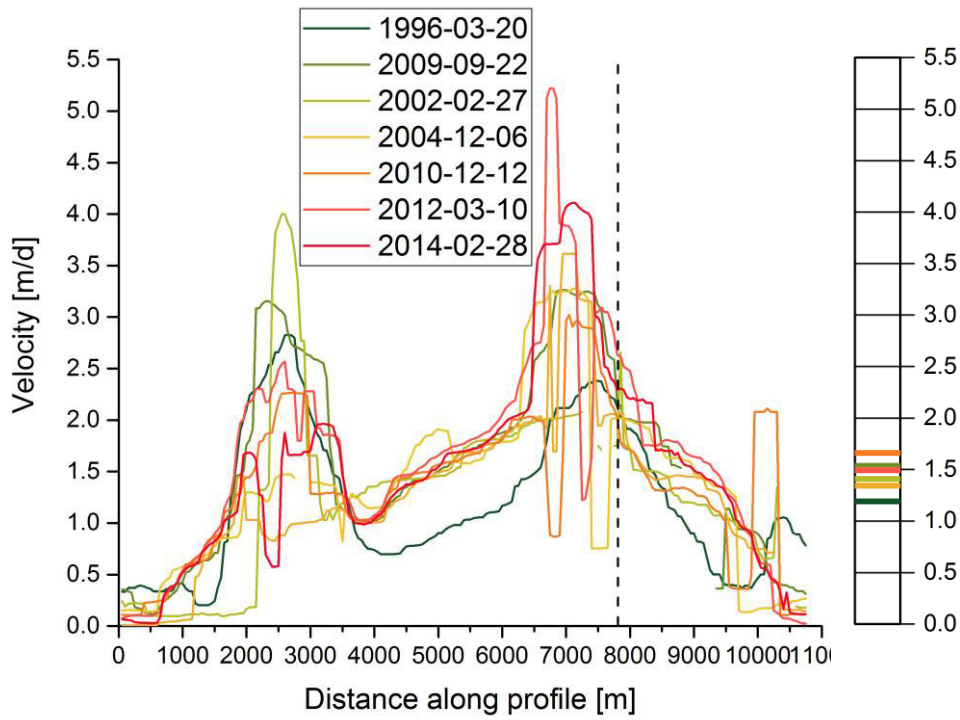


Figure S155. Surface velocity across the terminus of Temple Glacier (left) and median values of each profile (right). Dashed line: maximum ice thickness of across glacier profile

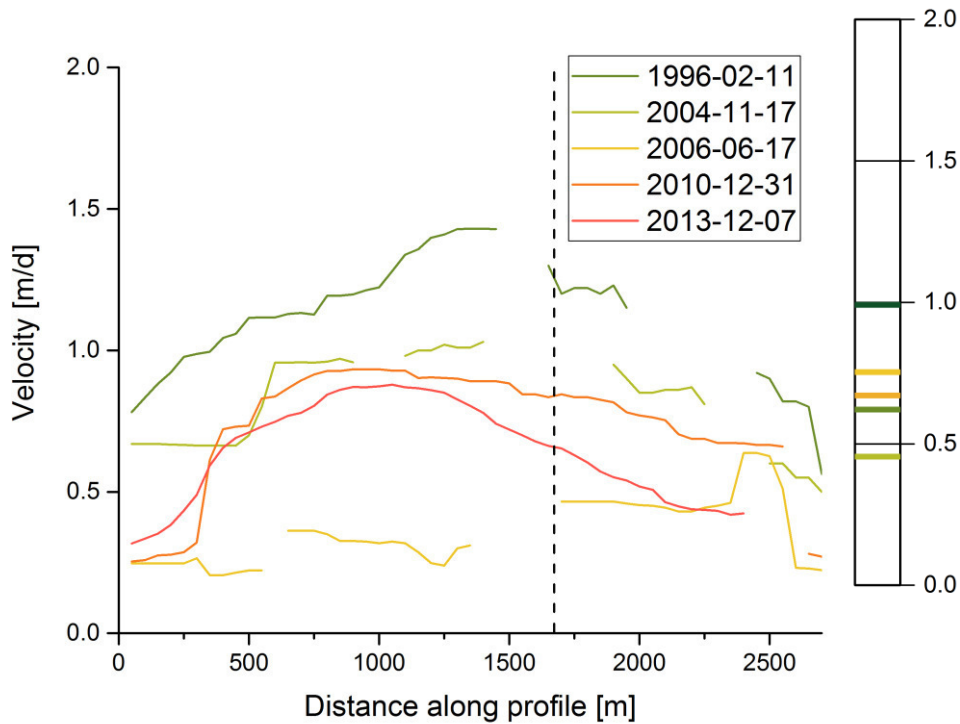


Figure S156. Surface velocity across the terminus of TPE8 Glacier (left) and median values of each profile (right). Dashed line: maximum ice thickness of across glacier profile

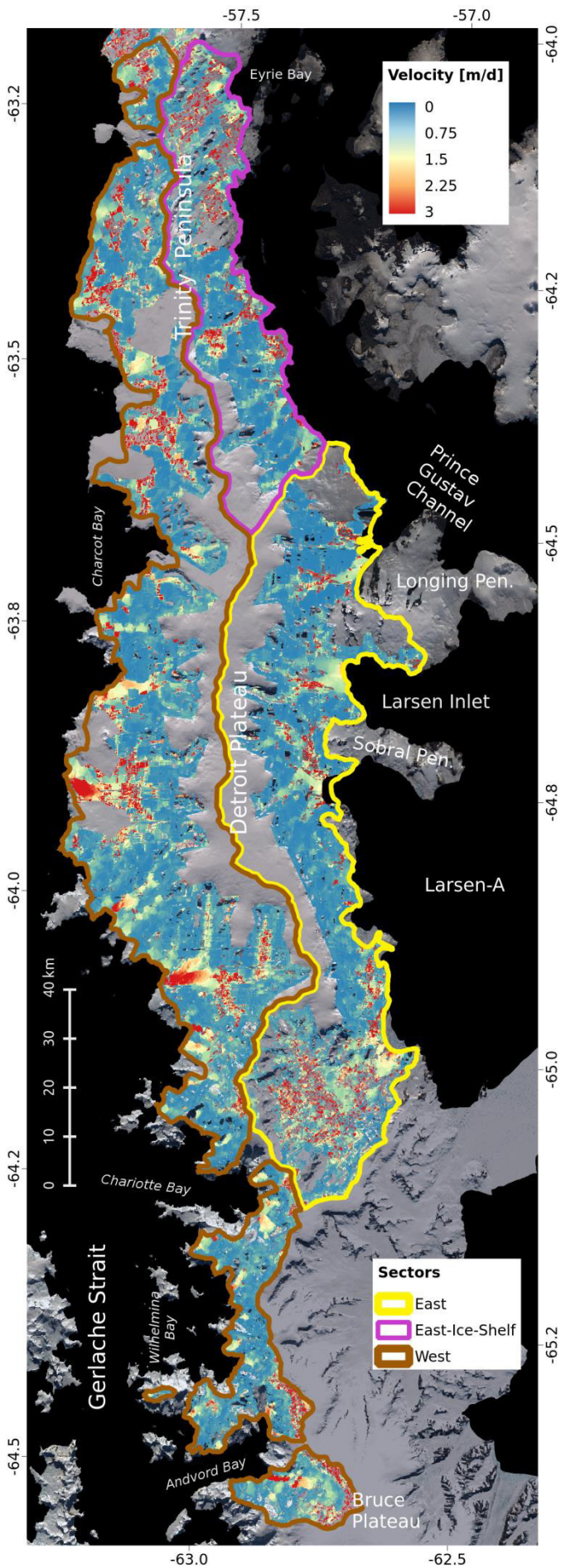


Figure S157. Surface velocity fields of outlet glaciers derived from multiple ERS SAR acquisitions (1996-1997). Background: Landsat LIMA Mosaic USGS, NASA, BAS, NSF. Note: Red speckle patterns indicate erroneous tracking results (noise).

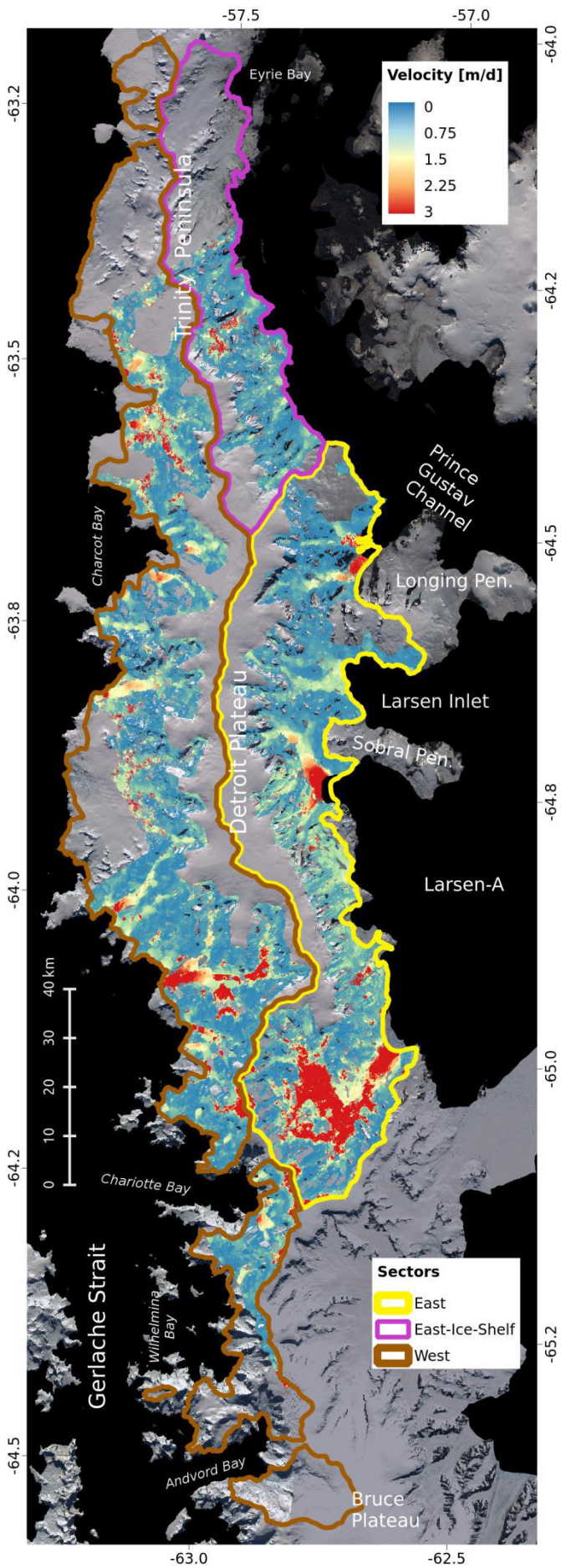


Figure S158. Surface velocity fields of outlet glaciers derived from multiple ENVISAT SAR acquisitions (2005-2006). Background: Landsat LIMA Mosaic USGS, NASA, BAS, NSF. Note: Red speckle patterns indicate erroneous tracking results (noise).

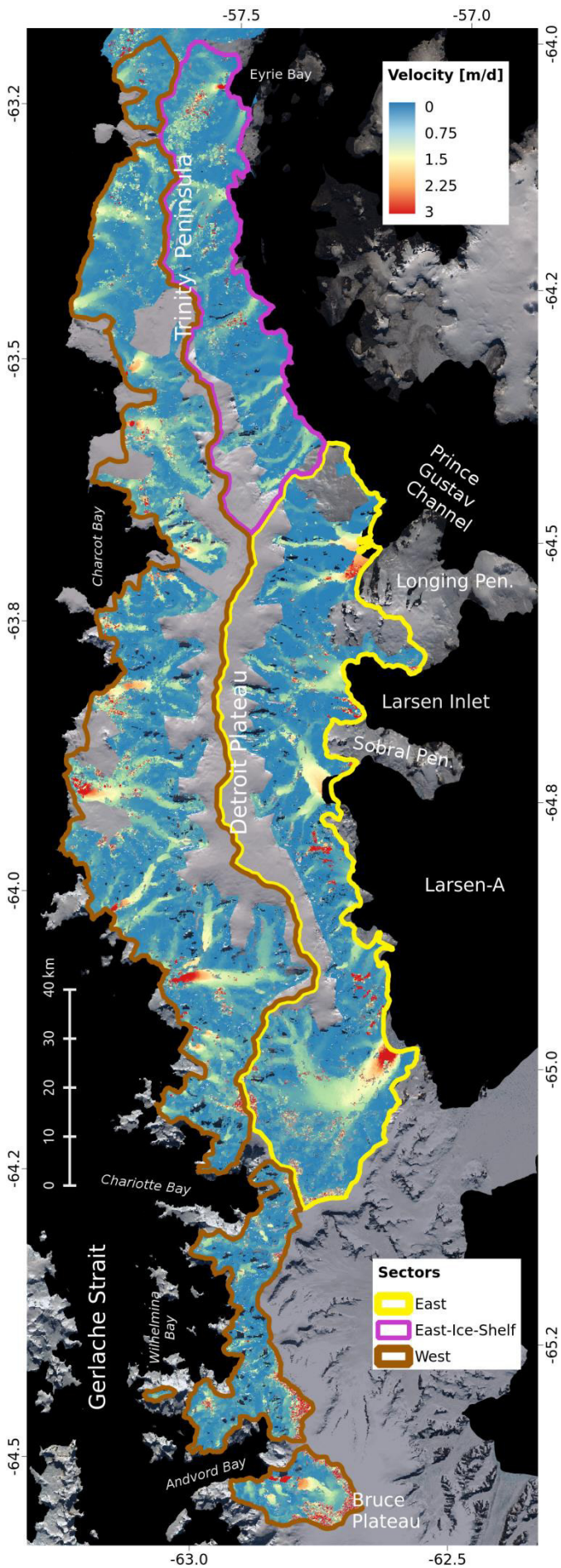


Figure S159. Surface velocity fields of outlet glaciers derived from multiple ALOS PALSAR acquisitions (2008-2010). Background: Landsat LIMA Mosaic USGS, NASA, BAS, NSF. Note: Red speckle patterns indicate erroneous tracking results (noise).

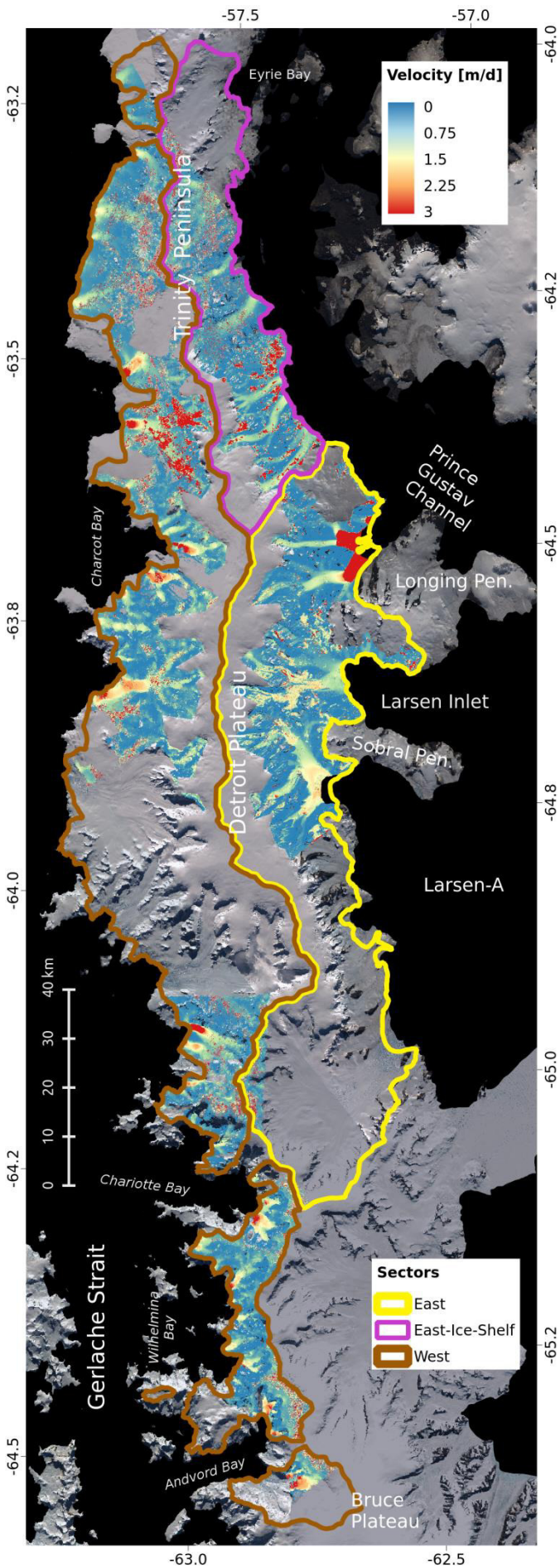


Figure S160. Surface velocity fields of outlet glaciers derived from multiple TerraSAR/TanDEM-X SAR acquisitions (2011-2012). Background: Landsat LIMA Mosaic USGS, NASA, BAS, NSF. Note: Red speckle patterns indicate erroneous tracking results (noise).

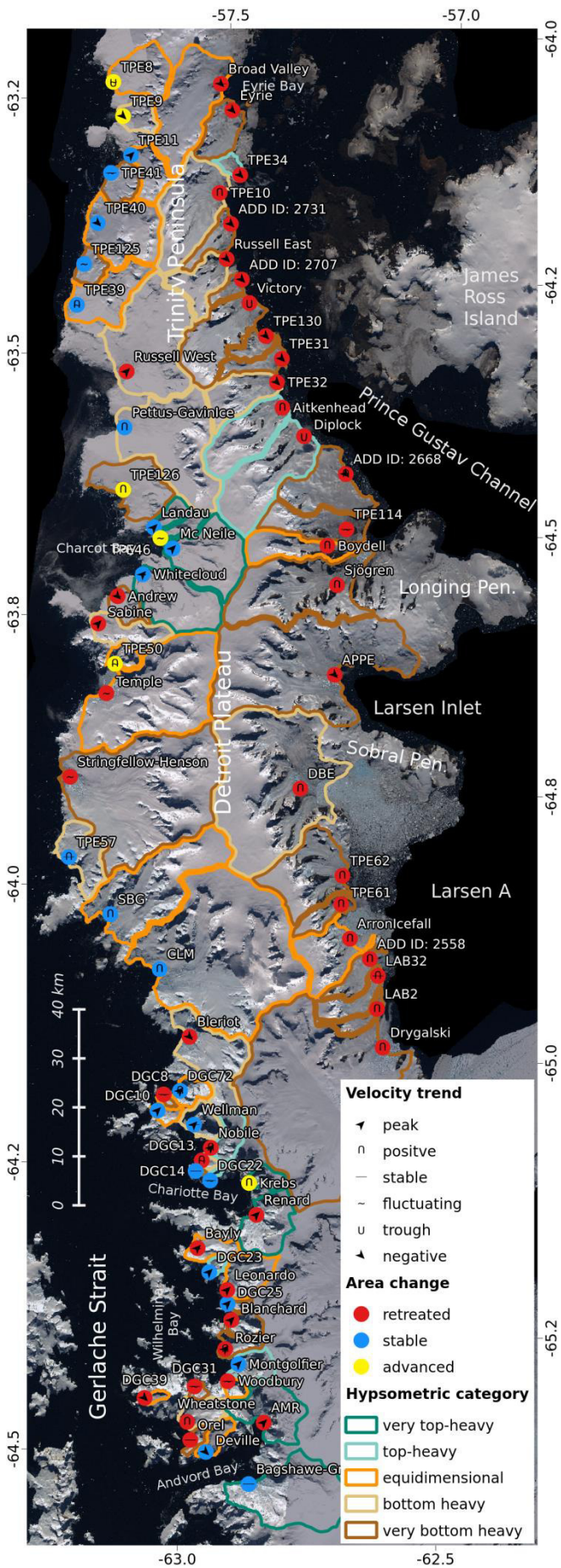


Figure S161. Categorizations of glaciers based on the temporal variations of area changes (dots) and flow velocities measured at the maximum ice thickness at the terminus profiles (symbols). Colors of catchment delineation indicate Hypsometric categories according to Jiskoot et al. (2009). Background: Landsat LIMA Mosaic USGS, NASA, BAS, NSF

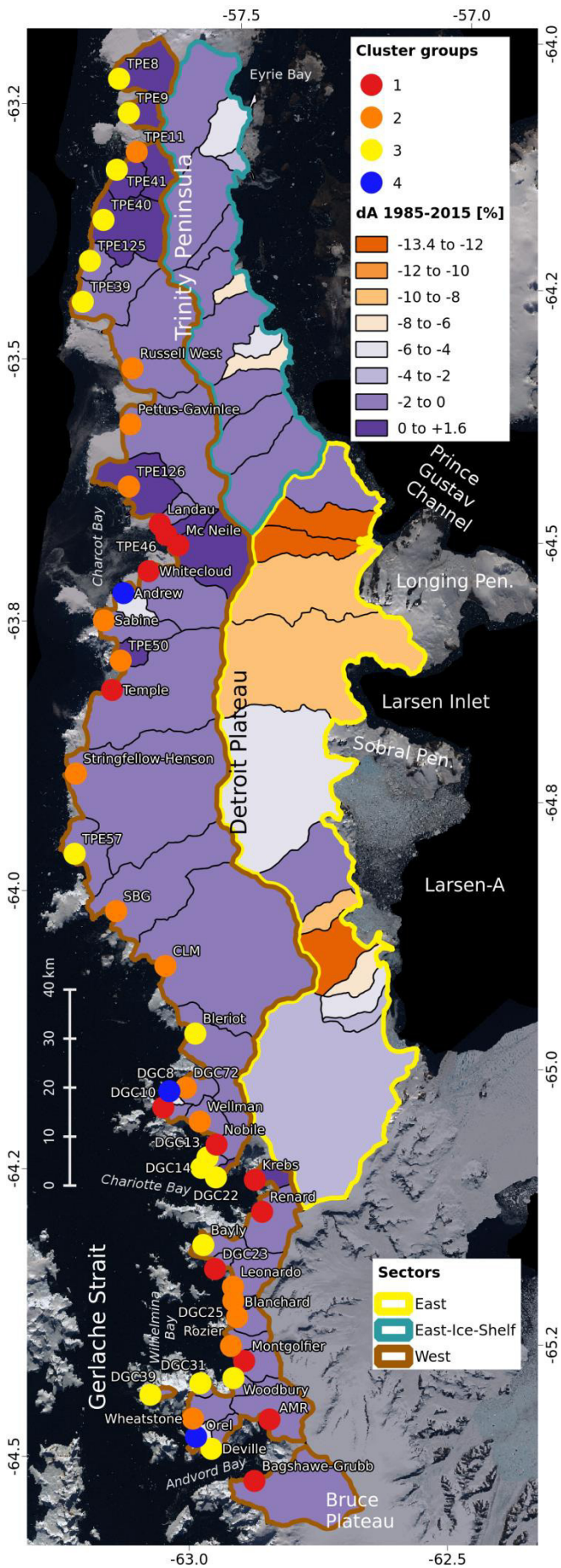


Figure S162. Spatial distribution of glacier types along the west coast (based on velocity measurements at the maximum ice thickness at the terminus profiles). Glaciers are group based on a hierarchical cluster analysis (dots). Individual glacier catchment colors: relative area change in the period 1985-2015. Colored polygon outlines: Boundaries of the three sectors. Background: Landsat LIMA Mosaic USGS, NASA, BAS, NSF

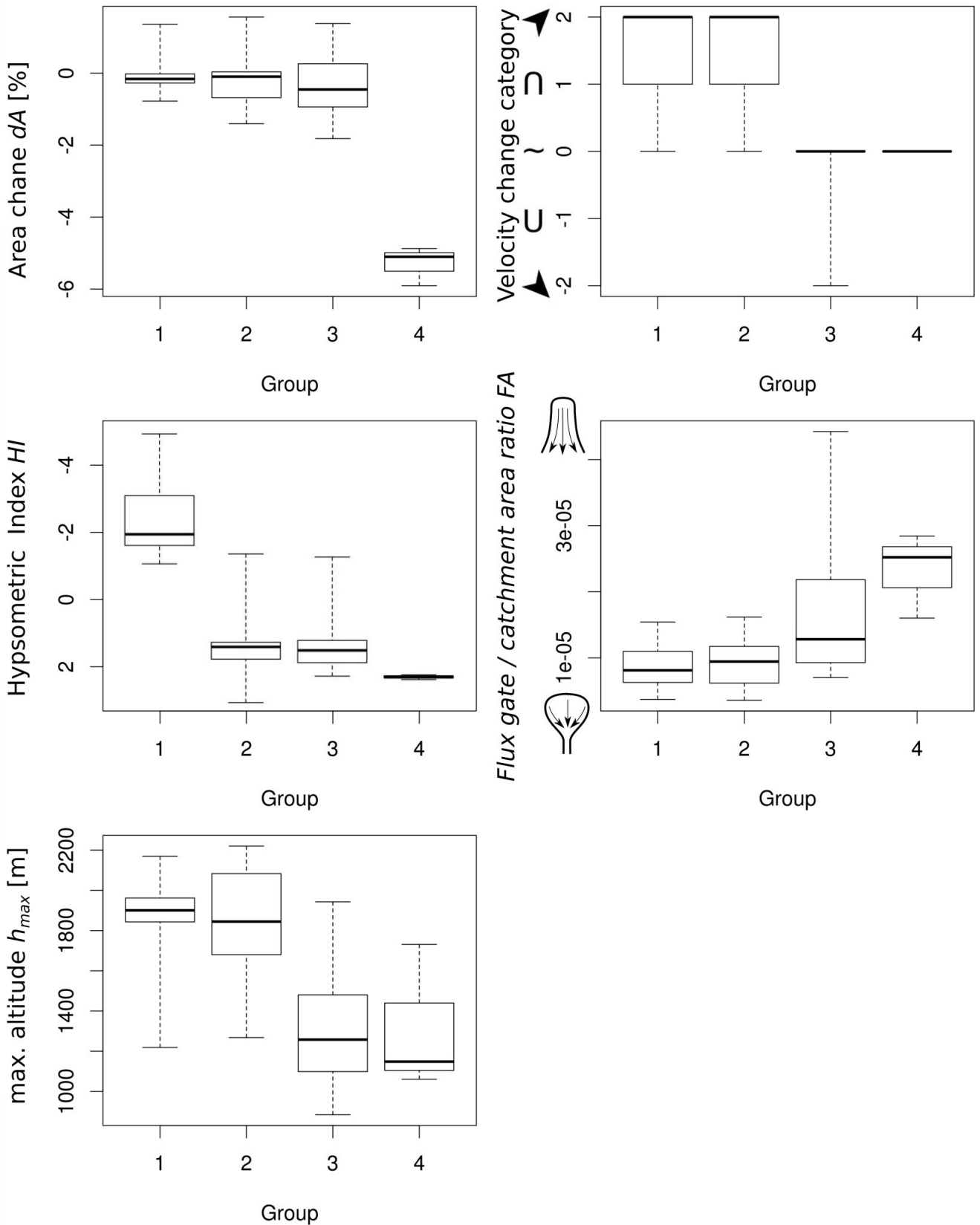


Figure S163. Boxplots of cluster analysis input variables (Sector “West”) for each group. Whiskers extend to the most extreme data points. Velocities were measured at the maximum ice thickness at the terminus profiles.

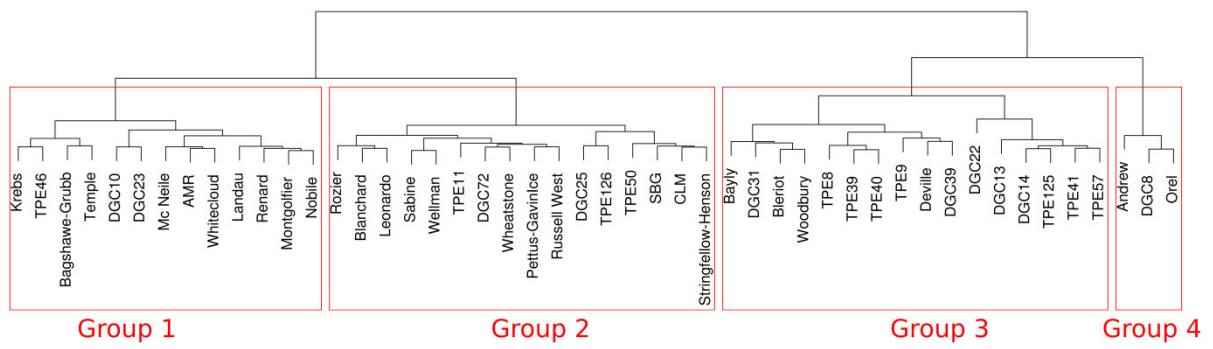


Figure S164. Dendrogram of hierarchical cluster analysis of glaciers in sector "West" coast (based on velocity measurements at the maximum ice thickness at the terminus profiles). The glaciers are assorted in four groups (red rectangles). See also Section 5.3.

Table S1: Observed parameters of the individual glaciers (median velocities measured along terminus profiles). Table continues next page.

Sector	Basin	l_t [m]	$A_{1985-1990}$ [km ²]	$A_{2010-2015}$ [km ²]	dA [km ²]	Area change category	Date v_s [yyyy-mm-dd]	Date v_E [yyyy-mm-dd]	dt [a]	v_s [m d ⁻¹]	v_E [m d ⁻¹]	dv [m d ⁻¹]	dv [%]	n_v	Vel. change category	h_{max} [m a.s.l.]	HI	Hypsometric category	FA	Group
East	ADD ID: 2707	5535	28.78	26.82	-1.96	retreated	1995-12-18	2013-12-24	18.03	0.276	0.107	-0.170	-61.375	31	decreased	1278	5.14	very bottom-heavy	0.0056	
	ADD ID: 2731	10955	56.92	55.85	-1.06	retreated	1995-12-18	2010-12-31	15.05	0.358	0.093	-0.265	-73.985	8	decreased	1327	2.93	very bottom-heavy	0.0055	
	Aitkenhead	6532	156.70	155.11	-1.59	retreated	1995-12-18	2013-11-04	17.89	0.108	0.145	0.037	34.679	32	peak	1746	-1.23	top-heavy	0.0024	
	Broad Valley	5948	246.73	246.08	-0.64	retreated	1995-12-18	2010-10-17	14.84	0.310	0.353	0.043	13.815	5	stable	1118	-1.02	equidimensional	0.0005	
	Diplock	8916	235.30	234.14	-1.16	retreated	1995-12-18	2014-03-27	18.28	0.559	0.449	-0.110	-19.743	27	trough	1845	-1.44	top-heavy	0.0017	
	Eyrie	6570	89.53	84.35	-5.18	retreated	1992-12-25	2010-12-31	18.03	0.865	0.169	-0.696	-80.499	7	decreased	1076	2.39	very bottom-heavy	0.0035	
	Russell East	2156	93.75	93.38	-0.37	retreated	1992-12-25	2013-12-07	20.96	0.963	0.389	-0.573	-59.559	34	decreased	1370	1.48	bottom-heavy	0.0035	
	TPE10	5465	225.96	225.24	-0.72	retreated	1995-12-20	2010-10-17	14.84	0.277	0.137	-0.140	-50.635	4	peak	1386	1.43	bottom-heavy	0.0033	
	TPE130	4493	40.58	38.72	-1.86	retreated	1996-02-29	2013-12-24	17.83	0.680	0.201	-0.479	-70.498	33	peak	983	2.07	very bottom-heavy	0.0076	
	TPE31	11684	52.70	48.76	-3.94	retreated	1992-12-25	2014-12-16	21.99	1.844	0.344	-1.500	-81.352	25	decreased	1490	3.50	very bottom-heavy	0.0076	
	TPE32	4071	108.63	108.24	-0.38	retreated	1992-12-25	2014-03-27	21.27	1.549	0.755	-0.794	-51.271	36	decreased	1646	1.46	bottom-heavy	0.0037	
	TPE34	2814	22.91	22.25	-0.66	retreated	1992-12-25	2010-12-31	18.03	1.076	0.076	-1.000	-92.937	10	decreased	500	-1.37	top-heavy	0.0023	
	Victory	9975	180.30	178.75	-1.55	retreated	1994-02-28	2013-12-24	19.83	0.612	0.765	0.153	25.078	25	trough	1645	2.11	very bottom-heavy	0.0041	
Summary East	mean sum	85114	1538.78	1517.71	-21.07				18.22	0.729	0.306	-0.423	-57.983	277		1339				
East-Ice-Shelf	ADD ID: 2558	5890	60.2433	56.31	-3.94	retreated	1993-01-29	2010-12-29	17.93	0.435	0.353	-0.082	-18.758	30	peak	1840	9.08	very bottom-heavy	0.0067	
	ADD ID: 2668	20996	162.324	160.93	-1.39	retreated	1996-02-13	2014-12-16	18.85	0.435	0.340	-0.095	-21.821	23	peak	1342	2.88	very bottom-heavy	0.0041	
	APPE	31872	696.24	639.85	-56.39	retreated	1993-01-12	2014-12-16	21.94	0.869	0.853	-0.015	-1.766	114	fluctuating	1964	1.82	very bottom-heavy	0.0003	
	Arron Icefall	10557	152.356	131.88	-20.48	retreated	1993-01-12	2011-01-22	18.04	0.532	0.288	-0.244	-45.793	39	peak	1979	-1.08	equidimensional	0.0061	
	Boydell	1954	108.039	94.95	-13.09	retreated	1995-12-18	2014-12-16	19.01	0.290	0.975	0.685	236.007	37	peak	1842	-1.07	equidimensional	0.0009	
	DBE	12140	658.91	627.24	-31.67	retreated	1993-01-12	2014-02-27	21.14	0.535	0.950	0.415	77.569	85	peak	2167	1.37	bottom-heavy	0.0011	
	Drygalski	14018	990.41	964.49	-25.92	retreated	1993-01-29	2010-12-29	17.93	0.951	1.641	0.219	72.572	29	peak	2043	1.60	very bottom-heavy	0.0003	
	LAB2	4157	38.3889	37.47	-0.92	retreated	1993-01-29	2010-12-29	17.93	0.060	0.065	0.006	9.726	17	peak	1779	3.76	very bottom-heavy	0.0046	
	LAB32	5534	66.3816	63.60	-2.78	retreated	1993-01-12	2010-12-29	17.97	0.221	0.284	0.063	28.300	17	stable	1841	3.21	very bottom-heavy	0.0046	
	Sjögren	3838	329.298	300.73	-28.57	retreated	1992-12-25	2014-12-16	21.99	0.570	0.638	0.068	11.897	36	peak	1926	1.97	very bottom-heavy	0.0014	
	TPE114	7310	126.385	110.61	-15.78	retreated	1996-02-29	2014-12-16	18.81	0.098	0.190	0.092	93.627	39	stable	1759	2.96	very bottom-heavy	0.0014	
	TPE61	2943	54.3413	49.09	-5.25	retreated	1993-01-12	2011-01-22	18.04	0.406	0.276	-0.130	-31.942	42	peak	1981	2.78	very bottom-heavy	0.0022	
	TPE62	6700	211.811	209.40	-2.41	retreated	1992-12-25	2011-01-22	18.09	0.372	0.448	-0.076	20.424	42	peak	2118	2.43	very bottom-heavy	0.0013	
Summary East-Ice-Shelf	mean sum	127909	3655.13	3446.54	-208.59				19.05	0.444	0.562	0.118	26.480	550		1891				
West	AMR	7773	137.24	136.73	-0.51	retreated	1993-02-01	2014-08-22	21.57	0.157	0.837	0.679	431.515	21	increased	1884	-3.82	very top-heavy	0.0021	1
	Andrew	2951	47.05	44.41	-2.64	retreated	1992-12-25	2014-08-27	21.68	0.453	0.358	-0.095	-21.030	107	decreased	1731	1.99	very bottom-heavy	0.0057	4
	Bagshawe-Grubb	10720	280.43	280.17	-0.26	stable	1993-02-01	2010-12-22	17.90	0.302	0.233	-0.069	-22.782	14	stable	2169	-2.88	very top-heavy	0.0019	1
	Bayly	4149	47.89	47.32	-0.57	retreated	1993-02-01	2014-08-22	21.57	0.419	0.912	0.493	117.584	42	increased	1529	-1.06	equidimensional	0.0027	2
	Blanchard	2005	38.00	37.63	-0.36	retreated	1993-02-01	2014-08-22	21.57	0.341	1.084	0.744	218.153	30	increased	2060	1.53	very bottom-heavy	0.0025	2
	Blieriot	8527	182.20	180.69	-1.50	retreated	1993-02-01	2014-04-10	21.20	0.836	0.300	-0.536	-64.134	25	decreased	1943	1.28	bottom-heavy	0.0019	3
	CLM	12682	809.85	809.58	-0.27	stable	1993-02-01	2010-12-29	17.92	0.388	0.396	0.008	2.157	34	peak	2191	1.13	equidimensional	0.0016	2
	Deville	8699	34.99	34.79	-0.20	stable	1996-02-15	2010-12-22	14.86	0.364	0.127	-0.237	-65.116	12	decreased	1389	-1.19	equidimensional	0.0025	3
	DGC10	6423	23.47	23.40	-0.06	stable	1993-02-01	2014-04-10	21.20	0.116	0.580	0.465	401.477	20	increased	1219	-1.10	equidimensional	0.0064	2
	DGC13	1950	10.95	10.76	-0.18	retreated	1996-02-15	2014-04-10	18.16	0.285	0.205	-0.081	-28.256	24	peak	901	1.28	bottom-heavy	0.0071	3
	DGC14	1684	5.66	5.64	-0.02	stable	1996-02-15	2014-04-10	18.16	0.096	0.113	0.018	18.626	20	stable	884	1.90	very bottom-heavy	0.0109	3
	DGC22	2188	8.98	9.10	0.12	stable	1996-02-15	2014-04-10	18.16	0.190	0.084	-0.106	-55.993	24	stable	1113	-1.24	top-heavy	0.0148	3
	DGC23	1868	15.92	15.91	0.00	stable	1993-02-01	2014-08-22	21.57	0.414	1.025	0.611	147.314	36	increased	1379	-1.33	top-heavy	0.0023	2
	DGC25	2693	14.12	14.27	0.15	stable	1993-02-01	2014-08-22	21.57	0.363	0.820	0.457	125.807	37	increased	1850	1.52	very bottom-heavy	0.0028	2
	DGC31	1466	13.30	13.06	-0.24	retreated	1996-02-15	2010-12-11	14.83	0.132	0.204	0.072	54.579	8	stable	1488	1.86	very bottom-heavy	0.0029	2
	DGC39	1331	15.07	14.97	-0.10	retreated	1993-02-01	2010-12-22	17.90	0.529	0.164	-0.365	-69.044	8	decreased	1472	1.02	equidimensional	0.0040	3
	DGC72	4990	38.39	38.09	-0.30	stable	1993-02-01	2010-12-29	17.92	0.359	0.695	0.336	93.651	13	peak	1706	1.17	equidimensional	0.0027	2
	DGC8	3340	9.34	8.91	-0.43	retreated	1993-02-01	2014-04-10	21.20	0.177	0.241	0.064	36.012	32	stable	1061	2.07	very bottom-heavy	0.0094	4
	Krebs	3152	34.80	35.27	0.47	advanced	1993-02-01	2014-04-10	21.20	0.866	0.738	-0.128	-14.780	13	peak	2029	-2.00	very top-heavy	0.0006	1
	Landau	2330	33.99	33.90	-0.08	stable	1996-02-13	2014-08-27	18.55	0.069	0.727	0.658	954.866	48	increased	1747	-1.79	very top-heavy	0.0027	1
	Leonardo	3632	84.22	83.72	-0.49	retreated	1993-02-01	2014-08-22	21.57	0.281	1.493	1.212	431.732	24	increased	2106	1.06	equidimensional	0.0009	2
	Mc Neile	2507	184.56	184.66	0.10	stable	1995-12-19	2014-08-27	18.70	0.207	0.699	0.492	237.738	30	increased	1882	-4.58	very top-heavy	0.0006	1
	Montgolfier	4486	55.20	55.06	-0.13	stable	1993-02-01	2014-08-22	21.57	0.141	1.371	1.230	872.806	21	increased	1929	-1.32	top-heavy	0.0022	1
	Nobile	2361	57.04	56.78	-0.26	retreated	1993-02-01	2014-04-10	21.20	0.233	0.372	0.139	59.586	13	peak	1901	-1.28	top-heavy	0.0018	1
	Orel	5399	19.02	18.11	-0.92	retreated	1996-02-15	2010-12-22	14.86	0.229	0.172	-0.057	-25.010	8	stable	1148	1.95	very bottom-heavy	0.0066	4
	Pettus-Gavinlce	3535	330.88	330.67	-0.21	stable	1992-12-25	2014-08-05	21.62	0.686	0.385	-0.301	-43.827	33	peak	1846	1.24	bottom-heavy	0.0030	2

Sector	Basin	l_f [m]	$A_{1985-1990}$ [km ²]	$A_{2010-2015}$ [km ²]	dA [km ²]	Area change category	Date vs [yyyy-mm-dd]	Date vE [yyyy-mm-dd]	dt [a]	vS [m d-1]	vE [m d-1]	dv [m d-1]	dv [%]	n_v	Vel. change category	h_{max} [m a.s.l.]	HI	Hypsometric category	FA	Group
	Renard	5904	118.15	117.24	-0.91	retreated	1993-02-01	2014-08-22	21.57	0.212	1.698	1.486	699.238	36	increased	2043	-1.82	very top-heavy	0.0011	1
	Rozier	5984	35.57	35.07	-0.50	retreated	1996-02-15	2014-08-22	18.53	0.977	0.944	-0.033	-3.420	38	peak	2061	2.70	very bottom-heavy	0.0036	2
	Russell West	3450	329.28	328.95	-0.33	retreated	1996-02-29	2014-08-27	18.50	1.072	1.759	0.687	64.111	16	increased	1645	1.44	bottom-heavy	0.0028	2
	Sabine	1795	83.09	82.78	-0.31	retreated	1993-02-01	2014-08-27	21.58	0.239	0.348	0.109	45.520	82	increased	1843	1.21	bottom-heavy	0.0070	2
	SBG	10917	327.95	327.75	-0.20	stable	1993-02-01	2010-12-29	17.92	0.298	0.306	0.007	2.395	34	peak	2220	1.08	equidimensional	0.0047	2
	Stringfellow-Henson	7775	670.38	669.74	-0.64	retreated	1993-02-01	2014-02-28	21.09	1.100	1.233	0.132	12.029	22	fluctuating	2167	1.55	very bottom-heavy	0.0026	2
	Temple	12056	453.96	453.22	-0.74	retreated	1992-12-25	2014-08-11	21.64	1.544	1.516	-0.028	-1.821	90	fluctuating	1962	-1.06	equidimensional	0.0031	1
	TPE11	1947	70.06	70.13	0.07	stable	1995-12-20	2013-12-24	18.02	0.184	1.203	1.018	552.655	20	increased	1268	1.05	equidimensional	0.0028	2
	TPE125	8741	40.41	40.13	-0.27	stable	1992-12-25	2013-12-24	21.01	0.415	0.260	-0.155	-37.319	22	fluctuating	1104	1.82	very bottom-heavy	0.0116	3
	TPE126	16295	145.52	147.80	2.28	advanced	1995-12-19	2014-08-27	18.70	0.287	0.306	0.019	6.542	58	peak	1655	2.20	very bottom-heavy	0.0060	2
	TPE39	9931	139.49	139.40	-0.08	stable	1995-12-19	2013-12-07	17.98	0.341	0.690	0.348	102.092	21	peak	1384	1.13	equidimensional	0.0051	2
	TPE40	13405	184.11	184.69	0.58	stable	1992-12-25	2013-12-24	21.01	0.718	0.406	-0.312	-43.414	27	decreased	1386	1.01	equidimensional	0.0059	3
	TPE41	9256	53.13	53.24	0.11	stable	1995-12-19	2013-12-07	17.98	0.326	0.281	-0.046	-13.987	26	stable	1094	1.98	very bottom-heavy	0.0107	3
	TPE46	2785	33.94	34.34	0.41	advanced	1992-12-25	2014-08-27	21.68	0.935	0.881	-0.054	-5.756	42	fluctuating	1843	-1.86	very top-heavy	0.0026	1
	TPE50	2987	31.32	31.53	0.21	advanced	1992-12-25	2014-02-28	21.19	0.450	0.517	0.067	14.899	46	peak	1839	1.13	equidimensional	0.0023	2
	TPE57	20111	100.43	100.34	-0.10	stable	1993-02-01	2010-12-29	17.92	0.317	0.230	-0.087	-27.382	29	peak	1132	1.31	bottom-heavy	0.0090	3
	TPE8	5582	111.74	112.24	0.49	advanced	1996-02-11	2013-12-24	17.88	0.991	0.739	-0.252	-25.395	14	trough	1104	1.19	equidimensional	0.0035	3
	TPE9	3735	48.96	49.64	0.68	advanced	1995-12-20	2013-12-24	18.02	0.377	0.150	-0.227	-60.233	17	decreased	1085	1.41	bottom-heavy	0.0057	3
	Wellman	3449	48.67	48.48	-0.19	stable	1996-02-15	2014-04-10	18.16	0.161	0.255	0.094	58.300	19	stable	1772	1.47	bottom-heavy	0.0037	2
	Wheatstone	4642	52.66	52.18	-0.48	retreated	1993-02-01	2010-12-22	17.90	0.355	0.258	-0.097	-27.262	11	peak	1569	1.21	bottom-heavy	0.0029	2
	Whitecloud	3711	177.77	177.66	-0.11	stable	1992-12-25	2014-08-11	21.64	0.454	0.481	0.027	5.848	39	fluctuating	1950	-2.94	very top-heavy	0.0013	1
	Woodbury	1464	20.24	20.03	-0.21	retreated	1993-02-01	2014-08-11	21.54	0.155	0.239	0.084	53.784	23	stable	1862	1.02	equidimensional	0.0024	2
Summary West	mean sum	268763	5809.33	5800.18	-9.14				19.58	0.428	0.605	0.177	41.334	1429		1636				
Summary all glaciers	mean sum	481786	11003.23	10764.42	-238.81				19.25	0.484	0.545	0.061	12.646	2256		1629				

l_f – length of ice front

dA – change in glacier area between 1985 and 2015*

Date v_s - date of first velocity measurement

dt - mean time period of velocity measurements

v_E – mean of latest velocity measurements (2010-2014)

n_v – sum of velocity measurements in the observation period (dt)

h_{max} – average maximum altitude of individual basins

Hypsometric category – see Table 4

Group – classification of glaciers in sector “West” according to the hierarchical cluster analysis in Section 4.4.

*since 1995 for the former Larsen-A and Prince Gustav Ice Shelf tributaries (see Section 5.2)

A – glacier area in the respective period*

Area change category – see definition in Section 4.1

Date v_E – date of last velocity measurement

v_s – mean of earliest velocity measurements (1992-1996)

dv – mean velocity change

Velocity change category – see definition in Table 3

HI – Hypsometric Index of the basin

FA – flux gate to catchment size ratio

Table S2: Observed parameters of the individual glaciers derived from velocity data measured at maximum ice thickness at the terminus profiles. Table continues next page.

Sector	Basin	Date v_S [yyyy-mm-dd]	Date v_E [yyyy-mm-dd]	dt [a]	v_S [m d ⁻¹]	v_E [m d ⁻¹]	dv [m d ⁻¹]	dv [%]	n_v	Vel. change category	Longitude [°]	Latitude [°]	Group
East	ADD ID: 2707	1995-11-14	2013-12-24	18.12	2.212	0.140	-2.072	-93.676	40	decreased	-58.3480	-63.7806	
	ADD ID: 2731	1992-12-25	2010-12-31	18.03	0.391	0.134	-0.256	-65.654	9	decreased	-58.1603	-63.6990	
	Aitkenhead	1995-12-18	2014-12-16	19.01	1.266	1.280	0.014	1.134	34	peak	-58.6712	-63.9561	
	Broad Valley	1996-02-11	2010-12-31	14.90	0.445	0.070	-0.375	-84.243	3	decreased	-57.6730	-63.5434	
	Diplock	1995-12-18	2014-12-16	19.01	0.538	0.641	0.103	19.140	52	trough	-58.7446	-64.0382	
	Eyrie	1992-12-25	2010-12-31	18.03	1.123	0.682	-0.442	-39.311	5	decreased	-57.7725	-63.5999	
	Russell East	1992-12-25	2013-12-24	21.01	3.127	0.552	-2.575	-82.350	39	decreased	-58.2950	-63.7328	
	TPE10	1995-11-14	2010-12-31	15.14	1.258	1.154	-0.105	-8.327	6	peak	-58.0911	-63.6559	
	TPE130	1995-11-14	2014-03-27	18.38	4.998	0.273	-4.725	-94.540	50	decreased	-58.4762	-63.8652	
	TPE31	1995-12-18	2013-12-24	18.03	3.986	0.169	-3.816	-95.756	25	decreased	-58.5084	-63.9136	
	TPE32	1995-12-19	2014-12-16	19.01	1.848	0.625	-1.223	-66.185	49	decreased	-58.5985	-63.9253	
	TPE34	1992-12-25	2010-12-31	18.03	1.369	0.365	-1.004	-73.345	6	decreased	-57.9752	-63.6675	
	Victory	1995-11-14	2013-12-02	18.06	1.284	1.222	-0.062	-4.852	37	trough	-58.3952	-63.8057	
	Summary East	mean sum			18.06	1.834	0.562	-1.272	-69.360				
East-Ice-Shelf	ADD ID: 2558	1993-01-29	2010-12-29	17.93	0.332	0.297	-0.035	-10.600	39	peak	-60.4713	-64.6331	
	ADD ID: 2668	1995-12-19	2014-03-27	18.28	1.068	0.367	-0.701	-65.626	24	decreased	-58.7338	-64.0949	
	APPE	1992-12-25	2014-12-16	21.99	2.276	1.230	-1.046	-45.972	126	decreased	-59.5048	-64.3030	
	Arron Icefall	1993-01-12	2010-12-29	17.97	0.479	1.298	0.819	170.781	30	peak	-60.4392	-64.5916	
	Boydell	1996-02-13	2014-12-16	18.85	0.367	1.149	0.782	213.226	37	peak	-59.0689	-64.1694	
	DBE	1993-01-29	2014-02-27	21.09	1.710	1.392	-0.318	-18.603	115	peak	-59.9281	-64.3595	
	Drygalski	1993-01-29	2010-12-29	17.93	1.610	5.490	3.879	240.893	22	peak	-60.7602	-64.7437	
	LAB2	1993-01-29	2010-12-29	17.93	0.053	0.084	0.030	56.272	23	peak	-60.6258	-64.6894	
	LAB32	1993-01-29	2010-12-29	17.93	0.270	0.378	0.108	39.865	23	peak	-60.5046	-64.6596	
	Sjögren	1996-02-13	2014-12-16	18.85	0.758	1.661	0.904	119.255	61	peak	-59.1731	-64.2164	
	TPE114	1996-02-13	2014-12-16	18.85	0.237	0.379	0.143	60.225	55	fluctuating	-58.9343	-64.1937	
	TPE61	1993-01-12	2011-01-22	18.04	0.343	0.136	-0.207	-60.310	44	peak	-60.3090	-64.5320	
	TPE62	1992-12-25	2011-01-22	18.09	0.374	0.067	-0.308	-82.175	40	peak	-60.1646	-64.5031	
	Summary East-Ice-Shelf	mean sum			18.75	0.760	1.071	0.312	41.000				
West	AMR	1993-02-01	2014-08-22	21.57	0.112	2.065	1.954	1750.085	18	increased	-62.3704	-64.8692	1
	Andrew	1992-12-25	2014-08-27	21.68	0.430	0.339	-0.091	-21.211	112	fluctuating	-59.7202	-63.8728	4
	Bagshawe-Grubb	1996-02-15	2010-11-29	14.80	0.211	0.163	-0.048	-22.789	5	stable	-62.6231	-64.9147	1
	Bayly	1993-02-01	2014-08-22	21.57	0.806	0.886	0.080	9.931	37	fluctuating	-61.8628	-64.6094	3
	Blanchard	1993-02-01	2014-08-22	21.57	0.937	1.390	0.453	48.342	37	increased	-62.0656	-64.7283	2
	Bleriot	1996-02-15	2014-04-10	18.16	1.375	1.267	-0.107	-7.793	27	fluctuating	-61.1699	-64.4075	3
	CLM	1993-02-01	2010-12-29	17.92	0.288	0.394	0.106	36.932	24	peak	-60.9489	-64.3093	2
	Deville	1996-02-15	2010-12-22	14.86	1.386	0.259	-1.127	-81.322	10	decreased	-62.5725	-64.8107	3
	DGC10	1993-02-01	2014-04-10	21.20	0.232	0.774	0.542	234.115	30	increased	-61.4458	-64.4220	1
	DGC13	1996-02-15	2014-04-10	18.16	0.354	0.457	0.102	28.864	23	fluctuating	-61.5345	-64.5383	3
	DGC14	1996-02-15	2014-04-10	18.16	0.096	0.124	0.028	28.973	29	stable	-61.5777	-64.5362	3
	DGC22	1996-02-15	2014-04-10	18.16	0.272	0.543	0.271	99.864	33	fluctuating	-61.5535	-64.5763	3
	DGC23	1993-02-01	2014-08-22	21.57	0.414	0.960	0.545	131.621	37	increased	-61.9237	-64.6491	1
	DGC25	1993-02-01	2014-08-22	21.57	0.096	1.049	0.953	994.935	38	increased	-62.0029	-64.7076	2
	DGC31	1993-02-01	2010-12-22	17.90	0.719	0.211	-0.509	-70.700	7	fluctuating	-62.3808	-64.7243	3
	DGC39	1993-02-01	2010-12-22	17.90	0.645	0.153	-0.493	-76.339	11	decreased	-62.5177	-64.6534	3
	DGC72	1993-02-01	2014-04-10	21.20	0.269	2.387	2.118	787.360	25	increased	-61.3022	-64.4380	2
	DGC8	1993-02-01	2014-04-10	21.20	0.169	0.384	0.215	127.060	40	fluctuating	-61.3651	-64.4162	4
	Krebs	1993-02-01	2014-04-10	21.20	0.866	1.119	0.253	29.203	20	peak	-61.5201	-64.6377	1
	Landau	1996-02-13	2014-08-27	18.55	0.068	1.349	1.281	1876.773	43	increased	-59.3685	-63.8722	1
	Leonardo	1993-02-01	2014-08-22	21.57	0.155	2.523	2.368	1525.056	28	increased	-61.9568	-64.6961	2
	Mc Neile	1995-11-14	2014-08-27	18.80	0.650	5.146	4.496	691.683	33	increased	-59.4035	-63.9233	1
	Montgolfier	1993-02-01	2014-08-22	21.57	0.250	2.624	2.374	949.476	31	increased	-62.2203	-64.7800	1
	Nobile	1993-02-01	2014-04-10	21.20	0.235	1.226	0.991	421.633	18	increased	-61.4705	-64.5422	1
	Orel	1993-02-01	2010-12-22	17.90	0.519	0.344	-0.174	-33.577	10	stable	-62.5638	-64.7635	4
	Pettus-Gavinlce	1992-12-25	2014-08-05	21.62	5.651	1.951	-3.700	-65.473	29	peak	-59.1464	-63.7450	2

Sector	Basin	Date vs [yyyy-mm-dd]	Date vE [yyyy-mm-dd]	dt [a]	vS [m d-1]	vE [m d-1]	dv [m d-1]	dv [%]	n _v	Vel. change category			Group
	Renard	1993-02-01	2014-08-22	21.57	0.213	1.273	1.060	498.781	42	increased	-61.6438	-64.6709	2
	Rozier	1996-02-29	2014-08-27	21.57	1.777	2.210	0.433	24.342	59	increased	-62.1835	-64.7457	2
	Russell West	1993-02-01	2014-08-27	18.50	0.196	0.341	0.145	73.631	105	increased	-58.8902	-63.6830	2
	Sabine	1993-02-01	2010-12-12	21.58	0.577	2.814	2.238	388.165	31	peak	-59.8056	-63.8741	2
	SBG	1996-02-13	2011-02-08	17.87	4.106	4.029	-0.077	-1.885	20	fluctuating	-60.8223	-64.1623	2
	Stringfellow-Henson	1992-12-25	2014-02-28	15.00	1.390	1.283	-0.106	-7.660	98	fluctuating	-60.4311	-63.9752	1
	Temple	1995-11-14	2013-12-24	21.19	1.272	1.881	0.609	47.843	28	increased	-60.1247	-63.9419	2
	TPE11	1992-12-25	2013-12-24	18.12	0.526	0.384	-0.142	-26.927	31	fluctuating	-58.1397	-63.4734	3
	TPE125	1992-12-25	2014-08-27	21.01	0.150	0.277	0.127	84.605	50	peak	-58.6190	-63.5057	2
	TPE126	1995-12-19	2013-12-24	21.68	1.081	0.993	-0.088	-8.144	25	fluctuating	-59.3057	-63.7796	3
	TPE39	1992-12-25	2013-12-24	18.03	0.649	0.408	-0.241	-37.191	25	fluctuating	-58.7693	-63.5361	3
	TPE40	1995-12-19	2013-12-24	21.01	0.472	0.454	-0.018	-3.798	17	fluctuating	-58.3804	-63.4791	3
	TPE41	1992-12-25	2014-08-27	18.03	1.390	1.025	-0.365	-26.229	47	fluctuating	-58.2347	-63.4585	1
	TPE46	1992-12-25	2014-08-27	21.68	1.312	0.852	-0.459	-35.021	113	fluctuating	-59.3930	-63.8914	2
	TPE50	1993-02-01	2010-12-29	21.68	0.473	0.275	-0.198	-41.828	22	stable	-59.9269	-63.9387	3
	TPE57	1996-02-11	2013-12-24	17.92	0.671	0.692	0.021	3.134	12	fluctuating	-60.6700	-64.0238	3
	TPE8	1995-12-19	2013-12-24	17.88	4.396	0.605	-3.791	-86.236	24	decreased	-57.9284	-63.3700	3
	TPE9	1996-02-15	2014-04-10	18.03	0.196	0.855	0.658	335.252	21	increased	-58.0371	-63.4244	2
	Wellman	1993-02-01	2010-12-22	18.16	0.455	0.530	0.075	16.501	12	peak	-61.4298	-64.4846	2
	Wheatstone	1992-12-25	2014-08-27	17.90	1.017	3.375	2.359	232.018	99	increased	-62.5189	-64.7362	1
	Whitecloud	1993-02-01	2014-08-22	21.68	0.153	0.237	0.085	55.585	44	fluctuating	-59.5585	-63.9000	3
	Woodbury	1993-02-01	2014-08-22	21.57	0.213	1.273	1.060	498.781	42	increased	-62.3053	-64.7749	2
Summary West	mean sum			19.65	0.831	1.200	0.369	44.461					1742
Summary all glaciers	mean sum			19.21	0.994	1.065	0.071	7.143					2736

Date v_s - date of first velocity measurement

dt - mean time period of velocity measurements

v_E – mean of latest velocity measurements (2010-2014)

n_v – sum of velocity measurements in the observation period (dt)

Latitude/Longitude – position of velocity measurements (maximum ice thickness at terminus profiles)

Group – classification of glaciers in sector “West” according to the hierarchical cluster analysis in Section 4.4.

Date v_E – date of last velocity measurement

v_s – mean of earliest velocity measurements (1992-1996)

dv – mean velocity change

Velocity change category – see definition in Table 3

Table S3: Uncertainty σ_v of intensity tracking results. Table continues next pages.

Date [yyyy-mm-dd]	Satellite	dt [d]	σ_v^C [m d ⁻¹]	n	σ_v^T [m d ⁻¹]	σ_v [m d ⁻¹]
1992-12-25	ERS	35	0.13	9721	0.05	0.14
1992-12-25	ERS	35	0.25	23678	0.05	0.26
1993-01-12	ERS	70	0.07	9880	0.02	0.07
1993-01-29	ERS	35	0.10	6090	0.05	0.11
1993-01-29	ERS	35	0.23	4533	0.05	0.24
1993-02-01	ERS	35	0.20	6321	0.05	0.21
1994-02-01	ERS	21	0.35	22007	0.08	0.36
1994-02-18	ERS	54	0.07	28834	0.03	0.08
1994-02-28	ERS	33	0.16	26276	0.05	0.17
1995-10-31	ERS	1*	0.41	150	1.60	0.41
1995-11-14	ERS	1*	0.36	1961	1.60	0.36
1995-11-16	ERS	1*	0.29	448	1.60	0.29
1995-12-18	ERS	71	0.02	68711	0.02	0.03
1995-12-18	ERS	70	0.03	77246	0.02	0.04
1995-12-19	ERS	71	0.02	70974	0.02	0.03
1995-12-19	ERS	70	0.06	67287	0.02	0.06
1995-12-19	ERS	69	0.12	66877	0.02	0.12
1995-12-20	ERS	70	0.04	70897	0.02	0.04
1995-12-21	ERS	70	0.08	10755	0.02	0.08
1995-12-21	ERS	69	0.09	9000	0.02	0.10
1996-01-22	ERS	1*	0.24	49973	1.60	0.24
1996-01-23	ERS	1*	0.34	546	1.60	0.34
1996-02-11	ERS	35	0.12	10215	0.05	0.12
1996-02-11	ERS	35	0.14	8164	0.05	0.15
1996-02-13	ERS	35	0.06	23882	0.05	0.08
1996-02-15	ERS	35	0.14	9379	0.05	0.15
1996-02-29	ERS	35	0.02	39573	0.05	0.05
1996-03-03	ERS	34	0.05	18324	0.05	0.07
1996-03-03	ERS	35	0.05	18395	0.05	0.07
1996-03-20	ERS	1*	0.30	9049	1.60	0.30
1997-02-13	ERS	35	0.04	44246	0.05	0.06
1997-02-15	ERS	35	0.11	14969	0.05	0.12
1997-02-18	ERS	35	0.09	6705	0.05	0.10
1998-02-03	ERS	35	0.07	3176	0.05	0.08
1999-11-09	ERS	1*	0.34	4022	1.60	0.34
2002-02-07	ERS	35	0.07	9893	0.05	0.09
2002-11-29	ERS	35	0.13	61073	0.05	0.13
2002-12-03	ERS	35	0.13	19079	0.05	0.13
2002-12-08	ERS	35	0.29	1965	0.05	0.29
2002-12-21	ERS	70	0.05	21331	0.02	0.05
2002-12-21	ERS	35	0.27	3396	0.05	0.27
2002-12-26	ERS	70	0.13	2437	0.02	0.13
2003-01-07	ERS	35	0.05	24658	0.05	0.07
2003-01-08	ERS	70	0.19	4794	0.02	0.19
2003-01-12	ERS	35	0.09	2548	0.05	0.10
2003-01-25	ERS	35	0.10	14207	0.05	0.11
2004-11-01	ERS	35	0.17	30346	0.05	0.17
2004-11-17	ERS	70	0.06	71277	0.02	0.07
2004-11-19	ERS	70	0.08	32153	0.02	0.09
2004-12-06	ERS	35	0.11	33520	0.05	0.12
2004-12-24	ERS	70	0.11	34409	0.02	0.11
2004-12-25	ERS	35	0.14	12592	0.05	0.14
2005-01-10	ERS	35	0.28	23466	0.05	0.28

Date [yyyy-mm-dd]	Satellite	dt [d]	σ_v^C [m d ⁻¹]	n	σ_v^T [m d ⁻¹]	σ_v [m d ⁻¹]
2006-11-03	ERS	35	0.19	56628	0.05	0.19
2006-11-04	ERS	35	0.14	70277	0.05	0.14
2008-10-29	ERS	35	0.07	9881	0.05	0.08
2010-02-08	ERS	35	0.18	18041	0.05	0.19
2010-02-26	ERS	70	0.11	19172	0.02	0.11
2010-03-15	ERS	35	0.10	23486	0.05	0.11
2000-09-22	R1	24	0.10	20810	0.06	0.12
2000-09-22	R1	24	0.14	33870	0.06	0.15
2000-10-01	R1	24	0.06	30397	0.06	0.09
2006-08-22	R1	24	0.07	57259	0.06	0.10
2006-08-22	R1	24	0.08	21635	0.06	0.10
2003-12-22	ENVISAT	35	0.31	38866	0.05	0.31
2004-01-09	ENVISAT	70	0.03	61495	0.02	0.04
2004-01-10	ENVISAT	35	0.13	1790	0.05	0.13
2004-01-28	ENVISAT	70	0.16	1510	0.02	0.16
2004-02-14	ENVISAT	35	0.09	1898	0.05	0.10
2004-03-20	ENVISAT	35	0.13	3299	0.05	0.14
2004-04-24	ENVISAT	35	0.12	3505	0.05	0.13
2004-05-29	ENVISAT	35	0.10	3623	0.05	0.11
2004-07-03	ENVISAT	35	0.10	3546	0.05	0.11
2004-07-19	ENVISAT	35	0.03	60612	0.05	0.06
2004-08-07	ENVISAT	35	0.11	3418	0.05	0.12
2004-09-11	ENVISAT	35	0.14	3400	0.05	0.15
2004-10-16	ENVISAT	35	0.15	3449	0.05	0.16
2004-12-06	ENVISAT	35	0.06	63965	0.05	0.08
2005-01-28	ENVISAT	70	0.02	62239	0.02	0.03
2005-03-05	ENVISAT	35	0.15	2744	0.05	0.15
2005-03-21	ENVISAT	35	0.19	64254	0.05	0.19
2005-04-09	ENVISAT	35	0.13	2904	0.05	0.14
2005-05-14	ENVISAT	35	0.17	3016	0.05	0.17
2005-06-18	ENVISAT	35	0.13	3631	0.05	0.14
2005-07-23	ENVISAT	35	0.14	2943	0.05	0.14
2005-08-08	ENVISAT	35	0.12	68061	0.05	0.13
2006-02-15	ENVISAT	35	0.07	61205	0.05	0.08
2006-03-25	ENVISAT	35	0.14	2755	0.05	0.15
2006-07-08	ENVISAT	35	0.08	3488	0.05	0.09
2006-08-09	ENVISAT	35	0.06	60954	0.05	0.08
2006-08-12	ENVISAT	35	0.15	3302	0.05	0.15
2006-09-16	ENVISAT	35	0.14	3295	0.05	0.15
2006-10-21	ENVISAT	35	0.16	2741	0.05	0.17
2007-02-18	ENVISAT	70	0.03	71538	0.02	0.04
2007-04-29	ENVISAT	70	0.04	65692	0.02	0.05
2007-06-20	ENVISAT	35	0.03	63862	0.05	0.05
2007-08-12	ENVISAT	70	0.04	61079	0.02	0.05
2007-09-01	ENVISAT	35	0.15	3391	0.05	0.16
2007-10-03	ENVISAT	35	0.10	61336	0.05	0.11
2007-10-06	ENVISAT	35	0.16	3255	0.05	0.16
2008-04-30	ENVISAT	35	0.10	63576	0.05	0.11
2008-06-22	ENVISAT	70	0.03	57922	0.02	0.04
2008-08-13	ENVISAT	35	0.07	60539	0.05	0.08
2009-03-11	ENVISAT	35	0.11	64638	0.05	0.12
2009-07-29	ENVISAT	35	0.03	61130	0.05	0.05
2006-06-10	ALOS	46	0.02	15503	0.02	0.02
2006-06-17	ALOS	46	0.01	61958	0.02	0.02
2006-06-25	ALOS	46	0.08	581	0.02	0.09
2006-07-14	ALOS	46	0.02	9476	0.02	0.02
2006-09-21	ALOS	92	0.02	9912	0.01	0.02

Date [yyyy-mm-dd]	Satellite	dt [d]	σ_v^C [m d ⁻¹]	n	σ_v^T [m d ⁻¹]	σ_v [m d ⁻¹]
2006-12-23	ALOS	46	0.08	5135	0.02	0.08
2007-12-04	ALOS	46	0.03	10220	0.02	0.04
2007-12-14	ALOS	46	0.04	2193	0.02	0.04
2008-05-14	ALOS	46	0.01	43889	0.02	0.02
2008-10-21	ALOS	46	0.02	10711	0.02	0.02
2008-10-31	ALOS	46	0.13	2461	0.02	0.13
2008-11-13	ALOS	92	0.02	10861	0.01	0.02
2008-11-14	ALOS	46	0.02	33136	0.02	0.02
2008-12-06	ALOS	46	0.04	10213	0.02	0.04
2008-12-07	ALOS	92	0.02	36230	0.01	0.02
2008-12-16	ALOS	46	0.07	2291	0.02	0.07
2008-12-29	ALOS	92	0.02	10998	0.01	0.02
2008-12-30	ALOS	46	0.04	37661	0.02	0.04
2009-01-21	ALOS	46	0.02	10677	0.02	0.03
2009-12-02	ALOS	46	0.05	3484	0.02	0.05
2009-12-09	ALOS	46	0.03	9707	0.02	0.03
2009-12-21	ALOS	46	0.05	2455	0.02	0.05
2009-12-26	ALOS	46	0.03	9385	0.02	0.03
2010-01-19	ALOS	46	0.02	15505	0.02	0.02
2010-10-08	ALOS	46	0.04	620	0.02	0.04
2010-10-17	ALOS	46	0.03	79294	0.02	0.03
2010-11-06	ALOS	46	0.08	2212	0.02	0.08
2010-11-08	ALOS	46	0.01	16076	0.02	0.02
2010-11-10	ALOS	46	0.02	422	0.02	0.03
2010-11-13	ALOS	46	0.04	9956	0.02	0.05
2010-11-29	ALOS	92	0.03	2069	0.01	0.03
2010-12-01	ALOS	92	0.01	18027	0.01	0.01
2010-12-03	ALOS	92	0.40	426	0.01	0.40
2010-12-06	ALOS	92	0.03	10352	0.01	0.03
2010-12-11	ALOS	92	0.04	4683	0.01	0.04
2010-12-12	ALOS	46	0.03	9480	0.02	0.04
2010-12-22	ALOS	46	0.05	1992	0.02	0.05
2010-12-26	ALOS	46	0.02	411	0.02	0.03
2010-12-29	ALOS	46	0.03	10478	0.02	0.04
2010-12-31	ALOS	46	0.01	46824	0.02	0.02
2011-01-18	ALOS	92	0.16	430	0.01	0.16
2011-02-08	ALOS	46	0.01	17569	0.02	0.02
2011-02-10	ALOS	46	0.01	394	0.02	0.02
2008-10-19	TSX/TDX	11	0.05	4560	0.02	0.05
2008-10-25	TSX/TDX	22	0.02	4362	0.01	0.02
2008-10-30	TSX/TDX	11	0.03	4507	0.02	0.04
2009-08-01	TSX/TDX	11	0.02	11170	0.02	0.03
2009-10-28	TSX/TDX	11	0.06	4220	0.02	0.07
2010-10-26	TSX/TDX	33	0.02	2678	0.01	0.02
2010-11-01	TSX/TDX	44	0.02	3442	0.01	0.02
2010-11-17	TSX/TDX	22	0.01	5995	0.01	0.01
2010-11-17	TSX/TDX	11	0.06	3599	0.02	0.07
2010-11-28	TSX/TDX	99	0.01	3063	0.00	0.01
2010-12-15	TSX/TDX	66	0.02	3476	0.00	0.02
2010-12-20	TSX/TDX	77	0.01	3524	0.00	0.01
2010-12-20	TSX/TDX	55	0.01	4297	0.00	0.02
2010-12-26	TSX/TDX	66	0.01	4341	0.00	0.01
2011-01-22	TSX/TDX	11	0.02	4722	0.02	0.03
2011-06-25	TSX/TDX	22	0.01	15556	0.01	0.02
2011-06-25	TSX/TDX	22	0.04	9886	0.01	0.04
2011-07-06	TSX/TDX	44	0.04	10380	0.01	0.04
2011-07-16	TSX/TDX	22	0.04	3582	0.01	0.04

Date [yyyy-mm-dd]	Satellite	dt [d]	σ_v^C [m d ⁻¹]	n	σ_v^T [m d ⁻¹]	σ_v [m d ⁻¹]
2011-07-17	TSX/TDX	22	0.01	15712	0.01	0.02
2011-07-16	TSX/TDX	22	0.10	1421	0.01	0.10
2011-07-17	TSX/TDX	22	0.03	10450	0.01	0.03
2011-07-28	TSX/TDX	44	0.02	10607	0.01	0.02
2011-08-03	TSX/TDX	22	0.40	614	0.01	0.40
2011-08-08	TSX/TDX	22	0.03	10394	0.01	0.04
2011-08-14	TSX/TDX	44	0.14	1556	0.01	0.14
2011-08-19	TSX/TDX	44	0.03	10054	0.01	0.03
2011-08-19	TSX/TDX	55	0.04	2385	0.00	0.04
2011-08-24	TSX/TDX	22	0.03	1894	0.01	0.03
2011-08-24	TSX/TDX	55	0.03	10578	0.00	0.03
2011-08-29	TSX/TDX	33	0.03	1856	0.01	0.03
2011-08-30	TSX/TDX	22	0.02	15605	0.01	0.02
2011-08-30	TSX/TDX	22	0.06	7157	0.01	0.06
2011-09-04	TSX/TDX	33	0.01	15878	0.01	0.01
2011-09-09	TSX/TDX	11	0.06	2325	0.02	0.06
2011-09-14	TSX/TDX	11	0.05	3667	0.02	0.05
2011-09-14	TSX/TDX	11	0.12	1279	0.02	0.12
2011-09-15	TSX/TDX	11	0.03	15546	0.02	0.03
2011-09-15	TSX/TDX	11	0.07	7819	0.02	0.07
2011-09-27	TSX/TDX	44	0.14	2001	0.01	0.14
2011-10-01	TSX/TDX	33	0.02	1956	0.01	0.02
2011-10-01	TSX/TDX	44	0.04	3582	0.01	0.04
2011-10-06	TSX/TDX	33	0.04	3602	0.01	0.05
2011-10-06	TSX/TDX	33	0.11	1353	0.01	0.11
2011-10-12	TSX/TDX	66	0.02	3453	0.00	0.02
2011-10-17	TSX/TDX	55	0.03	3541	0.00	0.03
2011-10-23	TSX/TDX	11	0.06	2018	0.02	0.06
2011-11-03	TSX/TDX	22	0.05	3533	0.01	0.05
2011-11-03	TSX/TDX	22	0.07	1209	0.01	0.07
2011-11-25	TSX/TDX	22	0.03	3507	0.01	0.03
2011-12-06	TSX/TDX	11	0.06	2432	0.02	0.06
2011-12-12	TSX/TDX	33	0.01	13467	0.01	0.01
2011-12-13	TSX/TDX	44	0.05	2328	0.01	0.05
2011-12-17	TSX/TDX	22	0.01	4172	0.01	0.02
2011-12-18	TSX/TDX	33	0.08	2365	0.01	0.08
2012-01-03	TSX/TDX	11	0.01	16220	0.02	0.03
2012-01-03	TSX/TDX	11	0.07	8576	0.02	0.07
2012-01-31	TSX/TDX	55	0.05	2338	0.00	0.05
2012-03-09	TSX/TDX	11	0.02	13279	0.02	0.03
2012-03-09	TSX/TDX	11	0.16	7483	0.02	0.16
2012-03-10	TSX/TDX	22	0.07	2343	0.01	0.07
2012-03-15	TSX/TDX	22	0.01	15451	0.01	0.01
2012-03-15	TSX/TDX	33	0.05	2290	0.01	0.05
2012-03-15	TSX/TDX	22	0.07	7142	0.01	0.07
2012-03-20	TSX/TDX	11	0.08	6422	0.02	0.08
2012-03-21	TSX/TDX	44	0.05	2265	0.01	0.05
2012-03-25	TSX/TDX	22	0.11	1258	0.01	0.11
2012-03-26	TSX/TDX	55	0.05	2143	0.00	0.05
2012-03-26	TSX/TDX	11	0.19	2259	0.02	0.19
2012-04-01	TSX/TDX	22	0.14	2362	0.01	0.14
2012-04-06	TSX/TDX	33	0.06	2248	0.01	0.06
2012-04-06	TSX/TDX	11	0.10	2316	0.02	0.10
2012-04-12	TSX/TDX	22	0.05	2100	0.01	0.05
2012-04-17	TSX/TDX	22	0.02	15486	0.01	0.02
2012-04-17	TSX/TDX	22	0.05	7244	0.01	0.05
2012-04-30	TSX/TDX	11	0.04	1747	0.02	0.05

Date [yyyy-mm-dd]	Satellite	dt [d]	σ_v^C [m d ⁻¹]	n	σ_v^T [m d ⁻¹]	σ_v [m d ⁻¹]
2012-05-08	TSX/TDX	66	0.02	3381	0.00	0.02
2012-05-09	TSX/TDX	22	0.02	15305	0.01	0.02
2012-05-09	TSX/TDX	55	0.04	2344	0.00	0.04
2012-05-09	TSX/TDX	22	0.05	6241	0.01	0.05
2012-05-13	TSX/TDX	77	0.02	3656	0.00	0.02
2012-05-15	TSX/TDX	44	0.04	2221	0.01	0.04
2012-05-19	TSX/TDX	22	0.03	3672	0.01	0.03
2012-05-19	TSX/TDX	22	0.10	1275	0.01	0.10
2012-05-20	TSX/TDX	55	0.04	2375	0.00	0.04
2012-05-24	TSX/TDX	33	0.04	1210	0.01	0.04
2012-05-30	TSX/TDX	33	0.03	2544	0.01	0.03
2012-06-04	TSX/TDX	11	0.05	3532	0.02	0.06
2012-06-04	TSX/TDX	11	0.10	1351	0.02	0.11
2012-06-05	TSX/TDX	33	0.01	15558	0.01	0.01
2012-06-11	TSX/TDX	11	0.09	2222	0.02	0.09
2012-06-15	TSX/TDX	11	0.08	3328	0.02	0.09
2012-06-15	TSX/TDX	11	0.10	1280	0.02	0.10
2012-06-21	TSX/TDX	11	0.07	2621	0.02	0.07
2012-06-27	TSX/TDX	11	0.06	7647	0.02	0.06
2012-06-28	TSX/TDX	44	0.04	2293	0.01	0.04
2012-07-03	TSX/TDX	55	0.04	2350	0.00	0.04
2012-07-03	TSX/TDX	33	0.05	2292	0.01	0.05
2012-07-09	TSX/TDX	44	0.04	2389	0.01	0.04
2012-07-13	TSX/TDX	33	0.03	2765	0.01	0.03
2012-07-19	TSX/TDX	33	0.02	15662	0.01	0.02
2012-07-25	TSX/TDX	11	0.09	2122	0.02	0.09
2012-08-04	TSX/TDX	11	0.07	2545	0.02	0.07
2012-08-09	TSX/TDX	11	0.07	3577	0.02	0.07
2012-08-09	TSX/TDX	11	0.12	1204	0.02	0.13
2012-08-10	TSX/TDX	11	0.07	7151	0.02	0.07
2012-08-11	TSX/TDX	44	0.08	2444	0.01	0.08
2012-08-16	TSX/TDX	55	0.04	2374	0.00	0.04
2012-08-22	TSX/TDX	44	0.04	2230	0.01	0.04
2012-09-07	TSX/TDX	11	0.14	1690	0.02	0.14
2012-09-23	TSX/TDX	33	0.05	1078	0.01	0.05
2012-09-29	TSX/TDX	55	0.04	1597	0.00	0.04
2012-09-29	TSX/TDX	33	0.06	2397	0.01	0.06
2012-10-05	TSX/TDX	44	0.08	2401	0.01	0.08
2012-10-10	TSX/TDX	55	0.05	2372	0.00	0.05
2012-10-20	TSX/TDX	33	0.03	2520	0.01	0.03
2012-10-21	TSX/TDX	11	0.09	2179	0.02	0.09
2012-10-27	TSX/TDX	22	0.08	2296	0.01	0.08
2012-11-01	TSX/TDX	11	0.10	2327	0.02	0.10
2012-11-01	TSX/TDX	33	0.17	1923	0.01	0.17
2012-11-05	TSX/TDX	11	0.05	3446	0.02	0.05
2012-11-05	TSX/TDX	11	0.13	1186	0.02	0.13
2012-11-07	TSX/TDX	44	0.05	2312	0.01	0.05
2012-11-12	TSX/TDX	33	0.05	2364	0.01	0.06
2012-11-12	TSX/TDX	11	0.12	2354	0.02	0.12
2012-11-18	TSX/TDX	22	0.07	2419	0.01	0.07
2012-11-23	TSX/TDX	11	0.08	2204	0.02	0.09
2012-12-26	TSX/TDX	55	0.03	2141	0.00	0.03
2013-02-23	TSX/TDX	77	0.01	3503	0.00	0.01
2013-03-01	TSX/TDX	11	0.08	2802	0.02	0.08
2013-03-17	TSX/TDX	11	0.06	3749	0.02	0.07
2013-03-17	TSX/TDX	11	0.14	1255	0.02	0.14
2013-03-23	TSX/TDX	22	0.03	3632	0.01	0.03

Date [yyyy-mm-dd]	Satellite	dt [d]	σ_v^C [m d ⁻¹]	n	σ_v^T [m d ⁻¹]	σ_v [m d ⁻¹]
2013-03-23	TSX/TDX	22	0.08	1196	0.01	0.08
2013-03-26	TSX/TDX	11	0.08	1992	0.02	0.08
2013-03-28	TSX/TDX	11	0.17	1347	0.02	0.18
2013-03-29	TSX/TDX	33	0.05	1148	0.01	0.05
2013-04-03	TSX/TDX	33	0.09	2117	0.01	0.09
2013-04-10	TSX/TDX	22	0.06	2172	0.01	0.07
2013-04-15	TSX/TDX	33	0.07	2237	0.01	0.07
2013-04-26	TSX/TDX	55	0.05	2275	0.00	0.05
2013-04-26	TSX/TDX	11	0.12	2379	0.02	0.13
2013-04-30	TSX/TDX	55	0.02	3261	0.00	0.03
2013-06-08	TSX/TDX	22	0.03	3820	0.01	0.03
2013-06-08	TSX/TDX	22	0.04	1021	0.01	0.04
2013-06-19	TSX/TDX	44	0.02	3719	0.01	0.02
2013-06-30	TSX/TDX	22	0.03	3813	0.01	0.03
2013-06-30	TSX/TDX	22	0.09	1258	0.01	0.09
2013-07-28	TSX/TDX	33	0.01	15233	0.01	0.02
2013-08-02	TSX/TDX	33	0.02	2763	0.01	0.02
2013-08-25	TSX/TDX	33	0.05	2311	0.01	0.05
2013-08-30	TSX/TDX	33	0.01	15399	0.01	0.01
2013-09-20	TSX/TDX	33	0.03	3602	0.01	0.03
2013-09-20	TSX/TDX	33	0.05	1292	0.01	0.05
2013-09-27	TSX/TDX	33	0.04	2235	0.01	0.04
2013-10-02	TSX/TDX	33	0.01	15262	0.01	0.01
2013-10-23	TSX/TDX	33	0.02	3578	0.01	0.02
2013-10-23	TSX/TDX	33	0.05	1283	0.01	0.05
2013-10-30	TSX/TDX	33	0.05	2317	0.01	0.05
2013-11-02	TSX/TDX	11	0.02	9090	0.02	0.03
2013-11-02	TSX/TDX	11	0.07	484	0.02	0.07
2013-11-04	TSX/TDX	33	0.02	15102	0.01	0.02
2013-11-09	TSX/TDX	11	0.05	2652	0.02	0.06
2013-11-10	TSX/TDX	55	0.04	2294	0.00	0.04
2013-11-15	TSX/TDX	22	0.04	2878	0.01	0.05
2013-11-20	TSX/TDX	22	0.03	3538	0.01	0.04
2013-11-20	TSX/TDX	33	0.04	2955	0.01	0.04
2013-11-20	TSX/TDX	11	0.08	2846	0.02	0.08
2013-11-20	TSX/TDX	22	0.10	1321	0.01	0.10
2013-11-21	TSX/TDX	11	0.08	2180	0.02	0.08
2013-11-25	TSX/TDX	33	0.02	3312	0.01	0.02
2013-11-25	TSX/TDX	33	0.05	1125	0.01	0.05
2013-11-26	TSX/TDX	11	0.03	15060	0.02	0.03
2013-11-26	TSX/TDX	22	0.04	2825	0.01	0.04
2013-11-26	TSX/TDX	11	0.08	6708	0.02	0.09
2013-11-27	TSX/TDX	22	0.08	2346	0.01	0.09
2013-11-30	TSX/TDX	44	0.00	8207	0.01	0.01
2013-12-01	TSX/TDX	44	0.02	3438	0.01	0.02
2013-12-01	TSX/TDX	33	0.03	2670	0.01	0.03
2013-12-01	TSX/TDX	11	0.06	2893	0.02	0.06
2013-12-02	TSX/TDX	22	0.01	14680	0.01	0.01
2013-12-02	TSX/TDX	33	0.04	2079	0.01	0.04
2013-12-02	TSX/TDX	22	0.06	6620	0.01	0.06
2013-12-02	TSX/TDX	11	0.23	1957	0.02	0.24
2013-12-06	TSX/TDX	11	0.05	3548	0.02	0.06
2013-12-06	TSX/TDX	11	0.15	1322	0.02	0.15
2013-12-07	TSX/TDX	11	0.02	14924	0.02	0.03
2013-12-07	TSX/TDX	22	0.04	2905	0.01	0.04
2013-12-07	TSX/TDX	11	0.11	8347	0.02	0.11
2013-12-08	TSX/TDX	22	0.08	2021	0.01	0.08

Date [yyyy-mm-dd]	Satellite	dt [d]	σ_v^C [m d ⁻¹]	n	σ_v^T [m d ⁻¹]	σ_v [m d ⁻¹]
2013-12-12	TSX/TDX	22	0.03	3508	0.01	0.03
2013-12-12	TSX/TDX	33	0.03	2814	0.01	0.03
2013-12-12	TSX/TDX	11	0.07	3039	0.02	0.08
2013-12-12	TSX/TDX	22	0.09	1242	0.01	0.09
2013-12-13	TSX/TDX	33	0.06	2306	0.01	0.06
2013-12-13	TSX/TDX	11	0.07	2024	0.02	0.08
2013-12-17	TSX/TDX	11	0.02	3978	0.02	0.03
2013-12-17	TSX/TDX	33	0.03	3323	0.01	0.03
2013-12-17	TSX/TDX	11	0.14	1290	0.02	0.14
2013-12-18	TSX/TDX	33	0.01	13920	0.01	0.01
2013-12-18	TSX/TDX	22	0.03	2741	0.01	0.04
2013-12-23	TSX/TDX	22	0.03	3725	0.01	0.03
2013-12-23	TSX/TDX	11	0.05	2877	0.02	0.06
2013-12-23	TSX/TDX	22	0.09	1118	0.01	0.10
2013-12-24	TSX/TDX	22	0.01	14893	0.01	0.01
2013-12-24	TSX/TDX	22	0.05	7587	0.01	0.05
2013-12-24	TSX/TDX	11	0.09	2342	0.02	0.09
2013-12-28	TSX/TDX	11	0.05	3475	0.02	0.05
2013-12-28	TSX/TDX	11	0.14	1096	0.02	0.15
2013-12-30	TSX/TDX	44	0.03	2034	0.01	0.03
2014-01-03	TSX/TDX	33	0.02	2819	0.01	0.02
2014-01-04	TSX/TDX	55	0.04	2128	0.00	0.04
2014-01-04	TSX/TDX	33	0.05	1939	0.01	0.05
2014-01-09	TSX/TDX	22	0.03	2828	0.01	0.03
2014-01-10	TSX/TDX	44	0.03	2083	0.01	0.03
2014-01-10	TSX/TDX	22	0.10	2104	0.01	0.10
2014-01-14	TSX/TDX	44	0.01	3685	0.01	0.01
2014-01-15	TSX/TDX	33	0.05	2236	0.01	0.05
2014-01-19	TSX/TDX	33	0.02	3652	0.01	0.02
2014-01-31	TSX/TDX	22	0.03	2647	0.01	0.03
2014-02-27	TSX/TDX	44	0.03	3163	0.01	0.03
2014-02-28	TSX/TDX	55	0.05	2235	0.00	0.05
2014-03-24	TSX/TDX	11	0.08	1958	0.02	0.08
2014-03-27	TSX/TDX	11	0.03	15610	0.02	0.03
2014-04-04	TSX/TDX	33	0.04	1921	0.01	0.04
2014-04-10	TSX/TDX	22	0.05	1895	0.01	0.05
2014-07-25	TSX/TDX	11	0.07	1184	0.02	0.08
2014-08-05	TSX/TDX	33	0.05	1130	0.01	0.05
2014-08-06	TSX/TDX	22	0.03	2495	0.01	0.03
2014-08-11	TSX/TDX	33	0.02	2649	0.01	0.02
2014-08-11	TSX/TDX	22	0.08	1340	0.01	0.08
2014-08-22	TSX/TDX	11	0.08	3049	0.02	0.08
2014-08-27	TSX/TDX	11	0.08	1215	0.02	0.09
2014-12-16	TSX/TDX	11	0.03	15265	0.02	0.03
datasets		Mean values:				
382	All		0.07	11717	0.05	0.08
59	ERS		0.14	26475	0.04	0.15
5	R1		0.09	32794	0.06	0.11
41	ENVISAT		0.11	30240	0.04	0.12
43	ALOS		0.05	13868	0.01	0.05
234	TSX/TDX		0.06	4414	0.01	0.06

Date - mean date of SAR acquisitions

dt - time interval in days between consecutive SAR acquisitions

σ_v^C - uncertainty of image coregistration

σ_v^T - uncertainty of intensity tracking process

* if $dt = 1d \rightarrow \sigma_v = \sigma_v^C$ see manuscript Section 4.2